Development of weak cation exchange membrane adsorbers for protein capture

by

Yung Priscilla Lai

A thesis

presented to the University of Waterloo

in fulfillment of the

thesis requirement for the degree of

Master of Applied Science

in

Chemical Engineering

Waterloo, Ontario, Canada, 2015

Author’s declaration

I hereby declare that I am the sole author of this thesis. This is a true copy of the thesis, including any required final revisions, as accepted by my examiners.

I understand that my thesis may be made electronically available to the public.

Abstract

To reduce therapeutic protein production costs in bioprocessing such as monoclonal antibodies production, the downstream purification step needs to be optimized. Protein A resins for the chromatographic purification of such proteins have long been used but are expensive, diffusion limited, and may leach into the stream due to proteolysis. Weak cation exchange membrane adsorbers are a viable alternative, enabling lower costs and lower mass transfer limitations from diffusion for higher throughput.

The proposed synthesis route to develop weak cation exchange membrane adsorbers was to graft poly(acrylic acid) directly from a regenerated cellulose (RC) membrane surface by aqueous activator regenerated by electron transfer atom transfer radical polymerization (ARGET ATRP), a type of reversible deactivation radical polymerization (RDRP) technique. The technique allows for polymerization under limited amounts of oxygen in aqueous media and for controlled polymerization. The initiator, 2-bromoisobutyryl bromide (BiBB), was first immobilized on the RC membrane followed by ARGET ATRP.

The first part of the work investigated the immobilization of BiBB on RC membranes in a heterogeneous acylation reaction. The optimal ratio of BiBB to triethylamine (TEA, used in the reaction to neutralize the hydrogen bromide by-product) was 1/0.67. The effect of NaOH treatment on the methanol-washed RC membrane (i.e. no NaOH or 2 M NaOH), BiBB quantity used per membrane disc for immobilization (0.41, 0.74, or 2.67 mmol), and immobilization solvent (*N*,*N*-dimethylformamide, DMF, or tetrahydrofuran, THF) on BiBB immobilization was studied. Relative and absolute immobilized BIBB quantities were studied using attenuated total reflectance Fourier transform infrared spectroscopy (ATR-FTIR) peak area ratios and the degree of substitution (DS) of the RC membranes were calculated from gravimetry, respectively. The highest BiBB immobilization was obtained with the higher BiBB quantity used per membrane disc for immobilization, 2 M NaOH-treated, methanol-washed RC membrane, and DMF as immobilization solvent (ANOVA, 95% confidence level). The uniformity of BiBB immobilized across the surface was found to be improved when larger quantities of BiBB were added to the reaction (i.e. 0.74 mmol per membrane disc or greater). For ARGET ATRP, the amine ligand, 2,2′-bpyridine (bpy), was selected at a $CuBr_2$/bpy/ascorbic molar ratio of 1/2/2 based on $CuBr_2$

reduction studies by ascorbic acid. Using bpy, various ARGET ATRP reactions were conducted to determine the polymerization conditions that produced membranes with high and low poly(acrylic acid) contents (PAA, polymer ATR-FTIR peak area ratios of ~0.7 and ~0.48, respectively). The polymerization conditions that produced high PAA contents and low PAA contents were tested for their static protein binding capacity with lysozyme. The lysozyme static protein binding capacities were 235 mg mL^{-1} and 510 mg mL^{-1} for the poly(acrylic acid)-grafted RC membranes (PAA-*g*-RC) with low and high PAA contents, respectively.

The second part of the work investigated the effect of RC membrane treatment conditions and BiBB quantity used per membrane disc on immobilized BiBB in a 3^2 factorial design (i.e. methanol-washed RC membrane, 0nD; methanol-washed RC membrane with DMF storage for two weeks prior to immobilization, 0D; and methanol-washed RC membrane with 0.5 M NaOH treatment along with DMF storage prior to immobilization, 0.5D; with either 0, 0.74, and 2.67 mmol BiBB used per membrane disc). Energy dispersive x-ray spectroscopy (EDX) and thermogravimetric analysis (TGA) complemented ATR-FTIR and gravimetry in confirming the presence of immobilized BiBB. ANOVA analysis (95% confidence level) of the relative BiBB quantities determined from the ATR-FTIR peak area ratios and the absolute initiator quantities expressed as the degree of substitution (DS) determined by gravimetry confirmed the increased amount of immobilized BiBB when 0D and 0.5D treatments on the RC membranes were used over 0nD. Moreover, increasing the BiBB quantity used per membrane disc gave an increased amount of immobilized BiBB. The BiBB-modified 0D membrane using 2.67 mmol BiBB per membrane disc (0D 2.67) was then used for subsequent ARGET ATRP due to the high DS values without the need for the extra NaOH treatment.

The final part of the work investigated the characteristics of the grafted poly(acrylic acid) (i.e. conversion, grafting ratio, and theoretical number-average molecular weight) via gravimetry and ATR-FTIR. Low monomer conversions of 1.8-3.4 % were achieved, resulting in oligomeric theoretical number-average molecular weights (682-1052 g mol^{-1}). However, grafting ratios of 109-202 % were obtained and the PAA-*g*-RC membrane swelled from a 47 mm diameter circle into an ellipse with a 60 mm long major axis and a 50 mm long minor axis. The PAA-*g*-RC membrane swelled 8 times its own weight in pH 5 acetate buffer. Finally, the dynamic protein binding capacity for human immunoglobinG (IgG) at 10% breakthrough ($DBC_{10\%}$) for the 0D,

0D 2.67, and PAA-*g*-RC membranes were measured. 0D and 0D 2.67 were statistically similar while PAA-*g*-RC membranes (47 mm diameter discs) achieved the highest $DBC_{10\%}$ (4.4, 5.7, and 30 mg mL^{-1}, respectively, t-test with 95% confidence level). Successful protein capture was therefore achieved with the weak cation exchange membrane adsorbers developed in this work based on RC membrane supports.

Acknowledgements

I would like to thank my supervisors Dr. Christine Moresoli and Dr. Mario Gauthier for their guidance, support, and time. I am grateful for the opportunities they have provided to me that allowed for personal and professional growth. Their advice has been invaluable towards the completion of my thesis.

Financial support from the Natural Sciences and Engineering Research Council of Canada (NSERC), Monoclonal Antibody Network (MabNet), and the University of Waterloo are acknowledged.

My sincere thanks also goes to the following Moresoli and Gauthier lab members for their guidance, training, support, and for providing a welcoming and friendly work environment: Dr. Katharina Hassel, Huayu Niu for her advice and for the swelling experiments, Rasool Nasseri Pourtakalo, Nagma Zerin, Joseph Khouri, Jason Tran for the DBC experiments, Jan Weggen for the modified ÄKTA MATLAB code, Aklilu Worku, Ala Alturk, Dr. Deepak Vishnu, Mosa Alsehli, Ryan Amos, Joanne Fernandez, Dr. Hemali Lad, and An Nguyen.

I am thankful to the reader of my thesis Dr. Neil McManus for his time and feedback.

Lastly, special thanks to Nina Heinig for her assistance with the ESEM, Ralph Dickhout for his assistance with XRD and TGA, Dr. Jean Duhamel for access to the UV-vis spectrophotometer, Dr. Marc Aucoin for access to the ÄKTA prime system, Bert Habicher for his patience in repairing the lab shaker, and Dr. Howard Siu and Dr. Jake Fisher for their assistance with the ATR-FTIR equipment.

Table of Contents

List of Figures

List of Tables

List of Abbreviations and Symbols

$[Cu^{I}]$	Concentration of copper(I) [mol L^{-1}]
$[Cu^{II}\text{-}X]$	Concentration of copper(II) [mol L^{-1}]
[M]	Concentration of monomer [mol L^{-1}]
$[P^{\bullet}]$	Concentration of active radicals [mol L^{-1}]
[R-X]	Concentration of dormant chain ends [mol L^{-1}]
0.5D 0.74	BiBB-modified (0.74 mmol BiBB used per membrane disc) regenerated cellulose membrane methanol-washed, treated with 0.5 M NaOH, and stored in dry DMF prior to immobilization
0.5D 2.67	BiBB-modified (2.67 mmol BiBB used per membrane disc) regenerated cellulose membrane methanol-washed, treated with 0.5 M NaOH, and stored in dry DMF prior to immobilization
0.5D	Regenerated cellulose membrane methanol-washed, treated with 0.5 M NaOH and stored in dry DMF prior to immobilization
0D 0.74	BiBB-modified (0.74 mmol BiBB used per membrane disc) regenerated cellulose membrane methanol-washed, untreated with NaOH, and stored in dry DMF for at least two weeks prior to immobilization
0D 2.67	BiBB-modified (2.67 mmol BiBB used per membrane disc) regenerated cellulose membrane methanol-washed, untreated with NaOH, and stored in dry DMF for at least two weeks prior to immobilization
0D	Regenerated cellulose membrane methanol-washed, untreated with NaOH, and stored in dry DMF for at least two weeks prior to immobilization
0nD 0.74	BiBB-modified (0.74 mmol BiBB used per membrane disc) regenerated cellulose membrane methanol-washed, untreated with NaOH, and not stored in dry DMF prior to immobilization
0nD 2.67	BiBB-modified (2.67 mmol BiBB used per membrane disc) regenerated cellulose membrane methanol-washed, untreated with NaOH, and not stored in dry DMF prior to immobilization
0nD	Regenerated cellulose membrane methanol-washed, untreated with NaOH and not stored in dry DMF prior to immobilization
AA	Acrylic acid
Am + Ars	Acrylamide and artemisinin monomers for imprinting
ANOVA	Analysis of variance

ARGET ATRP	Activator regenerated by electron transfer atom transfer radical polymerization
ATR-FTIR	Attenuated total reflectance Fourier transform infrared spectroscopy
ATRP	Atom transfer radical polymerization
BA	Butyl acrylate
BiBB	2-Bromoisobutyryl bromide
bpy	2,2′-Bipyridine
c_0	Feed protein concentration in ÄKTA Prime system [mg mL^{-1}]
c	Protein concentration measured at outlet [mg mL^{-1}]
C_{bf}	Final protein concentration in buffer solution [mg mL^{-1}]
C_{bi}	Initial protein concentration in buffer solution [mg mL^{-1}]
CO_2	Carbon dioxide
CPPUA	11-(4′-Cyanophenyl-4″-phenoxy) undecyl acrylate
CTMP	Chemi-thermomechanical pulp
Cu	Copper
$CuBr_2$	Copper(II) bromide
DBC	Dynamic protein binding capacity
$DBC_{10\%}$	Dynamic protein binding capacity at 10% breakthrough
DEAEMA	2-(Diethylamino)ethyl methacrylate
deriv	Derivative
DF	Degree of freedom
DMAEMA + EB	2-(Dimethylamino)ethyl methacrylate and ethyl bromide for quaternization
DMF	*N*,*N*-Dimethylformamide
DNA	Deoxyribonucleic acid
DS	Degree of substitution
DTRP	Degenerative transfer radical polymerization
DVBSPA	*N*,*N*-Dimethyl-*N*-(p-vinylbenzyl)-*N*-(3-sulfopropyl) ammonium
EA + Sty	Ethyl acrylate and styrene (monomers to make copolymer)

eATRP	Electrochemical atom transfer radical polymerization
EDX	Energy dispersive x-ray spectroscopy
EGMA + DEGMA	(Ethylene glycol) methyl ether methacrylate and di(ethylene glycol) methyl ether methacrylate (DEGMA) (monomers to make block copolymer)
ESEM	Environmental scanning electron microscope
F	F-value
F_{crit}	Critical f-value
FRP	Free radical polymerization
FTIR	Fourier transform infrared spectroscopy
GMA	Glycidyl methacrylate
HHal	Acid product from immobilization, where Hal is a halogen
HMTETA	*N*,*N*,*N′*,*N″*,*N‴*,*N‴*-Hexamethyltriethylenetetramine
HPLC	High-performance liquid chromatography
ICAR ATRP	Initiator for continuous activator regeneration atom transfer radical polymerization
IgG	Immunoglobin G
k_a	ATRP activation rate constant
k_d	ATRP deactivation rate constant
K_{eq}	Equilibrium rate constant or ATRP rate constant [-]; also k_a/k_d
k_p	Polymerization rate constant [L mol^{-1} s^{-1}]
k_t	Rate constant of termination
MA + HEMA	Methyl acrylate and 2-hydroxyethyl methacrylate (monomers to make block copolymer)
MA	Methyl acrylate
mAbs	Monoclonal antibodies
Max.	Maximum
MBA	4-Mercaptobenzoic acid
MCC	Microcrystalline cellulose

Me_6TREN	Tris[2-(dimethylamino)ethyl]amine
MeOH	Methanol
MMA	Methyl methacrylate
$M_{n,theo}$	Theoretical number-average molecular weight of polymer determined by gravimetry
MS	Mean sum of squares
MS_E	Mean square of error
$MW_{monomer}$	Molecular weight of monomer [g mol^{-1}]
n_1	Refractive index of the ATR crystal
n_2	Refractive index of the sample
N_A	Avogadro's number
NaBr	Sodium bromide
NaOH	Sodium hydroxide
n_{BiBB}	Quantity of BiBB immobilized [mol]
NIPAAm	*N*-Isopropylacrylamide
n_{m0}	Quantity of monomer initially added [mol]
NMP	Nitroxide mediated radical polymerization
NMR	Nuclear magnetic resonance
PA	Polyamide
PAA	Poly(acrylic acid)
PAA-*g*-RC	Poly(acrylic acid) grafted regenerated cellulose membrane
PAR	ATR-FTIR peak area ratio
PE	Polyethylene
PEGMA	Poly(ethylene glycol) methacrylate
pI	Isoelectric point
pKa	Acid dissociation constant
PMDETA	*N,N,N′,N′,N″*-Pentamethyldiethylenetriamine
PP	Polypropylene

PS	Polysulfone
PVDF	Poly(vinylidene fluoride)
RAFT	Reversible addition fragmentation chain transfer polymerization
RC	Regenerated cellulose
RDRP	Reversible deactivated radical polymerization
rep	Replicate
RH	Relative humidity
R_p	Rate of polymerization [mol L^{-1} s^{-1}]
S4SS	Sodium 4-styrenesulfonate
SARA ATRP	Supplemental activator and reducing agent atom transfer radical polymerization
SBC	Static protein binding capacity
SEC	Size exclusion chromatography
SPMAK	3-Sulfopropyl methacrylate
SRMP	Stable radical mediated polymerization
SS	Sum of squares
tBA	*tert*-Butyl acrylate
TEA	Triethylamine
temp.	Temperature [°C]
TGA	Thermal gravimetric analysis
THF	Tetrahydrofuran
TPMA	Tris(2-pyridylmethyl)amine
UF	Ultrafiltration
UV	Ultraviolet
UV-vis	Ultraviolet-visible spectroscopy
V	Volume [mL]
V_0	Dead volume of set-up in breakthrough mode [mL]
V_b	Volume of buffer solution [mL]

V_m	Membrane volume [mL]
VP	4-Vinylpyridine
V_p	Loading volume of protein solution at 10% breakthrough [mL]
W_i	Mass of BiBB immobilized membrane [mg]
W_p	Mass of PAA-*g*-RC [mg]
x	Unit length
x_1	BiBB quantity used per membrane disc [mmol]
x_2	TEA quantity used per membrane disc [mmol]
XPS	X-ray photoelectron spectroscopy
y	Unit length or ATR-FTIR peak area ratio
z	Normalized peak area ratios at one point of the membrane surface
z_0	Maximum normalized peak area ratio of one
ZnSe	Zinc selenide
θ	Angle of incident light [°]
λ	Wavelength of incident light [cm]

1. Introduction

1.1 Research motivation

It is no surprise that treatments for cancer or other serious diseases like autoimmune diseases are expensive [1]. A price reduction for therapeutic proteins such as monoclonal antibodies (mAbs) would be the most direct conduit to improve access to these essential treatments, by improving production economy. Currently, therapeutic proteins are commercially produced by mammalian protein expression systems in batch or fed batch reactors [1]. More cost effective protein expression systems such as *E.coli*, yeast cells, or plants are also being developed [1]. Due to the improved yields in the upstream protein expression process, the downstream purification of the proteins has become the bottleneck [1–3]. Higher throughputs in downstream bioprocesses are needed. Chromatographic membrane adsorbers that are inexpensive, robust, and disposable represent a viable solution, in contrast to resins used in traditional packed bed chromatography [1,4].

1.2 Objectives

The development of weak cation exchange membrane adsorbers from a regenerated cellulose (RC) support layer was realized by a surface-initiated aqueous activator regenerated by electron transfer atom transfer radical polymerization (ARGET ATRP). The two-step process consisted of the initiator immobilization, 2-bromoisobutyryl bromide (BiBB), onto RC membrane discs (47 mm diameter), and subsequent aqueous ARGET ATRP directly from the surface.

The first objective was to identify factors that would provide control over the BiBB immobilization. This included observing the effects of BiBB to triethylamine (TEA) ratios, 2 M NaOH treatment of the methanol-washed RC membrane, the BiBB quantity used per membrane disc (i.e. 0.41, 0.74 or 2.67 mmol), and the solvent type (i.e. tetrahydrofuran (THF), or *N*,*N*-dimethylformamide (DMF) on the amount of immobilized BiBB. Moreover, suitable immobilized BiBB/amine ligand/ascorbic acid/$CuBr_2$ molar ratios with varying NaBr concentrations were investigated for successful grafting of poly(acrylic acid) from RC membrane

(PAA-*g*-RC). The PAA-*g*-RC membranes were then characterized for their static protein binding capacity of lysozyme.

The second objective was to determine whether methanol-washed RC membranes (0nD), methanol-washed RC membranes stored in DMF for at least two weeks prior to BiBB immobilization (0D), methanol-washed RC membrane treated with 0.5 M NaOH and subsequent DMF storage prior to immobilization (0.5D), and the BiBB quantity used per membrane disc (0, 0.74, or 2.67 mmol) would have a significant effect on the amount of BiBB immobilized. PAA-*g*-RC membranes were then tested for their dynamic protein binding capacity (DBC) of IgG. Basic polymerization properties such as the grafting ratio, estimated molecular weight by gravimetry and PAA-*g*-RC swelling factor were estimated to correlate to the breakthrough curves from DBC.

2. Literature review

2.1 Downstream bioprocessing

Downstream bioprocessing can be described as a series of purification steps to isolate a protein of interest [5]. Figure 2.1 illustrates a traditional process for monoclonal antibodies (mAbs, a type of therapeutic protein) production from mammalian cell culture. The purification starts with centrifugation and depth filtration to remove the cells and cell media [6,7]. Subsequently, protein A (originating from the cell wall of *Staphylococcus aureus* [8]) chromatography is employed for capture. Its excellent binding affinity with mAbs has made it the ligand of choice in most downstream mAbs processes [6]. Next, mAbs are eluted and undergo polishing steps to remove any DNA, viruses, host cell particles, or other impurities [6,7]. The polishing steps include cation exchange chromatography, which is run in bind and elute mode, and anion exchange chromatography, which is run in a flow through mode [6].

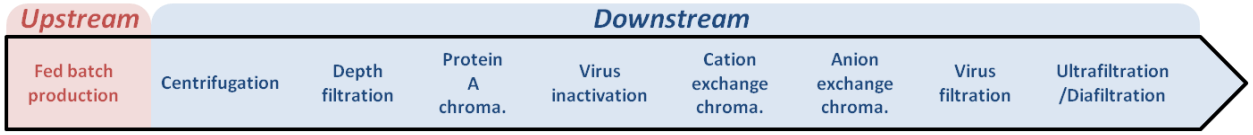

Figure 2.1: Generic mAbs production process as described in [5]

Improvement to the downstream process can come from optimizing the protein capture step, which uses protein A chromatography. This would serve to reduce costs (as the protein A resins are expensive), to increase production throughput over time by replacing it with materials with higher protein binding capacity, and lastly to eliminate the leaching of protein A into the stream by proteolysis [4,7–9]. Thus, alternatives to protein A chromatography are needed.

2.2 Membrane adsorber

Protein A chromatography resins can be replaced by ion exchange membrane adsorbers. Ion exchange membrane adsorbers are more cost effective due to lower materials costs and the ability to tailor them to higher protein binding capacities. Furthermore, mass transfer is limited by convection rather than intraparticle diffusion as in resins, enabling for faster mass transfer in its larger pore sizes (Figure 2.2) [10]. Resins, in comparison, have smaller pore sizes but are

highly porous, which allows for a larger surface area of binding sites, but the small diameter of the resin beads may lead to a higher pressure drop along the chromatography column [10]. For example, pores in regenerated cellulose-based membrane adsorbers are up to one or two micron large, which leads to a lower pressure drop even when these membranes are stacked on top of each other [8,11]. Protein binding takes place on the membrane surfaces and within its pores [12].

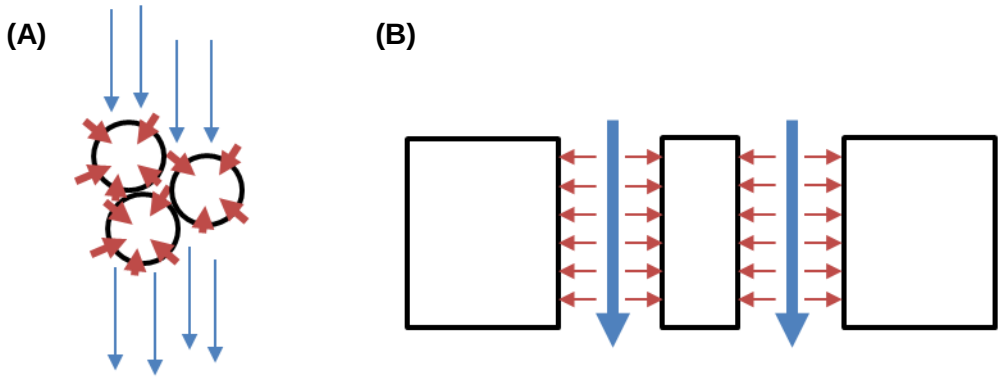

Figure 2.2: Mass transfer in (A) chromatographic resins and (B) membrane adsorbers; Blue arrows = convection, Red arrows = diffusion, Black circles = resin beads, Black rectangles = membrane.

To develop membrane adsorbers, a support layer must first be selected. This serves as the structural basis for the membrane. Typical support layers include cellulose, polysulfone (PS), polyamide (PA), polypropylene (PP), or poly(vinylidene fluoride) (PVDF) [8,13–24]. Cellulose, PS and PA have functional groups on their backbones available for substitution [16]. However, PP or PVDF support materials lack these sites and require plasma treatment to activate their surface for further modification [16], or the adsorption or physical entrapment of photoinitiator on their surface for subsequent UV-polymerization to impart functionality [23,24]. Activated support layers can thus be modified via conventional synthetic chemistry routes as described in [25] to create functional binding sites called ligands [2].

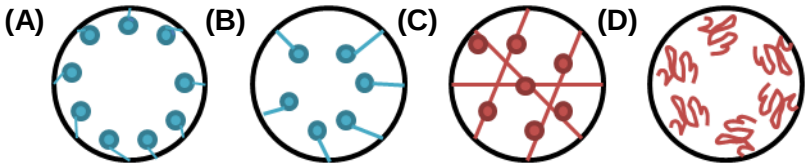

Figure 2.3: Cross-sectional view of functional binding sites in pores (A) ligand, (B) ligand with spacer arm, (C) gel-in-a-shell hydrogel, and (D) grafted polymer ligands; Circles represent binding sites except for (D), where the binding sites are contained within the polymer.

Traditional ligands and ligands with spacer arms have one functional site each, which allows for 2D protein binding (Figure 2.3A and B) [2]. Alternatively, polymer ligands allow 3D binding by creating a volume of binding sites enabling multi-layer protein binding (Figure 2.3C and D) [2,23]. The multi-layer protein binding would equate to higher protein binding capacities. However, a gel-in-a-shell hydrogel structure may affect mass transfer due to blocking of the pores by the hydrogel, making polymer grafting (Figure 2.3D) more advantageous for the process [10]. For ion exchange membrane adsorbers with polymer ligands, monomers with either cationic or anionic charges can be selected to capture positively or negatively charged proteins, respectively.

2.3 Surface initiated polymerization

In the previous section, various architectures of ligands were presented where polymer-based ligands can achieve higher protein binding due to multilayer binding versus single layer binding in conventional ligands. Gel-in-a-shell hydrogels have been mainly used with ceramic membranes and synthesized by immersing the support layer into a monomer solution with subsequent free radical polymerization, with or without cross-linker addition during the synthesis (Figure 2.3C) [10,26]. Alternatively, polymer ligands have been produced on the surface by ceric ion free radical polymerization [2], immersion of the support layer in a polymer solution with a photoinitiator to create UV-initiated polymer brushes with subsequent crosslinking between the brushes [2,23,24], or polymer grafting-from or grafting-to the surface using reversible deactivation radical polymerization (RDRP) techniques [2,13–20,27]. The first two techniques give limited control over the polymerization and consequently a higher polydispersity as compared to RDRP, which directly affects protein binding capabilities as well as the mass

transfer properties [10]. Moreover, the second option is not a permanent modification of the support layer due to the noncovalent bonding of the photoinitiator to the support layer, and may degrade over time as compared to covalent grafting techniques such as ceric ion polymerization and RDRP [19]. Hence, grafting-from or grafting-to RDRP techniques offer some advantages over other polymerization methods.

Grafting-from and grafting-to are two common methods to covalently attach polymers on surfaces. The grafting-from method enables polymerization to occur directly from the surface, as opposed to the grafting-to method which grafts prefabricated polymers onto the surface [28]. The former method enables higher grafting densities, whereas the latter is favoured in industrial applications since prefabricated polymers have known characteristics [28]. However in terms of higher grafting densities, the grafting-to method is less efficient due to the increasing steric hindrance from the prefabricated polymers during grafting [28]. Thus, grafting-from RDRP would offer significant advantages in terms of grafting density control.

2.3.1 Reversible deactivated radical polymerization (RDRP) for the functional layer

Many studies have used RDRP for surface initiated polymerizations [13–20,22,28–50]. It has become widely used due to its ability to produce controlled molecular weights, polymerize a range of monomers and create different topologies, in contrast to free radical polymerization (FRP) [51]. Similarly to FRP, RDRP consists of monomer addition to an active radical center for polymer propagation. In FRP however, dead end termination of propagating chains can occur, resulting in a broad molecular weight distribution, while RDRP polymerization is based on a dynamic equilibrium between the active and dormant polymer chain ends, enabling “reversible termination” and thereby narrower molecular weight distributions [51]. The classification of RDRP techniques is based on the reactivation mechanism of the dormant species into active species [51]. The three classifications are atom transfer radical polymerization (ATRP), stable radical mediated polymerization (SRMP, e.g. nitroxide mediated polymerization), and degenerative transfer radical polymerization (DTRP, e.g. reversible addition fragmentation chain transfer polymerization or RAFT) [51]. As the name infers, the chain ends in ATRP are reversibly terminated by atom transfer via a catalyst. For SRMP, alkoxyamines may be used to reversibly terminate the chain ends, and DTRP makes use of a chain transfer agent to reversibly terminate the propagating chain ends but requires a radical to activate it again [51]. The

advantage of ATRP over other methods is the ability to perform polymerizations under ambient, mild conditions with control using readily available reagents [51].

In ATRP, the dormant species are reactivated via an atom transfer, generally a halogen atom, mediated by a transition metal. Common transition metals for ATRP applications are copper, iron, ruthenium, nickel, and rhodium [51–54]. Since these transition metals are toxic, a variety of ATRP methods have been developed in order to minimize the catalyst quantity and to easily handle catalyst deactivated by exposure to oxygen during large scale production. In order to minimize the catalyst quantity, researchers have looked into reactivating it within the reaction (Table 2.1).

Table 2.1: Types of ATRP and method of catalyst reactivation

Type of ATRP	Method of catalyst reactivation	Ref.
Initiator for continuous activator regeneration (ICAR ATRP)	FRP initiators reactivate catalyst	[51]
Supplemental activator and reducing agent (SARA ATRP)	Zero valent metals act as an activator for propagation and reducing agent to reactivate the catalyst	[51]
Electrochemical ATRP (eATRP)	Electrodes reactivate the catalyst via a REDOX reaction	[51]
Activators regenerated by electron transfer (ARGET ATRP)	Reducing agent added to reactivate the catalyst (e.g. ascorbic acid)	[51]
Photoinduced ATRP	UV or visible light reactivates the catalyst	[55]

As observed in Table 2.1, the ability to regenerate the catalyst in eATRP, ARGET ATRP, and photoinduced ATRP allows the use of deactivated catalyst at the start of the polymerization, which is favourable for large scale production. Among these ARGET ATRP is of particular interest, as it does not require auxiliary equipment such as electrodes or UV light sources.

ARGET ATRP has the same mechanism as ATRP. The exception is the reducing agent, which reduces the $Metal^{n+1}$/Ligand to regenerate the catalyst for polymerization. The mechanism is shown in Figure 2.4.

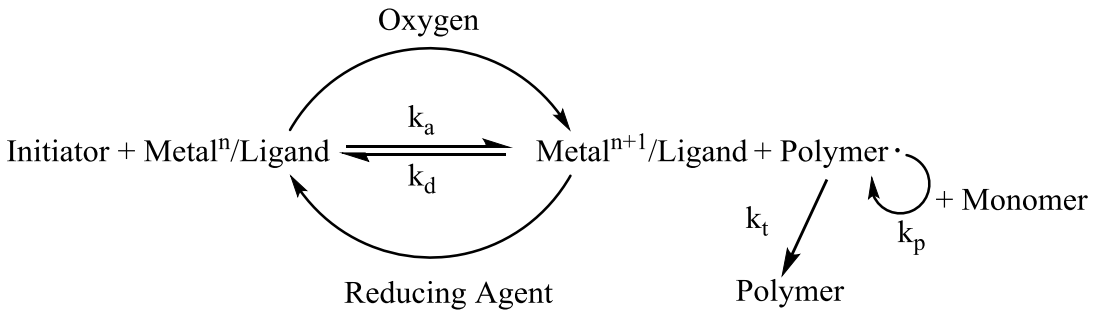

Figure 2.4: ARGET ATRP Mechanism.

A common initiator employed for surface initiated polymerizations (i.e. heterogeneous reactions) is 2-bromoisobutyryl bromide (BiBB). For homogeneous reactions, initiator such as ethyl 2-bromoisobutyrate have been used. Common amine ligands are *N,N,N′,N″,N‴,N‴*-hexamethyltriethylenetetramine (HMTETA), *N,N,N′,N′,N″*-pentamethyldiethylenetriamine (PMDETA), 2,2′-bipyridyine (bpy), tris[2-(dimethylamino)ethyl]amine (Me_6TREN), and tris(2-pyridylmethyl)amine (TPMA) [51,56,57].

In practice, strictly deoxygenated environments are not required as the reducing agent can both reduce O_2 in the solvent and regenerate the copper catalyst [51,58,59]. Moreover, due to the regeneration of the copper catalyst, lower amounts of catalysts are used, making it a greener polymerization method [51,58]. Additionally, hydrophilic polymers can be created using ARGET ATRP in aqueous media [51,59]. In summary, the use of water, ppm levels of catalysts, ascorbic acid as reducing agent, and ambient operating conditions in the presence of limited oxygen is applicable for scale-up to industrial scale as compared to conventional ATRP and other RDRP methods. More recently, biocatalysts have been used for ATRP such as horseradish peroxidase [53] and hemoglobin [52], eliminating the disadvantages of metal catalysts altogether. The potential to use biocatalysts would definitely make ATRP a more attractive technique for the synthesis of materials for biomedical applications.

2.3.2 Difficulties with aqueous ARGET ATRP

Unfortunately, there are competing interactions among reagents that can affect the control of the polymerization, especially with the widely used CuX_2 catalysts in water (X is usually bromine or chlorine). For example, water can dissociate CuX_2 and disproportionate CuX, leading

to lower catalyst efficiency. Moreover, the copper catalyst may complex with acidic monomers and ascorbic acid [51,54,59–62]. Other reagents in the medium may also interact with each other. Ascorbic acid can protonate the amine ligand, limiting its ability to complex with CuX_2 [60]. The copper catalyst can also reduce or oxidize radicals to form ions and coordinate with the free radicals, rendering the polymerization less efficient [54,60]. Some of these issues can be mitigated as described in the next section.

2.3.3 Mitigation strategies for ARGET ATRP

Excess amine ligand can be used to ensure that ligands are still available for the stabilization of the catalyst, even in the presence of ascorbic acid protonation [60,63]. However this is not the only role of the ligand that should be taken into account to control the polymerization [56,57]. Some groups have claimed that amine ligands such as Me_6TREN can function as a reducing agent, effectively reducing CuX_2. However the reduction of CuX_2 by Me_6TREN was not observed by [55] when the polymerization was conducted away from visible light sources. In effect, [55] argued that it was photoinitiated ATRP which reduced CuX_2 rather than the excess reducing agent. For all purposes, surface initiated ARGET ATRP may need to be performed away from light sources depending on the ligand, to eliminate potential photoinitiation effects.

The amine ligand should also be stable at the pH of the reaction, which may fluctuate over the course of the reaction [57]. For example, in [57], a less basic ligand like TPMA was more stable in acidic aqueous media than PMDETA. Thus, changing the pH conditions to an alkaline pH also ensures that the amine ligand would be deprotonated, such that it can complex with the copper catalyst. This is especially true in the case of aqueous reaction media if the CuX_2-ligand complex is only soluble above the ligand's pKa (e.g. 2,2′-bipyridine) [64]. Various groups have adjusted the pH to around 8-9 when polymerizing sodium methacrylate [32,64,65]. The optimum pH involved a balance between deprotonation of the amine ligand and ensuring that the polymerization rate was not impeded due to the charge repulsion of the monomers [64].

Other strategies for the control of the polymerization included adding a salt to mitigate catalyst dissociation and complexation [59,61]. In Simakova *et al.* [59], different salts (sodium chloride, tetraethylammonium chloride, and tetraethylammonium bromide) and salt concentrations were considered. It was hypothesized that a salt may help to stabilize the

dissociation and complexation of the copper catalyst in water, and also avoid its complexation with charged anions [61]. As a result, an increased sodium chloride concentration also decreased the conversion/polymerization rate as observed in [59]. This may be due to an increase in concentration of deactivating species, CuX_2, with increased X ions in solution [59,66]. All these adjustments should ensure that the rate of deactivation is greater than the rate of activation for good control of the polymerization (Figure 2.4).

2.4 Surface initiated grafting-from cellulose

For polymerization to occur directly from a cellulose support layer surface (i.e. grafting-from method), the initiator needs to be immobilized on the surface prior to ARGET ATRP.

2.4.1 Immobilization of initiator

The immobilization of the initiator on the support material is critical, as the amount of initiator affects the grafting density during polymerization. Several techniques have been used to control the amount of initiator for surface initiated ATRP and/or its variants on any substrate applicable to immobilization on cellulose I or II polymorphs: i) controlling the concentration of initiator [14], ii) controlling the ratio of initiator and a blocking agent [67–69], and iii) immobilizing the initiator and degrading some of it via irradiation [70] (this method was not used with cellulose I or II as the support layers).

There are two interconnected limitations in the successful substitution of initiator on all cellulose polymorphs surfaces for heterogeneous reactions: i) physical limitations and ii) chemical limitations. Physical limitations relate to the complex structure of all the cellulose polymorphs that hinders the accessibility of reactive species from the initiator. Chemical limitations relate to the competitive side reactions and impurities that limit the yield of the initiator immobilization reaction. The following section will discuss the structure and reactivity of cellulose, and techniques applicable to improve the immobilization yield on the common cellulose polymorphs, cellulose I and II.

2.4.1.1 Cellulose structural characteristics

Cellulose used as a support layer is favourable as it does not require surface activation for functionalization. Moreover, it is an ideal chromatographic material because it is renewable, abundant, biodegradable, insoluble in most solvents, chemically and mechanically resilient,

possesses large pores, has “low nonspecific interactions”, and is hydrophilic [71–75]. To functionalize the cellulose surface, it is important to understand the structure and chemistry of cellulose.

A three-level structural hierarchy exists in cellulose: a molecular level, a supermolecular level, and an ultrastructural level [76,77]. At the molecular level, cellulose is a biopolymer comprising cyclic anhydroglucose repeating units joined by β 1→4 glycosidic linkages. Due to intermolecular and intramolecular hydrogen bonding, these cellulose chains can be organized into various crystal polymorphs forming the supermolecular structure [76,78]. Four types of polymorphs exist: cellulose I, II, III, and IV. Cellulose I polymorphs, cellulose Iα and Iβ, are naturally produced by bacteria and plants, production of the former being favoured by bacteria and production of the latter being favoured by plants [77]. The polymorph cellulose Iα has a triclinic crystalline structure, whereas Iβ has a monoclinic structure [77]. The cellulose chains are all running in the same direction, parallel to each other. However, in cellulose II, every second cellulose chain is inverted 180° (i.e. antiparallel orientation) [75–79]. It is the most thermodynamically stable of all the cellulose polymorphs [78,80]. Various processes are used to produce cellulose II, either by treating cellulose I with sodium hydroxide, a cuprammonium solution, or using the greener Lyocell process (where N-methylmorpholine N-oxide is used for cellulose dissolution) [75–77,80,81]. For cellulose III, there also exists cellulose IIIα and cellulose IIIβ polymorphs [77,81]. The former is derived from liquid ammonia treatment of cellulose I, and the latter from liquid ammonia treatment of cellulose II [77,81]. This treatment is reversible, whereas the transition from cellulose I to II is not. From the heat treatment of cellulose IIIα and IIIβ in glycerol, cellulose IVα and IVβ are formed, respectively [77,81]. However, this process is unreliable and full conversion to cellulose IV has not been achieved. Cellulose IV is therefore not well characterized [77,81]. Hence, most cellulose that is used for materials applications is either cellulose I or cellulose II. As a result, these two polymorphs will be discussed further in the ensuing sections.

When comparing the supermolecular structure of cellulose Iβ (derived from plant sources) and cellulose II, the differences lie in the intermolecular bonding in the crystalline regions and the void space in the amorphous regions [76,80,81]. In the crystalline regions of cellulose II, the chains arrange in a monoclinic structure as in cellulose Iβ, however with

dissimilar dimensions due to the antiparallel orientation of the chains [76,78]. The antiparallel chain orientation also leads to more complex hydrogen bonding in cellulose II, where the hydrogen atom from O2 of the cellulose II chains can hydrogen bond with O2 in the antiparallel chains, which is not seen for cellulose I [76,78,81]. Consequently, the average hydrogen bonding length of cellulose II and cellulose I from plant sources are 0.272 nm and 0.280 nm, respectively, and much tighter hydrogen bonding is found within dry cellulose II [76,78]. In the amorphous region of cellulose II, void spaces are also smaller than in cellulose I from plant sources according to x-ray diffraction measurements [76]. However, cellulose II has larger amounts of amorphous regions than cellulose I, where hydroxyl groups are more accessible to reagents for functionalization in comparison to the hydroxyl groups in the crystalline structure due to hydrogen bonding [71,82].

A generalized model for cellulose supermolecular structure describes the amorphous regions connecting crystalline regions (10-20 nm long) together to form elementary fibrils 2-4 nm wide and ~100 nm in length, where the structure can be described as a fringe fibrillar model [76]. By the aggregation of elementary fibrils, longer fibrils called microfibrils are formed through hydrogen bonding interactions, with a less ordered structure than those within the elementary fibrils [76]. Other proposed models for cellulose supermolecular structure categorize the microfibril (10-20 nm wide, made of 24-36 cellulose chains) as the smallest fibril possible [77,81]. A fringe micellar model can be used to describe the micelles of crystalline regions connected together by long cellulose chains, which form amorphous regions making the microfibrils [76,77,81]. Depending on the processing conditions and the cellulose source, both models can be valid [76]. Further agglomeration of these microfibrils through secondary hydrogen bonding interactions forms macrofibrils [75,76,81].

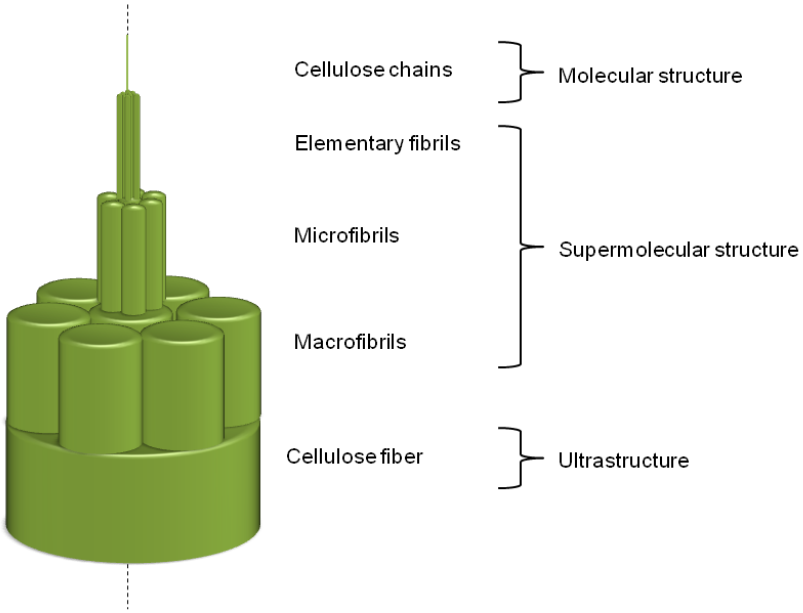

Figure 2.5: Simplified schematic of cellulose structural hierarchy (--- fibre axis).

The macrofibrils in turn make up the cellulose fibres. In plant-based cellulose I there are primary, secondary, and/or tertiary walls depending on the plant source, where the primary wall can be stripped during the bleaching process [76]. The orientation of the microfibrils and macrofibrils into the wall structure along the fibre axis defines the ultrastructure of the plant-based cellulose I fibre [76]. The wall includes a series of channels, voids, and pores [76]. However, cellulose II fibres do not have a wall structure due the effects of processing, where the ultrastructure or orientation of fibre aggregates will be dictated by the processing method [76]. In this respect the channels, voids, and pores in the ultrastructure of cellulose II fibres were observed to be smaller than in plant-based cellulose I [76]. By understanding the structure of cellulose, it is observed that the structural hierarchy would contribute to the challenge of its functionalization, since reactive compounds need to diffuse into the fibres for functionalization.

2.4.1.2 Structure and reactivity of cellulose

Especially for cellulose II (also called regenerated cellulose or mercerized cellulose), a lower void space and more complex hydrogen bonding in the supermolecular structure is observed [76]. Furthermore, the morphology of these fibrils is a complex structure of pores, channels, and voids where each layer of the structural hierarchy adds to the diffusive challenge in

accessing the hydroxyl groups on dry regenerated cellulose [80]. However, due to greater amounts of amorphous region in cellulose II (theoretically leading to better accessibility of the initiator to the reactive sites, and also being an ideal material for chromatography [71,82]), it has been predominately used in the development of membrane adsorbers [13–15,17,18,20].

In the literature, the crystalline structure and the fibre morphology of cellulose I and II affects the accessibility of hydroxyl groups for chemical modification or derivatization [75,76,79,80,83–85]. Bhattacharyya and Maldas [84] also reported in 1984 that when acetylating a thicker cellulose I film, a lower degree of substitution occurred due to diffusion limitations in thicker films (~300 μm), which could similarly occur in cellulose II. A mitigation strategy was to perform a chemical treatment on cellulose I to disturb the hydrogen bonding among the hydroxyl groups, in order to activate them/increase their reactivity [34,75,79,80,86]. These treatments include immersion in acid, base, solvent and salt etc. [34,75,79,80]. Ruckenstein and Guo [71] proposed in 2001 to mercerize native cellulose or cellulose I to convert it to cellulose II to increase its amorphous content and improve accessibility. The treatment improved the immobilization of epoxy groups on Whatman filter paper [71]. In work by Roy *et al.* in 2005 [79], the treatment of cellulose I with 2 M sodium hydroxide for 16 hours followed by ethanol washing and solvent exchange with THF resulted in detectable amounts of initiator by ATR-FTIR analysis, for subsequent RAFT polymerization, although the filter paper swelled after treatment. The treatment of cellulose (either I or II) in NaOH turns the second and third hydroxyl groups into salts, thus effectively breaking down intermolecular hydrogen bonding and increasing the reactivity of the groups (the pKa of the hydroxyl groups on the 2^{nd} and 3^{rd} carbons is 10-12) [11,80,87]. Furthermore, the cellulose I was never dried prior to the reaction to minimize the reformation of hydrogen bonds [79], a phenomenon called hornification [76,88]. Thus swelling and keeping the regenerated cellulose fibres in a wet state prior to functionalization could alleviate the effects of hydrogen bonding and lower void space in the supermolecular structure of regenerated cellulose as compared to cellulose I for improved chemical modification [86].

2.4.1.3 Chemistry and reactivity of cellulose

The chemistry of the reaction between cellulose (applicable to all polymorphs, since all have the same chemical composition) and the ATRP initiator for subsequent ATRP is generally

not elaborated in the literature, due to greater interest in the optimization of the polymerization step. The esterification of cellulose with acyl components has been described as a nucleophilic acyl substitution reaction [89,90], where the hydroxyl groups of cellulose acts as a nucleophile towards the acyl halide (i.e. the ATRP initiator). The primary hydroxyl group on the anhydrous glucose unit should be more readily substituted under these conditions due to decreased steric effects [75,76,89,91].

To obtain high levels of substitution on cellulose, competing reactions need to be suppressed. Strazzonlini *et al.* 1994 [92] looked into the analogous reaction between acyl halides and alcohols and the possible reaction pathways. Accordingly, various substitution reactions yielded a combination of products: esters, acids, carboxylic acid products, and/or alkyl halides [92]. Esterification was found to act as an intermediate step where the acid product (HHal) could react with any remaining alcohol, yielding water and an alkyl halide product (Figure 2.6: General reaction mechanism of alcohol and acyl halide system as in [92]Figure 2.6) [92]. Furthermore, the presence of water or hydroxyl group-containing impurities in the system would result in carboxylic products and more acid (HHal), since smaller molecules like water are "more effective nucleophiles than hydroxyl groups on cellulose" [92,93]. In addition, the resulting acid (HHal) product can contribute to the degradation of the cellulose substrate by breaking down the glycosidic ester bonds into alkyl halides, which is unfavourable if the substrate structure needs to be preserved [89,92]. Thus, dry reagents are used for the substitution reaction and the free acid (HHal) should be eliminated. Amine bases are thus added to the substitution reaction. Their role is to neutralize the acid (HHal) not only to prevent cellulose degradation, but also to push the equilibrium towards the ester product formation and to prevent the formation of water and carboxylic acid that compete for the acyl halide [92,94].

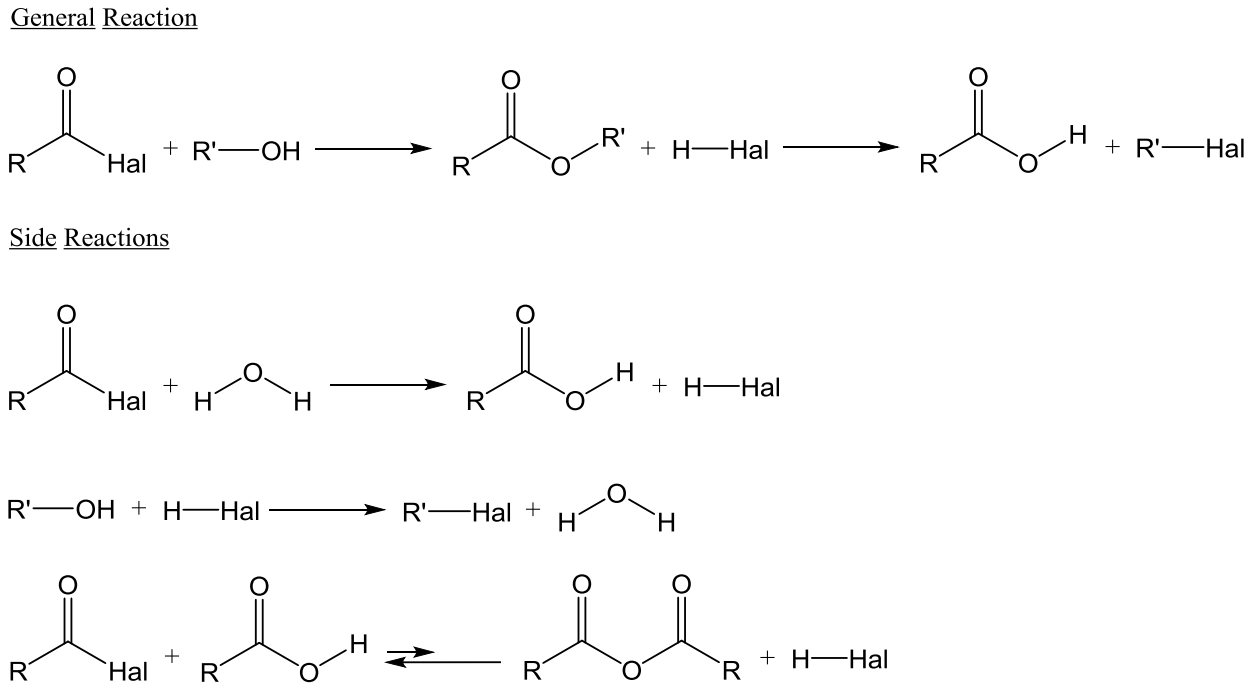

Figure 2.6: General reaction mechanism of alcohol and acyl halide system as in [92] where Hal = halogen.

The choice of the amine base is important. Various investigations have used triethylamine as the base due to its availability and affordability [13–15,19,22,27,28,33,35,37,39,42,44,46,48,50,62,67,95,96]. However triethylamine can react with the commonly used initiator 2-bromoisobutyryl bromide (BiBB) and result in a brown tar, as reported in [95]. Hence, it can also lower the yield of the desired product. Belegrinou *et al*. [95] reported that for nucleophilic acyl substitution between dimerized 11-mercapto-1-undecanol and BiBB, a lower yield of desired product was attained when triethylamine was used (64%) as compared to pyridine (92%) as the base in the reaction. Pyridine and *N*-ethyldiisopropylamine (Hünig's base) were thus suggested as alternative bases for the reaction [95]. Otherwise, others also allowed the esterification of cellulose with BiBB for 30 minutes before adding triethylamine dropwise, possibly to prevent the reaction of BiBB with triethylamine too early in the reaction [97]. Furthermore, multiple groups have used an excess of acyl halide to immobilize the initiator over the stoichiometric amount of available hydroxyl groups to offset the low yield issues [69,79,96,98]. The excess acyl halide can also serve to consume impurities, such that more of the hydroxyl groups from cellulose can be substituted [98].

2.4.1.4 Solvent choice

Another important aspect of cellulose reactivity and immobilization of the initiator is the solvent. Suitable solvent choice helps to disturb interfibrillar interactions (i.e. increases the distance among the chains) for swelling similarly to a sodium hydroxide treatment [76,91]. DMF is a polar, aprotic solvent which is of interest for the nucleophilic substitution reaction between the ATRP initiator and cellulose. Its polarity enables the cellulose (i.e. cellulose I or II) to swell and it disrupts noncovalent interactions within cellulose [91]. Secondly, the use of strong polar aprotic, basic solvents such as DMF is favourable for nucleophilic substitution reaction over other polar, aprotic solvents such as THF [89,92]. Previous work demonstrated that DMF swelled native cellulose (i.e. cellulose I) and mercerized cellulose (i.e. cellulose II) more as compared to other polar, aprotic solvents such as THF [83]. Moreover, Freire *et al.* in 2006 [99] achieved higher fatty acid substitution on pulp fibres when using DMF over toluene as solvent, which swells pulp fibres less than DMF. Thus better substitution arises when interfibrillar swelling occurs (i.e. the distance among cellulose chains increases) [76,84,100,101]. The hydroxyl groups are more accessible to react.

2.4.1.5 Characterization of initiator immobilization on cellulose surfaces

All acyl halide initiators like BiBB commonly used for ATRP contain a carbonyl bond and require an ester linkage to all cellulose polymorphs for covalent attachment to its surface. Moreover, an increase in bromine content on the cellulose surface would be observed due to initiator immobilization. Thus, many researchers characterized initiator immobilized on cellulose (either I or II) surfaces based on these properties. Characterization of the initiator immobilized on the cellulose surface (either I or II) is of importance, as the initiator quantity per unit surface area (i.e. density) is critical to the subsequent polymerization step. If there are relatively low initiator quantities on the surface (with no sacrificial initiator used), a low polymer density would result, and controlling the polymerization could become challenging due to the low amount of initiating species [40].

ATR-FTIR is a popular characterization method for initiator immobilization monitoring as it provides quick, qualitative measurements for the initiator on the surface, with no sample preparation required. Quantitative measurements can be difficult with this method: The absorbance is related to the sample concentration as well as to the contact surface area and

pressure exacted on the sample by the ATR crystal, contrary to spectra obtained by FTIR analysis in the transmission mode [102]. In single point reflection ATR-FTIR, the incident light is reflected off the crystal at a single point towards the detector and an evanescent wave penetrates perpendicularly to the surface of the sample. The depth of penetration is a function of the refractive index of the crystal and the refractive index of the sample material, where the pressure and contact surface area can affect the resulting absorbance intensities (2.1). Thus, a longer wavelength or lower wavenumber increase the depth of penetration (usually in the nanometre range, even though the wavelength is in micrometre range),

$$Depth = \frac{\lambda}{2\pi\sqrt{\sin^2\theta - (n_2 / n_1)^2}} \qquad (2.1)$$

where λ = wavelength of incident light [μm], θ = angle of incident light [°], n_1 = refractive index of the crystal, n_2 = refractive index of the sample.

Extended ATR correction algorithms may be used to correct the peak shift and intensity of ATR-FTIR spectra if a sample refractive index is known. Otherwise, ATR-FTIR spectra analysis can be achieved by taking the ratio of the area of the peak characteristic for the initiator and the area of a reference peak. The ratio accounts for changing contact areas among samples that would affect the individual absorbance intensity of the peaks of interest. In terms of calibration for solids, the preparation of standards or internal standards would present a challenge for grafted polymer membranes, which may vary in consistency in terms of polymer chain grafting density over the whole membrane. Hence, semi-quantitative analysis of the relative initiator quantities may be more feasible.

Alternatively, x-ray photoelectron spectroscopy (XPS) [27,35,47–50] or energy dispersive x-ray spectroscopy (EDX) [69] has been used to provide a quantitative measure of the initiator on the membrane surface when initiator levels were below the detection limit of ATR-FTIR. Reported relative contents of bromine element by XPS ranged from 0.48 atomic % - 2.06 atomic % on various cellulose paper surfaces [27,35,47–50].

Other approaches confirming the presence of BiBB or BiBB analogues were by measuring the water contact angle before and after the immobilization reaction [38,40,103], or

measuring the amount of polymer on the surface via the cleavage of BiBB analogue containing a disulfide bond [37]. Cleavage of the disulfide bond and subsequent testing gave a measure of the covalently bonded BiBB analogue on the surface [37]. Finally, other methods to confirm initiator immobilization on the surface included qualitative colour change when the substrate was coated with a dopamine initiator solution [104,105].

There have been a number of strategies proposed to circumvent low BiBB concentrations on the surface disabling ATR-FTIR detection. These strategies include: i) using excess amounts of BiBB as compared to the stoichiometric amount needed [69,96,98,106], ii) treating the cellulosic material in sodium hydroxide solution for swelling and activating the hydroxyl groups [79], and iii) substitution of triethylamine with pyridine during the immobilization reaction [69,95,107]. The work by Wang *et al.* [107] in particular combined the three conditions and confirmed the presence of the BiBB using ATR-FTIR for wheat, which in contrast to cellulose contains predominantly starch, but is similarly made of connecting glucose chains but with α 1→4 linkages. First the wheat was treated with ammonia and nitric acid to obtain higher hydroxyl group reactivities and to remove the undesired cell wall of the wheat [107]. Then during the immobilization step, excess BiBB and pyridine were used [107].

2.4.1.6 Loss of mechanical integrity of cellulose substrate

Solvents play a role in the loss of mechanical integrity of cellulose substrates. It is important to note that the group of Malmström favoured the use of THF over DMF for the purpose of limiting the swelling of the their cellulose I paper, to preserve its physical integrity [45]. They conceded, however, that this also limited the accessibility of hydroxyl groups to the initiator [45]. Another factor that can negatively affect mechanical strength may be the initiator substituted on the cellulose chains. Some groups indeed reported having problems with mechanical integrity after the immobilization of initiator on cellulosic substrates like filter paper and other paper products (e.g. Whatman filter paper [79], and dissolved pulp paper in [40]). The loss of crystallinity may be an explanation since in a similar case, the crystallinity of cellulose nanowhiskers (sulfuric acid-treated Avicel PH101) [108] and cellulose nanofibres (kenaf bast fibres, *Hibiscus cannabinus*) [109] decreased after substitution of their hydroxyl groups. The crystallinity may have decreased due to the introduction of the initiator breaking the "intermolecular and intramolecular hydrogen bonding among the cellulose chains" [75,78].

Hence, any cellulose polymorph may be partially degraded, as seen in [69] and [98], with excess initiator. Moreover, with increasing reaction time, lower crystallinity was found in microcrystalline cellulose and cellulose nanofibres from a plant source [108,109]. Alternate solutions to avoid any potential cellulose degradation or structural modification during initiator immobilization have been employed. The initiator was thus attached with xyloglucan using the enzyme xyloglucan endotransglycosylase and adsorbed to the cellulose filter paper surface before ATRP [110]. A dopamine compound with the acyl halide initiator was also synthesized, and the cellulose support layer was dip coated into the dopamine initiator solution prior to ATRP [104,105]. Integrity was preserved since the initiator was only coated onto the cellulose surface, which did not disrupt the hydrogen bonding between the cellulose chains or produced destructive side products that could degrade the cellulose.

2.4.2 Surface initiated ARGET ATRP from cellulose surfaces

After successful initiator immobilization, ARGET ATRP can proceed. ARGET ATRP can be conducted in a heterogeneous or homogeneous reaction setting. As cellulose is insoluble in many common organic solvents, the polymerization is mainly heterogeneous unless the cellulose is solubilized into for example, ionic liquids [89,93,111]. In the case of regenerated cellulose membrane support layers, ARGET ATRP is a heterogeneous reaction.

2.4.2.1 Monomer choice for cation exchange membrane chromatography

The monomer for cation exchange membrane adsorber development should exhibit a negative charge for therapeutic protein capture. Cation exchange is preferred over anion exchange as the pI of the mAbs protein is in the range of 6.5-9, so cation exchangers operating in the pH range of 5-6 are ideal for electrostatic protein binding [6]. Monomers acting as strong cation exchangers traditionally contain sulfonic groups, whereas monomers for weak cation exchangers contain carboxylic acid groups. As the charge of the polymer ligand would not be constant over a broad pH range for a weak cation exchanger [6], it would be easier to manipulate the operating conditions to separate various proteins in the stream during binding [9]. Thus, monomers polymerized to produce poly(acrylic acid) would be a suitable choice, since commercially available membrane adsorbers for weak cation exchange such as Natrix and Sartobind have also employed poly(acrylic acid), in addition to those reported in the literature [18].

To obtain poly(acrylic acid) three different monomers have been used, namely *tert*-butyl acrylate [112], acrylic acid [18], and sodium acrylate [62]. *tert*-Butyl acrylate has been used due to the inability to polymerize acrylic acid directly via ATRP initially [62,64]. The *tert*-butyl group protects the carboxylic acid during polymerization from reactions with the catalyst [62,64]. However, the *tert*-butyl groups can cause steric hindrance leading to a lower polymerization rate [64]. Furthermore, acid hydrolysis is needed to deprotect the acrylic acid units, which may also inconveniently cleave the grafted polymer from the cellulose surface [62]. Pyrolysis has also been used for deprotection, however the use of other monomer alternatives would not require this extra step [62]. Therefore it could be more efficient to directly polymerize acrylic acid or its salt form on the surface. Work by Ashford *et al.* in 1999 [64] successfully demonstrated the polymerization of sodium methacrylate under aqueous conditions via ATRP. Singh *et al.* in 2008 [18] has also successfully polymerized acrylic acid from regenerated cellulose membranes. However inhibitors needed to be removed from the acrylic acid monomer, followed by deprotonation by the addition of an excess of sodium chloride, effectively creating sodium acrylate [18]. To simplify the process, sodium acrylate can be purchased directly and used as in [62] for ATRP or ARGET ATRP. Furthermore, the sodium form of acrylic acid may help to mitigate metal carboxylate formation between the copper catalyst and the acid monomers [64].

2.4.2.2 Reagent ratios for surface initiated aqueous ARGET ATRP on cellulose

Earlier, the advantages of ARGET ATRP over traditional ATRP were stated, namely that less catalyst was needed, and the ability to perform the polymerization in the presence of a limited amount of O_2, as well as in aqueous media, providing a greener alternative. The main reagents for surface initiated aqueous ARGET ATRP on cellulose I or cellulose II support layers are the following:

i. CuX_2 catalyst, where X is a halogen
ii. Amine ligand (e.g. PMDETA, 2,2′-bipyridine)
iii. Monomer (sodium acrylate, as aforementioned)
iv. Reducing agent (e.g. ascorbic acid or tin(II) 2-ethylhexanoate [40,58])
v. Optional sacrificial initiator in solution for better control of the surface initiated polymerization (e.g. ethyl 2-bromoisobutyrate [40])
vi. Initiator-modified regenerated cellulose support layer
vii. Water

The ratios of these reagents are of importance to ensure molecular weight control for the grafted polymer. As aforementioned, the rate of deactivation (k_d) should be greater than the rate of activation (k_a) for improved control as it allows for activation of propagating sites for a short time before deactivation of the active chain ends, thus reducing the polydispersity of the polymer's molecular weight [59]. Thus, a lower amount of copper catalyst is used in comparison to the initiating sites. In [28,40], the quantity of copper catalyst was around three orders of magnitude lower than the amount of sacrificial initiator and initiator on the cellulose substrate. Moreover, the amine ligand was added in excess of the copper catalyst. Typical copper catalyst to amine ligand molar ratios for ARGET ATRP on cellulose based materials are 1/2 [15,47] and 1/10 [28,40,63]. The reducing agent can be either continuously fed into the reaction medium [59] or added batch-wise [15,28,40,47,58]. Various molar ratios of reducing agent to amine ligand for batch-wise addition have been reported: 1/1 [28], 1/2 [47], or ranges from 1/2 to 1/18 [15]. The reagent molar ratios directly affected the polymerization, which resulted in varying protein binding capacities as seen in [15].

To determine the best set of reagent ratios for polymerization, UV-vis spectroscopy can help to observe the consumption of the copper catalyst by the reducing agent (e.g. ascorbic acid) over time. The absorbance of the d-d orbital group of CuX_2 appears in the ~700 nm range, depending on the solvent. As it is consumed, the peak should decrease in intensity and give rise to a peak around 400-500 nm [57]. The new peak has been described to the absorbance of ascorbic acid and copper catalyst charge transfer transition [65].

2.4.2.3 Characterization of polymer grafting

The characterization of the polymers grafted from cellulose surfaces (i.e. cellulose I and II) has proven to be a challenge. Many have used ellipsometry to measure the polymer thickness on the surface of silicon wafers [13,17,19,32,58,62,65,70,112–114], gold substrates [18,61], cellulose membranes (notably from an unspecified cellulose source) [115], or poly(glycidyl methacrylate)-coated silicon wafers spin coated with a membrane of dissolved regenerated cellulose [20]. However cellulose-based materials are rough, making it difficult to deduce the true thickness of the grafted polymers. Moreover, the polymer thickness is a function of the moisture level, particularly for hydrophilic polymers such as poly(acrylic acid).

Another method to characterize the grafted polymers is to cleave them from the surface, either through acid hydrolysis or using a base, followed by solvent removal [68,79,110,116,117]. Hence, NMR analysis can be employed for chemical microstructure and number-average molecular weight determination, or SEC for molecular weight distribution analysis. However, if there are insufficient quantities of polymers cleaved from the surface for characterization, ATR-FTIR can also be employed for a semi-quantitative evaluation of polymers on the surface. Many authors were able to detect polymers in the subsequent polymerization step via ATR-FTIR [13–15,18,22,27,40], even though the initiator quantities were below the detection limit of ATR-FTIR. If the polymer-modified surfaces were washed inadequately, detection could be attributed to physisorbed polymers on the membrane surface rather than to those covalently attached to the initiator, as discussed in [40] and [44].

2.4.2.4 Applications of ATRP and ARGET ATRP on cellulose

Previous work has explored the use of atom transfer radical polymerization techniques to produce functionalized cellulose substrates (either cellulose I or II) using various ATRP techniques (Table 2.2 and Table 2.3). The target applications included creating novel materials for anti-fouling membranes and responsive membrane materials.

Table 2.2: Cellulose substrates functionalized via surface initiated ATRP or ARGET ATRP for novel material development

Application	Monomer	Substrate	Ref.
Dual responsive material	VP + NIPAAm for block copolymer	Whatman filter paper 1	[36]
Dual responsive membrane[a]	NIPAAm and DEAEMA on each face of the membrane	Cross-linked cellulose membrane	[106]
Biocomposites	MMA	Cellulose filter paper	[110]
Self-cleaning surfaces	GMA	Whatman filter paper	[38]
Antibacterial properties	tBA	Cellulose filter paper from Hangzhou Xinhua Paper Co.	[118]
Blood-compatible materials	DVBSPA	Cellulose membrane from Sigma Aldrich	[119]
Anti-microbial properties	DMAEMA + EB	Whatman filter paper or aminopropyltrimethoxysilane-coated microscope slides	[68]
Thermoplastic elastomers[a]	BA + MMA	Wood pulp	[120]
pH-Responsive membranes	AA	RC Satorius 0.45 µm	[50]
Molecular imprinted membranes	Am + Ars	RC Sartorius 0.45 µm	[21]
Antifouling membrane	PEGMA	RC UF with PE support	[19]

VP + NIPAAm = 4-vinylpyridine and *N*-isopropylacrylamide to form block copolymer; DEAEMA = 2-(diethylamino) ethyl methacrylate; MMA = methyl methacrylate; GMA = glycidyl methacrylate; tBA = *tert*-butyl acrylate; DVBSPA = *N*,*N*-dimethyl-*N*-(p-vinylbenzyl)-*N*-(3-sulfopropyl) ammonium; DMAEMA + EB = 2-(dimethylamino) ethyl methacrylate and ethyl bromide for quaternization; BA + MMA = butyl acrylate and methyl methacrylate to form block copolymer; AA = acrylic acid; Am + Ars = acrylamide and artemisinin for imprinting; PEGMA = poly(ethylene glycol) methacrylate; RC = regenerated cellulose; UF = ultrafiltration; PE = polyethylene; [a] ARGET ATRP.

Other applications included investigating the polymerization kinetics or experimenting with ATRP to graft various monomers on cellulose surfaces (Table 2.3).

Table 2.3: Polymerization studies of various cellulose support functionalized via surface initiated ATRP and ARGET ATRP

Application	Monomer	Substrate	Ref.
Comparison of grafting-on and grafting-from approaches	MMA	Whatman filter paper 1	[28]
Industrial applications of ARGET ATRP[a]	MMA	Whatman filter paper 1 dissolving pulp, bleached and unbleached Kraft pulp CTMP papers	[40]
Polymer library	EA + Sty	Unbleached cotton fibres	[98]
Polymer library	EA	Wood pulp cellulose fibres obtained from Kraft process and Whatman filter paper as reference	[69]
Polymer library	CPPUA	Whatman filter paper 1	[43]
Polymer library	MA and Sty	Whatman filter paper 1, chitosan, MCC, RC dialysis membrane, Lyocell fibres, chitosan films	[33]
Polymer library	MA + HEMA	Whatman filter paper 1	[35]
Polymer library	MA	Whatman filter paper	[44]
Polymer library[a]	EGMA + DEGMA	Hydroxypropylcellulose	[41]
Polymer library[a]	NIPAAm	Cellulose nanocrystals	[121]

MMA = methyl methacrylate; EA + Sty = ethyl acrylate and styrene to form copolymer; CPPUA = 11-(4′-cyanophenyl-4″-phenoxy) undecyl acrylate; MA = methyl acrylate; MA + HEMA = methyl acrylate and 2-hydroxyethyl methacrylate to form block copolymer; EGMA + DEGMA = (ethylene glycol) methyl ether methacrylate and di(ethylene glycol) methyl ether methacrylate (DEGMA) to form block copolymer; NIPAAm = *N*-isopropylacrylamide; RC = regenerated cellulose; MCC = microcrystalline cellulose; CTMP = chemi-thermomechanical pulp; [a] ARGET ATRP.

2.5 Protein capture by regenerated cellulose-based cation exchange membrane adsorbers

Examples of previous work in the development of regenerated cellulose cation exchange membrane adsorbers are listed in Table 2.4. Two ways to test the protein capture capability of these materials are by static protein binding and by dynamic protein binding capacity tests.

Table 2.4: Examples of cation exchange membrane adsorbers-based on regenerated cellulose (RC) supports functionalized via surface initiated ATRP

Application	Monomer	Substrate	Static protein binding capacities[a]	Ref.
Strong cation exchange	SPMAK	RC Whatman, 0.2, 0.45, 1 µm	79 ± 8 mg mL^{-1} lysozyme	[17]
Strong cation exchange	S4SS	RC Sartorius 0.45 µm	130 mg mL^{-1} lysozyme	[27]
Weak cation exchange	AA	RC Whatman 1 µm	99 mg mL^{-1} lysozyme	[18]
Multimodal (weak cation + hydrophobic interaction)	GMA + post modification with MBA	RC Whatman 1 µm	151 ± 9 mg mL^{-1} IgG	[20]

SPMAK = 3-sulfopropyl methacrylate; S4SS = sodium 4-styrenesulfonate; AA = acrylic acid; GMA = glycidyl methacrylate; MBA = 4-mercaptobenzoic acid; RC = regenerated cellulose; IgG = immunoglobin G; [a] Note: varying static protein binding capacity conditions.

The static protein binding capacity describes the maximum protein binding capacity of the material at equilibrium. Lysozyme has been extensively used for static protein binding capacity (SBC) characterization due to its affordability over mAbs. The lysozyme SBC of regenerated cellulose cation exchange membrane adsorbers ranged from 79-130 mg mL^{-1}, all under different equilibrium binding and elution conditions (Table 2.4). A multimodal chromatographic material with a mix of weak cation and hydrophobic interaction properties was used for the purification of IgG, a type of antibody [20]. Additional hydrophobic interactions enabled a higher specificity for IgG capture, and the reported SBC was 151 mg mL^{-1} [20]. Thus, the target IgG SBC for the development of novel weak cation exchange membranes should be in the range of 10^2 mg mL^{-1} or higher.

Dynamic protein binding capacity (DBC) measurements have been performed to characterize weak cation exchange membrane adsorber materials. They measure the protein binding capacity of the material in the presence of mass transfer effects, and is usually a fraction of the material's SBC [2]. Lysozyme has also been used as a model protein for DBC. The highest reported lysozyme dynamic protein binding capacity reported with unspecified breakthrough has been 71 mg mL^{-1} for a 5 mg mL^{-1} lysozyme solution in 10 mM potassium phosphate buffer at pH 7, using three poly(acrylic acid) modified RC membranes (11 mm diameter) at flow rate of 1 mL min^{-1} in an ÄKTA Purifier system [18].

3. Developing weak cation exchange membrane adsorbers – Understanding immobilization and polymerization

3.1 Introduction

Membrane adsorbers consist of a support layer and a functional layer [2]. Support layers such as regenerated cellulose (RC) can be used and are favoured due to their renewable and biodegradable nature. Moreover, RC has higher amorphous character over native cellulose leading to improved reactivity during its functionalization [71] and is suitable for use as chromatographic material given its insolubility in typical solvents, relatively inert behaviour, and excellent chemical properties for functionalization [71–74]. The functional layer can thus be tailored to achieve high protein binding.

Previously, membrane adsorbers functionalized with polymer brushes or "tentacle-like" arrangement on cellulose were created by free radical polymerization (FRP) techniques such as ceric ion polymerization [2,122]. With advances in polymer synthesis, surface initiated atom transfer radical polymerization (ATRP) has become popular for the development of membrane adsorbers on RC membrane supports [13–15,17,20]. ATRP enables control over the molecular weight distribution, while its subset aqueous ARGET ATRP enables polymerization in the presence of limited amounts of oxygen and requires lower quantities of metal catalysts. To perform surface initiated ARGET ATRP, an initiator first needs to be immobilized, to be followed by polymerization. The resulting polymer chains allow for three-dimensional binding of proteins, which enables higher, more efficient protein capture [2] as compared to conventional chromatographic ligands offering binding sites accessible surface sites rather than binding sites available through the volume of the polymer [10]. As a result, higher throughput for protein purification can be achieved with membrane materials prepared by aqueous ARGET ATRP, which also permits the use of lower catalyst concentrations and harmless solvent, water, for facile polymerization. Control of the polymer length can be achieved by optimizing each of the two steps, namely the immobilization of the initiator on the RC membrane and the subsequent polymerization by ARGET ATRP.

Initiator immobilization is affected by the accessibility of the initiator to the reactive hydroxyl groups on cellulose. To improve hydroxyl group accessibility and reactivity, leading to control over the amount of immobilized initiator on the surface, this chapter describes investigations into the effects of NaOH treatment of methanol-washed RC membranes, the amount of initiator BiBB used per membrane disc, and solvency conditions on the relative quantity of immobilized BiBB on the membrane surface. Furthermore, ARGET ATRP reagent ratios were investigated to identify conditions for successful grafting.

3.2 Materials and methods

3.2.1 Materials

Regenerated cellulose (RC) membranes from Whatman Inc. (RC60, pore size 1 μm, 47 mm diameter) were selected for use as the support layer and purchased from VWR International (Mississauga, ON, Canada). *N*,*N*-Dimethylformamide (DMF; 99.8%, Sigma Aldrich, Oakville, ON, Canada) was dried over CaH_2 overnight, followed by vacuum distillation. Tetrahydrofuran (THF; 99%, Sigma Aldrich, Oakville, ON, Canada) was distilled from a still with sodium benzophenone under N_2. Triethylamine (TEA; 99.5%, EMD Millipore Canada) was kept dry over 4 Å molecular sieves. 2-Bromoisobutyryl bromide (BiBB; 98%, Sigma Aldrich, Oakville, ON, Canada), copper (II) bromide (99.999%, Sigma Aldrich, Oakville, ON, Canada), sodium acrylate (97%, Sigma Aldrich, Oakville, ON, Canada), 2,2′-bipyridine (bpy; 99%, Sigma Aldrich, Oakville, ON, Canada), *N,N,N′,N′,N″*-pentamethyldiethylenetriamine (PMDETA; 99%, Sigma Aldrich, Oakville, ON, Canada), Milli-Q water, ascorbic acid (Food grade, J.T. Baker Chemical Co., Center Valley, PA, USA), sodium bromide (ACS grade, BDH Chemicals, Toronto, ON, Canada), sodium hydroxide pellets (NaOH; 97%, Sigma Aldrich, Oakville, ON, Canada), ethanol, methanol, citric acid (Fisher Scientific, Canada), sodium phosphate dibasic heptahydrate (Fisher Scientific, Canada), potassium chloride (Fisher Scientific, Canada), and lysozyme chloride (Neova Technologies, Abbotsford, BC, Canada) were used as is unless otherwise specified.

3.2.2 Membrane pre-treatment

Prior to immobilization, the RC membranes were soaked in methanol for 10 minutes, rinsed thoroughly with water and then THF, and dried in a vacuum oven overnight. These membranes were then either dipped into 0.5 M or 2 M NaOH for ten seconds, or were used as is.

All the NaOH-treated membranes were subsequently rinsed with ethanol until neutral pH, rinsed in dry DMF once, and stored in dry DMF until immobilization. Membranes that were not pre-treated with NaOH (i.e. 0 M NaOH treatment) were dried in a vacuum oven overnight prior to immobilization, unless otherwise specified.

3.2.3 Moisture regain and water vapour accessibility

Moisture regain was measured by subjecting the NaOH-treated membrane samples to 65% relative humidity (RH) at 25°C in an environmental chamber (MLR-351H, Sanyo Electric Co., Ltd., Moriguchi, Osaka, Japan). The samples were left in the chamber for 6 days to ensure that the mass was stabilized. During mass measurement of the wet samples, the humidity in the balance was maintained at ~60% RH by introducing a beaker of warm water. The membrane samples were then vacuum dried (30 in Hg, Fisher Scientific vacuum oven 280, Canada) at room temperature for at least three days prior to dry mass measurement. The water accessibility of the membrane was calculated by (3.1) according to [100].

$$\text{Moisture Regain } (\%) = 100\% \times \frac{\text{Mass@65\%RH} - \text{Dry mass}}{\text{Dry mass}} \qquad (3.1)$$

Water vapour accessibility was then calculated assuming 1.53 mol of water per anhydroglucose unit according to [100] (3.2). The value of 1.53 was derived from the extrapolated y-intercept of the empirical relationship of water molecules per anhydroglucose unit (derived from moisture regain measurement) versus degree of substitution of cellulose acetate in a homogeneous reaction [123].

$$\text{Accessibility of water vapour } (\%) = \text{Moisture regain } (\%) \times \frac{162\ \text{g mol}^{-1}\ \text{glucose}}{18\ \text{g mol}^{-1}\ \text{water}} \times \frac{1}{1.53} \qquad (3.2)$$

3.2.4 Immobilization of initiator

2-Bromoisobutyryl bromide (BiBB) was used as the initiator. One Whatman RC60 membrane disc (47 mm diameter) was placed into a 250 mL glass jar with a plastic screw cap cover in either 12 mL of dry DMF or dry THF. All the immobilization reactions were agitated using a stir bar either at a low stir rate (dial close to 2) or a high stir rate (dial close to the maximum) on a stirring plate (Thermolyne Nuova II magnetic stirrer, Thermo Fisher Scientific, Canada), or placed on an orbital shaker (Thermo Scientific 2309 lab rotator, Canada) at 125 rpm

immediately after adding the reagents. It should be noted that the volume of the solvent and diameter of the container (~58 mm) prevented the membrane from flipping over during agitation of the reaction medium. Three different BiBB quantities were considered per membrane disc with a BiBB/TEA molar ratio of ~1/0.67 in all cases (the average mass of the membrane was 40 mg):

i. Theoretical BiBB (0.41 mmol per membrane disc) - based on a degree of substitution (DS) of three and assuming that 56% of the hydroxyl groups were accessible to react (56% accessibility was calculated from the initial moisture regain values of the unmodified membrane based on gravimetry, Equation 3.1 and 3.2).
ii. Stoichiometric BiBB (0.74 mmol per membrane disc) - based on a DS of three and assuming 100% accessibility.
iii. Excess BiBB (2.67 mmol per membrane disc) - arbitrary value.

The jar containing one membrane disc and solvent was placed in an ice bath while the BiBB was added drop-wise. After 30 minutes, the ice bath was removed and the reaction medium was maintained at room temperature for at least 22 hours. All the immobilization reactions were performed under these conditions except for (iii), where TEA and BiBB were added in the following sequence: 0.1 mL TEA + 0.125 mL BiBB drop-wise in an ice bath + 0.15 mL TEA 15 minutes after the start of immobilization, and then 0.2 mL BiBB one hour after the first addition of BiBB. This sequence allowed for the consumption of impurities in the medium for improved immobilization. For condition (iii), the ice bath was removed ~45 minutes after the second addition of BiBB. Subsequently, the heterogeneous reaction conditions of (iii) were maintained at room temperature for at least 22 hours after the first addition of BiBB. All the BiBB-modified membranes were then washed with THF three times (10 minute soak, 5 second soak, 45 minute soak), rinsed with methanol three times, and dried in a vacuum oven overnight. Mass and ATR-FTIR measurements were then recorded for the RC membrane discs dried in a vacuum oven (30 in Hg, Fisher Scientific vacuum oven 280, Canada) at least overnight.

3.2.5 Reduction studies of $CuBr_2$ to CuBr by ascorbic acid independently from polymerization

A UV-Vis spectrophotometer (Cary 100, Varian Inc., USA) was used to determine the reduction of $CuBr_2$ (~0.024 mmol) by ascorbic acid with varying molar ratios of ascorbic acid

and amine ligands, i.e. 1/1/2 or 1/10/2 $CuBr_2$/PMDETA/ascorbic acid in 35 mL of Milli-Q water, or with a 1/2/2 $CuBr_2$/bpy/ascorbic acid molar ratio in 18 mL Milli-Q water. No monomer, BiBB-modified membrane, or salt were added; thus this study was conducted independently of polymerization. Only the headspace was purged with nitrogen gas prior to ascorbic acid addition, in order to understand the kinetics of the reduction even in the presence of residual oxygen. The absorbance of the aqueous solutions between 200-800 nm was measured before ascorbic acid addition, immediately after ascorbic acid addition, and 0.5, 1, 2, 4, 6, and 25 hours after ascorbic acid addition, unless otherwise specified. The pH of the aqueous solution containing 1/2/2 $CuBr_2$/bpy/ascorbic acid molar ratio was adjusted to 12 (as confirmed with pH paper) using 1 M NaOH.

3.2.6 ARGET ATRP

Deoxygenated Milli-Q water was used and produced by sparging with N_2 for at least 30 minutes. Two different polymerization scenarios were performed:

i. Starting with an intact BiBB-modified membrane disc (i.e. 47 mm diameter disc), solid membrane samples were collected at 0.5, 1, 2, 4, and 6 hours by ripping a small piece of the membrane off each time. The $CuBr_2$, 2,2′-bipyridine (bpy), and ascorbic acid quantities were determined based on the quantity of immobilized BiBB and the molar ratio 1/0.25/0.25/0.125 of immobilized BiBB/bpy/ascorbic acid/$CuBr_2$. Either 1 mM (condition I) or 5 mM (condition II) NaBr and 1 M sodium acrylate in 35 mL of deoxygenated Milli-Q water were used. The reagents were added sequentially under N_2 purge in a three-neck round bottom flask: $CuBr_2$, bpy, NaBr, 35 mL of Milli-Q water, sodium acrylate, ascorbic acid, and finally the BiBB-modified membrane (immobilization conditions: 2.67 mmol of BiBB per membrane disc, soaked in DMF for at least 2 weeks prior to immobilization). The pH of the solution was adjusted to ~8-9 with 1 M NaOH.

ii. With the BiBB-modified membrane disc divided into 6 pieces, where five pieces were each placed into one vial labelled 0.5, 1, 2, 4, and 6 hours, two different polymerization conditions were considered:

    a. Condition III - the immobilized BiBB/bpy/ascorbic acid/$CuBr_2$ molar ratios were 1/0.4/0.4/0.05, with 5 mM NaBr and 1 M sodium acrylate

according to 18 mL total solution volume in each vial. The pH was adjusted to 12 with 1 M NaOH.

b. Condition IV - the $CuBr_2$/bpy/ascorbic acid/immobilized BiBB molar ratios were 1/0.2/0.2/0.1, with a 1/16 $CuBr_2$/NaBr molar ratio and a 1/3240 $CuBr_2$/sodium acrylate molar ratio according to 18 mL total solution volume in each vial. The pH was adjusted with 1 M NaOH to 8-9.

The total amounts of $CuBr_2$, bpy, and NaBr needed for the five vials were all measured into one flask and solubilized into 30 mL of deoxygenated Milli-Q water. The total mass of ascorbic acid was measured and placed in a different flask and solubilized with 30 mL of deoxygenated Milli-Q water. The reagents were added in the following sequence: deoxygenated Milli-Q water (6 mL in each vial), $CuBr_2$/bpy/NaBr solution (6 mL in each vial), sodium acrylate (according to the mass needed for each vial), ascorbic acid solution (6 mL in each vial), and one membrane piece in each vial. All the additions of solution to the vials were carried out under N_2 purge of the headspace and were agitated using an orbital shaker (Thermo Scientific 2309 lab rotator, Canada) at ~125 rpm.

Immediately after the specified polymerization time, the membrane samples were rinsed in Milli-Q water thrice, soaked in water for at least 30 minutes, and rinsed with Milli-Q water again. The membrane samples were placed on Petri dishes or glass slides for drying under ambient conditions overnight. Afterwards, the membranes were placed into a vacuum oven at room temperature (30 in Hg, Fisher Scientific vacuum oven 280, Canada) at least overnight prior to mass and ATR-FTIR measurements.

3.2.7 ATR-FTIR

A Bruker Tensor 27 FTIR instrument (Billerica, MA, USA) with PIKE MiRacle ATR accessory (Madison, WI, USA) single point reflection with ZnSe crystal and an angle of incidence of 45° (64 scans, 4 cm^{-1} resolution) was used. Baseline correction and atmospheric correction for CO_2 were applied by the OPUS software. Twenty four points were measured across the membrane in a 4x6 grid to observe the spatial distribution of BiBB for the two surfaces of the membrane. Thus 48 repeated measurements were taken for each membrane sample unless otherwise specified.

The initiator functionalization levels were estimated by taking the peak area ratios between 1680-1800 cm^{-1} and 2700-3000 cm^{-1}, corresponding to the carbonyl [124] and C-H groups, respectively, using a baseline of zero. Polymer grafting was evaluated from the peak areas ratios between 1500-1600 cm^{-1} and 2700-3000 cm^{-1} for the ionized carboxylic groups [18] and C-H groups, respectively, using a baseline of zero for semi-quantitative analysis.

3.2.8 Static protein binding capacity with lysozyme

Prior to the protein static binding tests, an equilibration buffer was prepared by mixing solutions of 0.1 M citric acid and 0.2 M sodium phosphate dibasic heptahydrate to obtain phosphate citrate buffer at pH 5. Similarly, the binding buffer was prepared by adding lysozyme in the equilibration buffer at pH 5 for a final lysozyme concentration of 0.5 mg mL^{-1}. Finally, an elution buffer was prepared by mixing 0.1 M citric acid with 0.2 M sodium phosphate dibasic heptahydrate and KCl to obtain phosphate citrate buffer at pH 7 with 1 M KCl.

Cut membranes with dimensions of 1 cm x 1 cm were soaked into 5 mL of equilibration buffer for 2 hours. Next, the membrane sample was immersed into 10 mL of binding buffer for 24 hours. Finally, the lysozyme was eluted with an elution buffer for 2 hours. In all three steps, the samples were agitated with an orbital shaker (Thermo Scientific 2309 lab rotator, Canada) at 125 rpm.

The binding and elution solutions were then filtered with a 0.45 μm polyethersulfone membrane (Thermo Scientific, Ottawa, ON, Canada) prior to absorbance measurement with a UV-vis spectrophotometer (Genesys 10S, Thermo Scientific, Waltham, MA, USA). A lysozyme calibration curve for concentrations up to 1 mg mL^{-1} was prepared and the absorbance was measured at 280 nm. The static protein binding capacity was then computed with (3.3).

$$\text{Static protein binding capacity}\left[\text{mg mL}^{-1}\right] = \frac{(C_{bi}-C_{bf})V_b}{V_m} \qquad (3.3)$$

where C_{bi} = initial protein concentration in buffer solution [mg mL^{-1}], C_{bf} = final protein concentration in buffer solution [mg mL^{-1}], V_b = volume of buffer solution [mL], V_m = dry membrane volume [mL].

All the absorbance readings were taken three times from the same sample solution, and calibration curve readings were taken twice from the same solution. The dry membrane volume was estimated from the 1 cm x 1 cm dimensions and the dry thickness of the membrane sample. The thickness was measured with a digital micrometer (±0.002 mm, Marathon Watch Company, Richmond Hill, Canada), taking an average at three different points from each vacuum-dried membrane sample.

3.2.9 Statistical analysis

A polynomial equation (3.4) was used to represent the experimental ATR-FTIR peak area ratio (i.e. peak areas at 1680-1800 cm^{-1}/2700-3000 cm^{-1}) as a function of the TEA molar quantities used and BiBB molar quantities used, using the *fminsearch* function in MATLAB to minimize the sum of squares of error. This was to determine the optimal BiBB/TEA molar ratios for ATR-FTIR detection.

$$y = a_1 x_1 + a_2 x_2 + a_3 x_1 x_2 + a_4 + error \qquad (3.4)$$

Moreover, a 2^2 factorial design was employed to observe the effects of the BiBB quantity used per membrane disc and the 2 M NaOH-treated RC membrane on the ATR-FTIR peak area ratio (i.e. peaks at 1680-1800 cm^{-1}/2700-3000 cm^{-1}). A second 2^2 factorial design was used to investigate the effect of the BiBB quantity used per membrane disc and the immobilization solvent type on the ATR-FTIR peak area ratio (i.e. peaks at 1680-1800 cm^{-1}/2700-3000 cm^{-1}). Both studies employed ANOVA with a confidence level of 95%. T-tests measured the statistical difference between the samples, also with a confidence level of 95%. All the error bars representing the standard error are shown with the mean values.

3.3 Results and Discussion

3.3.1 Support layer characterization

3.3.1.1 ATR-FTIR

The support layer (i.e. Whatman RC60 membrane disc ~40 mg) was characterized by ATR-FTIR to obtain the baseline spectrum for the RC membrane (Figure 3.1). The peaks at 2700-3000 cm^{-1} were identified as the C-H functionality of cellulose, and at 3000-3500 cm^{-1} for the O-H functionality of cellulose. The fingerprint region of the spectra confirmed the presence

of the anhydroglucose rings with the C-O stretch at ~1000 cm^{-1} and the out-of-phase ring stretching at ~900 cm^{-1} (Figure 3.1) [125].

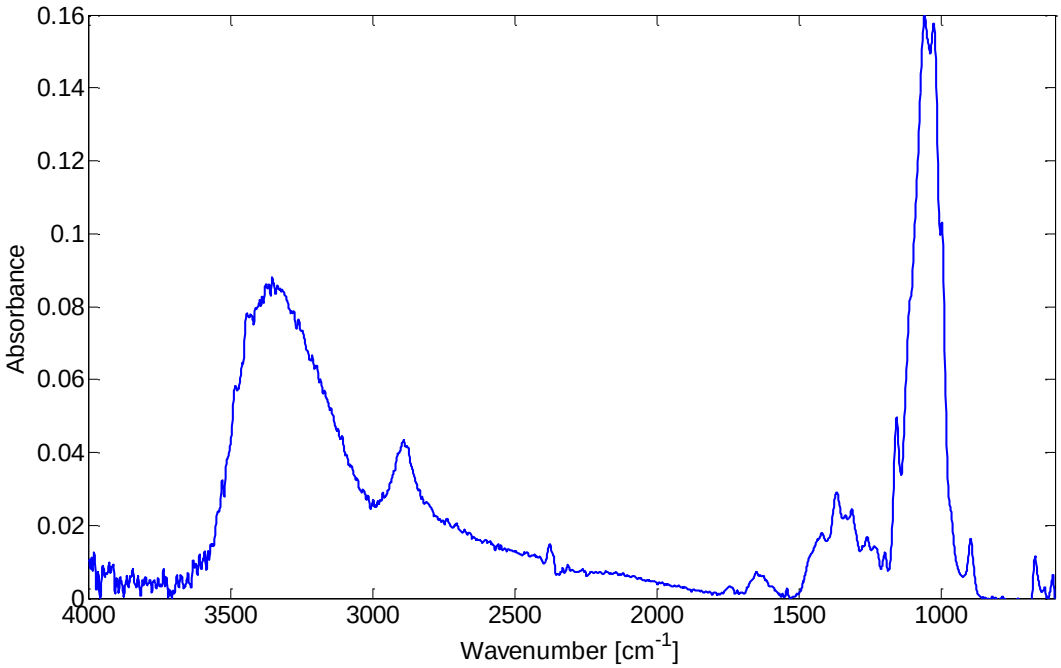

Figure 3.1: ATR-FTIR spectrum for the unmodified RC membrane.

3.3.1.2 Moisture regain and water vapour accessibility

Moisture regain experiments were conducted to determine the accessibility of hydroxyl groups in the RC membrane towards water vapour [100]. For a higher accessibility of water vapour to the hydroxyl groups, there should be a higher accessibility of reagents such as the initiator, BiBB, towards those groups allowing for greater BiBB immobilization. For the unmodified RC membrane (i.e. 0 M NaOH-treated, methanol-washed membrane), only 45% water vapour accessibility was observed (Table 3.1). NaOH treatment of the unmodified RC membrane was thus performed to determine whether the accessibility could be improved, as it is known that NaOH can swell cellulose fibres for greater accessibility [100,126].

Table 3.1: Accessibility of water after NaOH treatment of the methanol-washed RC membranes (n=2)

NaOH treatment [M]	Accessibility [%]
0	45.0 ± 1.9
0.5	53.8 ± 0.5
2	102.5 ± 28.9

All statistically the same (t-test, 95% confidence level)

A large standard error for the accessibility values of 2 M NaOH-treated, methanol-washed RC membrane was observed (Table 3.1). All the accessibility values were statistically similar (t-tests, 95% confidence level). The reported accessibility for mature Acala 4-42 cotton after 0 M NaOH treatment was 46%, similarly to the accessibility of 0 M NaOH-treated, methanol-washed RC membrane (Table 3.1) [100]. When Acala cotton was treated with 2 M NaOH for 30 minutes, the accessibility to water vapour was 45% [100]. The similarity in the accessibility values were explained by the sole occurrence of interfibrillar swelling (i.e. penetration of solvent only between fibres, as opposed to into it). The accessibility values in [100] only increased when higher NaOH concentrations (> 3 M) were used, due to their ability to promote intrafibrillar swelling (i.e. penetration of the solvent into the fibres), yielding a higher reactivity for the cotton. The results in literature may reflect the type of penetration by NaOH into the RC membrane where the statistically similar accessibility values among 0, 0.5, and 2 M NaOH-treated RC membranes demonstrated only interfibrillar swelling (Table 3.1).

3.3.2 Immobilization of BiBB

The measured accessibility of the reactive hydroxyl groups on the methanol-washed RC membrane support layer indicated that a degree of substitution (DS) of three on the RC membrane would not be feasible without degrading the membrane. According to the measured accessibility values, only ~45% of the stoichiometric amount of BiBB used per membrane disc (assuming a DS of 3 per membrane disc) would be immobilized due to the structural limitations (i.e. limited accessibility of the hydroxyl groups). However, preliminary BiBB immobilization results for the native RC membrane did not yield measurable mass increases, and unsuccessful BiBB detection by ATR-FTIR. Hence, the conditions for the BiBB immobilization reaction were studied by looking at the BiBB/TEA molar ratio, the BiBB amount used per membrane disc, NaOH treatment, and solvent effects on the immobilization.

3.3.2.1 Determining the optimal BiBB to TEA molar ratio

In the literature, the molar ratio of BiBB/TEA used is usually 1/1, as it is expected that TEA would consume the stoichiometric amount of hydrogen bromide produced. However, some of the BiBB may be consumed by TEA in the medium [95]. Furthermore, our initial experimental work indicated that a 1/1 BiBB/TEA molar ratio was ineffective in producing BiBB immobilization. Thus the influence of the BiBB and TEA amounts on BiBB immobilization was analyzed, by developing a polynomial equation based on the ATR-FTIR peak area ratios for nine different combinations of BiBB and TEA ranging from 0.41-9.10 mmol BiBB and 0.27-9.1 mmol TEA, respectively, per membrane disc that was 2 M NaOH-treated and methanol-washed (3.5).

$$y(x_1, x_2) = 0.0919x_1 - 0.0540x_2 - 0.0019x_1x_2 + 0.0967 \qquad (3.5)$$

where x_1 = BiBB quantity used per membrane disc [mmol], x_2 = TEA quantity used per membrane disc [mmol], y = ATR-FTIR peak area ratio (1680-1800 cm^{-1}/2700-3000 cm^{-1}).

The BiBB immobilization (based on the ATR-FTIR peak area ratio) estimated from (3.5) was then plotted for 0 to 3 mmol TEA and BiBB used per membrane disc and the model was bounded between 0 and 0.4 ATR-FTIR peak area ratio (Figure 3.2).

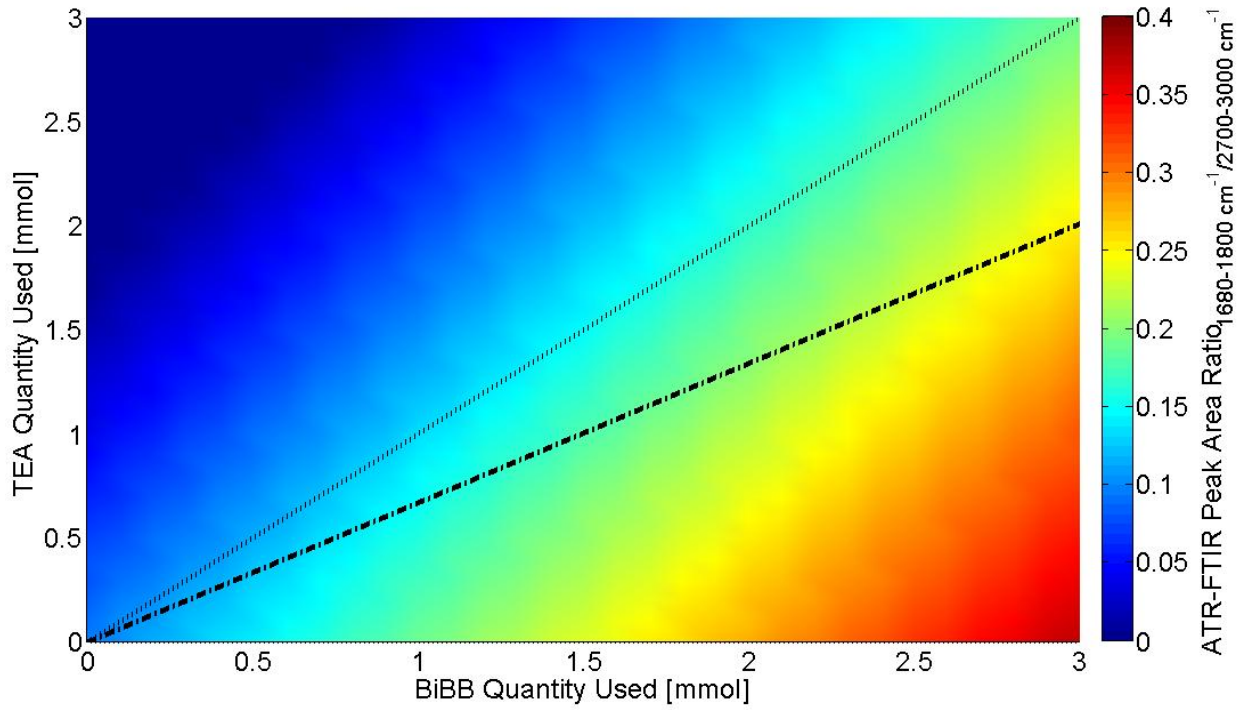

Figure 3.2: Polynomial representation of ATR-FTIR peak area ratio of peaks at 1680-1800 cm^{-1}/2700-3000 cm^{-1} (Coloured surface) vs. TEA quantity used [mmol] and BiBB quantity used [mmol] per membrane disc with 1:1 BiBB/TEA molar ratio (⋯) and 1/0.67 BiBB/TEA molar ratio (–.–.–.) on 2 M NaOH-treated RC membrane disc based on low stir speeds.

For comparison, the ATR-FTIR peak area ratio at 1680-1800 cm^{-1}/2700-3000 cm^{-1} for unmodified methanol-washed RC membrane was 0.027 ± 0.0010 (n=4). From the experimental work, anything near the border of the blue-coloured and cyan regions in Figure 3.2 would not be statistically different from the unmodified methanol-washed RC membranes' ATR-FTIR peak area ratios according to the t-test (95% confidence level), due to large standard errors across the BiBB-modified membrane. Thus, it was predicted that a lower BiBB/TEA molar ratio would provide a higher probability of statistically significant yields of immobilized BiBB, especially when small quantities of BiBB and TEA were used (i.e. in the 0 to 1 mmol BiBB range). Hence an arbitrary molar ratio of 1/0.67 BiBB/TEA was used for the rest of the work.

3.3.2.2 Effects of BiBB quantity used per membrane disc and of NaOH treatment on ATR-FTIR peak area ratios

Even though the accessibility of NaOH-treated, methanol-washed RC membranes was not significantly improved from a statistical viewpoint, the effects of the BiBB quantity used per membrane disc and of NaOH treatment on the BiBB immobilization were investigated in a 2^2 factorial design based on the ATR-FTIR peak area ratios (i.e. peaks at 1680-1800 cm^{-1}/2700-3000 cm^{-1}) (Table 3.2). This was to reconfirm whether the NaOH treatment had a direct effect on BiBB immobilization and whether the moisture regain measurements were ineffective. A 2 M NaOH treatment was selected based on the work of Zeronian *et al.* [86,126], because it was the minimum concentration that was observed to successfully convert cellulose I to cellulose II, leading to significant structural changes.

Table 3.2: 2^2 factorial design of BiBB quantity used per membrane disc and NaOH treatment in DMF and with stir bar agitation at low speed

Run #	BiBB quantity used per membrane disc [mmol]	NaOH pre-treatment [M]
1	+ (2.67)	+ (2)
2	+ (2.67)	- (0)
3	- (0.41)	+ (2)
4	- (0.41)	- (0)

The highest ATR-FTIR peak area ratio was observed for 2 M NaOH treatment and 2.67 mmol BiBB per membrane disc (Table 3.3). It should be noted that the degree of substitution of BiBB on cellulose determined by gravimetry was unreliable during measurement especially for 2 M NaOH-treated membranes. Moreover, the mass of NaOH-treated RC membranes were not directly measured due to storage in DMF prior to immobilization.

Table 3.3: ATR-FTIR peak area ratios at 1680-1800 cm^{-1}/2700-3000 cm^{-1} according to the BiBB quantity used per membrane disc and NaOH treatment (n=1, each sample measured three times)

	ATR-FTIR peak area ratios at 1680-1800 cm^{-1}/2700-3000 cm^{-1}	
	NaOH treatment [M]	
BiBB quantity used per membrane disc [mmol]	0	2
0.41	0.040 ± 0.00058	0.094 ± 0.040
2.67	0.052 ± 0.0096	0.37 ± 0.033

Table 3.4: ANOVA analysis of the effect of BiBB quantity used per membrane disc and NaOH treatment on BiBB immobilization detected from ATR-FTIR peak area ratios (n=1, each sample measured three times)

	SS	DF	MS = SS/DF	F = MS/MS_E	F_{crit}	
BiBB quantity used per membrane disc	0.064	1	0.064	30.56	5.32	Significant
NaOH treatment	0.11	1	0.11	50.44		Significant
Interaction	0.053	1	0.053	25.52		Significant
Error	0.017	8	0.0021			
Total	0.24	11				

SS = sum of squares; DF = degree of freedom; MS = mean square; MS_E = mean square of error; F = f-value; F_{crit} = critical f-value.

It was confirmed by ANOVA analysis (Table 3.4) that a higher BiBB amount used increased the ATR-FTIR peak area ratio, indicating higher BiBB immobilization as in [14]. Furthermore, ANOVA analysis confirmed that the 2 M NaOH treatment significantly increased BiBB immobilization. Although comparatively lower NaOH treatment for the methanol-washed RC membrane was used in this work (i.e. 2 M NaOH vs. > 3 M), the results agree with the literature where NaOH treatment increased the degree of substitution due to cellulose swelling and/or activation of the hydroxyl groups on the cellulose [76,79,86,126]. The ANOVA analysis may have thus indicated that the environmental humidity and hornification effects of drying and rewetting the methanol-washed RC membrane (i.e. reformation of the hydrogen bonds in the RC membrane) affected the estimated accessibility of hydroxyl groups after NaOH treatment.

3.3.2.3 Effects of BiBB quantity used per membrane disc and solvent on ATR-FTIR peak area ratios

An alternative method to improve the accessibility of the hydroxyl groups, and thus increase BiBB immobilization, was by swelling with solvent [83,99]. Two solvents were

considered based in previous studies for cellulose, namely tetrahydrofuran (THF) [13–15,17,20,28,33,35,37,42,48,50] and *N*,*N*-dimethylformamide (DMF) [127]. The effects of the BiBB quantity used per membrane disc and solvent on ATR-FTIR peak area ratios (i.e. peaks at 1680-1800 cm^{-1}/2700-3000 cm^{-1}) was investigated with a 2^2 factorial design (Table 3.5). In this study, lower NaOH treatment was used (i.e. 0.5 M NaOH) since 2 M NaOH treatment affected the structural integrity of the RC membrane by qualitative observation.

Table 3.5: 2^2 factorial design of BiBB quantity used per membrane disc and solvent type variations with stir bar agitation at high speeds

Run #	BiBB quantity used per membrane disc [mmol]	Solvent
1	+ (0.74)	+ (DMF)
2	+ (0.74)	- (THF)
3	- (0.41)	+ (DMF)
4	- (0.41)	- (THF)

The ATR-FTIR peak area ratio was highest with DMF as solvent and when 0.74 mmol BiBB per membrane disc was used (Table 3.6). The DS values determined by gravimetry also reflected this effect (Table 3.6). Statistical testing was not feasible for the DS values due to n=1.

Table 3.6: ATR-FTIR peak area ratios at 1680-1800 cm^{-1}/2700-3000 cm^{-1} (n=1, each sample measured 48 times by ATR-FTIR at different points across the membrane surface) and degree of substitution of BiBB on BiBB-modified RC membrane (n=1) as a function of the BiBB quantity used per membrane disc and solvent, for the top and bottom surfaces of the RC membrane

		ATR-FTIR peak area ratios at 1680-1800 cm^{-1}/2700-3000 cm^{-1}		Degree of substitution (DS)	
BiBB used per membrane disc [mmol]	Membrane surface	Solvent		Solvent	
		THF	DMF	THF	DMF
0.41	Top	0.075 ± 0.0024	0.18 ± 0.013	0.16	0.085
	Bottom	0.087 ± 0.0031	0.072 ± 0.0074		
0.74	Top	0.18 ± 0.0027	0.24 ± 0.0029	0.081	0.26
	Bottom	0.16 ± 0.0024	0.20 ± 0.0026		

Table 3.7: ANOVA analysis of membrane surface, BiBB quantity used per membrane disc, and solvent type effects on ATR-FTIR peak area ratios at 1680-1800 cm^{-1}/2700-3000 cm^{-1} (n=1, each sample measured 48 times)

	SS	DF	MS	F	F_{crit}	
Membrane surface	0.071	1	0.071	77.24	3.89	Significant
BiBB quantity used per membrane disc	0.40	1	0.40	438.20		Significant
Solvent	0.11	1	0.11	123.03		Significant
BiBB quantity used per membrane disc x Solvent Interaction	0.00050	1	0.00050	0.54		Not significant
Error	0.17	188	0.00092			
Total	0.76	191	0.0040			

SS = sum of squares; DF = degree of freedom; MS = mean square; F = f-value; F_{crit} = critical f-value.

ANOVA analysis was performed on the ATR-FTIR peak area ratios to investigate the relative amount of BiBB immobilized (Table 3.7). As indicated in the previous section, higher BiBB immobilization was observed for higher BiBB amounts used. As for the effect of the solvent, statistically higher BiBB immobilization was obtained in DMF as compared to THF. It is believed that more pronounced swelling of the cellulose fibres in DMF (either native or regenerated cellulose) as compared to THF, and its higher polarity enhanced the accessibility of BiBB to the hydroxyl groups and improved their reactivity for nucleophilic substitution with BiBB [83,89,91,92]. Thus DMF was adopted as the solvent to achieve higher BiBB immobilization for the subsequent reactions. Blocking of the data was also considered in the ANOVA analysis to evaluate whether there was a significant difference between the peak area ratios on the top and bottom surfaces of the membranes. As seen in Table 3.7, the two surfaces on the same membrane were significantly different from each other. This will be further discussed in the next section.

3.3.2.4 Uniformity of immobilized BiBB on the RC membrane discs and agitation

With the ability to manipulate the immobilized BiBB quantity via the BiBB amount used per membrane disc, NaOH treatment, and solvent, the uniformity of BiBB immobilization across each side of the membrane surface was investigated. First, the average ATR-FTIR peak area ratios for each side of a membrane surface were compared to evaluate their distribution. As

previously stated, there were differences in the relative amount of BiBB immobilized on the top and bottom surfaces of a given membrane. The stirring speed was increased, but BiBB immobilization remained relatively similar on both surfaces of the membrane (Figure 3.3B vs. D). This difference may therefore be due to the structural heterogeneity of the top and bottom surfaces of the membrane.

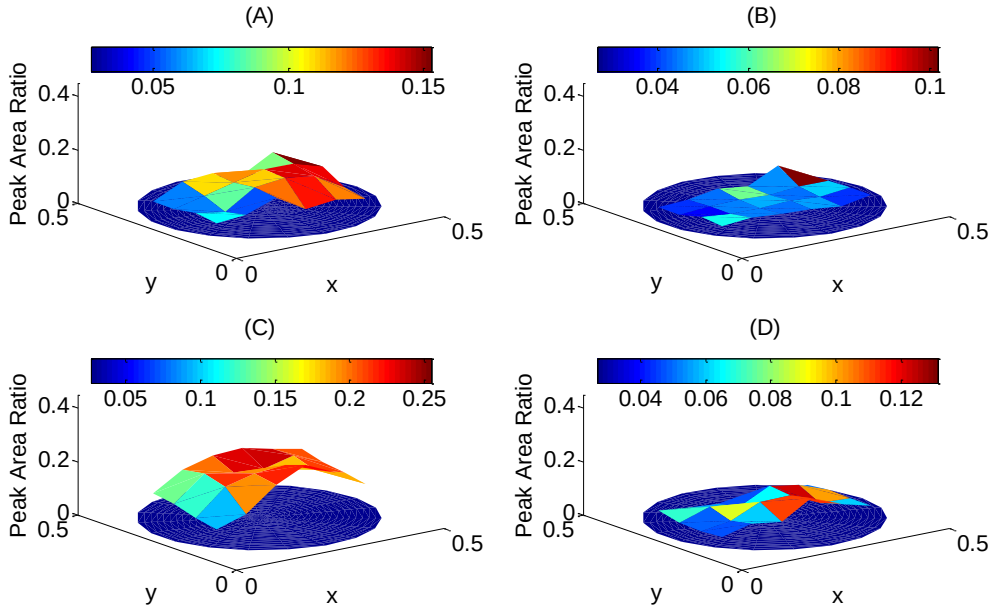

Figure 3.3: ATR-FTIR peak area ratios at 1680-1800 cm^{-1}/2700-3000 cm^{-1} for 0.5 M NaOH treatment and 0.41 mmol BiBB under (A) and (B) – low stir rate, top and bottom surface of the membrane, respectively; (C) and (D) – high stir rate, top and bottom surface of the membrane, respectively; where x and y = unit length and blue circle = unmodified membrane peak area ratio.

Next, the ATR-FTIR peak area ratios of surfaces for different immobilization conditions were compared. The sum of squares of normalized ATR-FTIR peak area ratios (SS) given by (3.6) was used. The ATR-FTIR peak area ratios were also normalized against the highest peak area ratio value, so that the maximum normalized value would be one.

$$SS = \sum (z - z_0)^2 \qquad (3.6)$$

where z = normalized ATR-FTIR peak area ratios (1680-1800 cm^{-1}/2700-3000 cm^{-1}) at one point of the membrane surface, $z_0 = 1$, SS = sum of squares.

Hence the lower SS, the less heterogeneous or more uniform the BiBB immobilization was across the surface (5.27, 6.84 and 2.79, 5.76 for (A), (B) and (C), (D) in Figure 3.3, respectively). From the SS estimates, uniformity improvements at the higher stir rate could not be confirmed. Statistical testing was not feasible due to n=1 for the heterogeneity (SS) values.

Ultimately, magnetic stirring during immobilization was not pursued due to potential physical damage to the membrane. The theoretical quantity of BiBB per membrane disc (i.e. 0.41 mmol) was also abandoned due to the low BiBB immobilization measured by ATR-FTIR. Moreover, the 0.74 mmol BiBB amount per membrane disc reduced the BiBB heterogeneity on the surface at high stir rate, even in different solvents (Table 3.8). Statistical testing was not feasible due to n=1 for the SS values.

Table 3.8: SS values for BiBB immobilization on 0.5 M NaOH-treated membranes using 0.41 mmol or 0.74 mmol BiBB per membrane disc and DMF or THF as solvent at high stir rate (n=1)

		SS values	
		Solvent type	
BiBB quantity used per membrane disc [mmol]	Membrane surface	THF	DMF
0.41	Top	1.45	2.79
	Bottom	1.82	5.76
0.74	Top	0.19	0.18
	Bottom	0.31	0.32

Consequently, the use of 0.41 mmol of BiBB per membrane disc was abandoned and an orbital shaker was used instead of magnetic stirring. Agitation of the membrane on the shaker yielded good BiBB uniformity on the membrane according to the SS values. A plot of the ATR-FTIR peak area ratio for both surfaces of a 0.5 M NaOH-treated, methanol-washed membrane exposed to 0.74 mmol BiBB per membrane disc in DMF and agitated with an orbital shaker is given in Figure 3.4. The SS values were 0.22 for both surfaces of the membrane, respectively. The relative immobilized BiBB amount measured by the ATR-FTIR peak area ratios for the two surfaces was statistically different (t-test with 95% confidence level). Thus all the subsequent

immobilizations were conducted on an orbital shaker with either 0.74 mmol or 2.67 mmol BiBB per membrane disc.

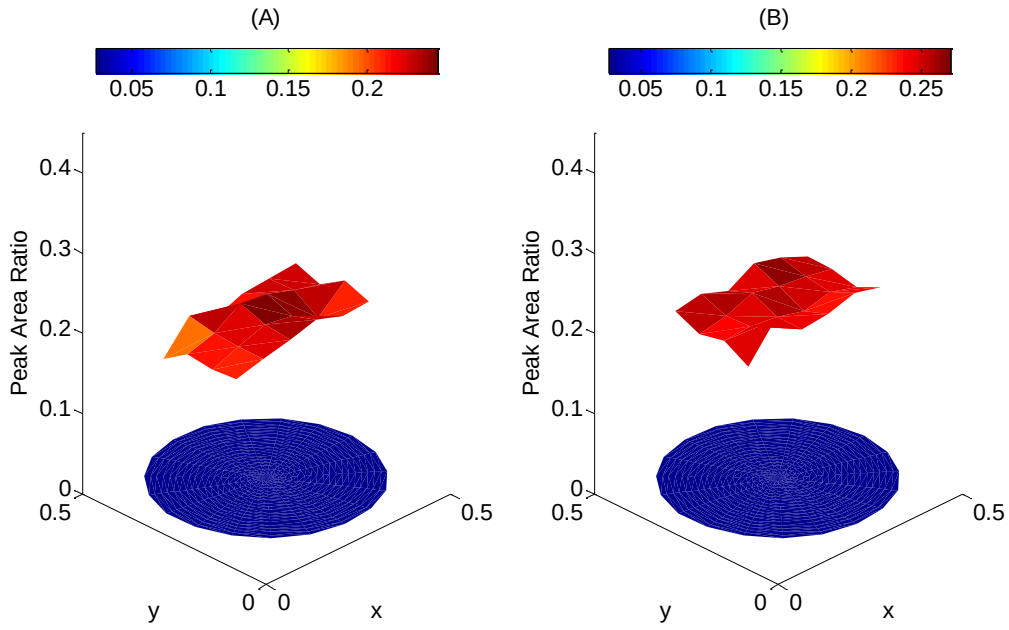

Figure 3.4: ATR-FTIR peak area ratios at 1680-1800 cm^{-1}/2700-3000 cm^{-1} for (A) top and (B) bottom surfaces of 0.5 M NaOH-treated membrane subjected to 0.74 mmol BiBB in DMF with agitation by shaking at 125 rpm.

3.3.3 Activator regenerated by electron transfer atom transfer radical polymerization (ARGET ATRP)

Following the analysis of the BiBB immobilization step, the ARGET ATRP polymerization conditions were investigated. First, the type of amine ligand and $CuBr_2$, ascorbic acid, and pH conditions were evaluated by UV-vis spectroscopy to investigate the $CuBr_2$ consumption by ascorbic acid over time in an aqueous medium. Second, polymer grafting and its evolution with time was evaluated from the ATR-FTIR peak area ratio using the optimal $CuBr_2$/amine ligand/ascorbic acid molar ratio determined by UV-vis spectroscopy.

3.3.3.1 UV-vis spectroscopy of $CuBr_2$/amine ligand/ascorbic acid molar ratios in aqueous media

$CuBr_2$ and ascorbic acid interactions were studied by UV-vis spectroscopy based on previous studies [55,56]. The $CuBr_2$ d-d transition is identified by a peak ranging in the 700-800 nm region [56]. Plots of the maximum absorbance in the 700-800 nm region as a function of time for different $CuBr_2$/amine ligand (PMDETA or bpy)/ascorbic acid molar ratios are presented in Figure 3.5.

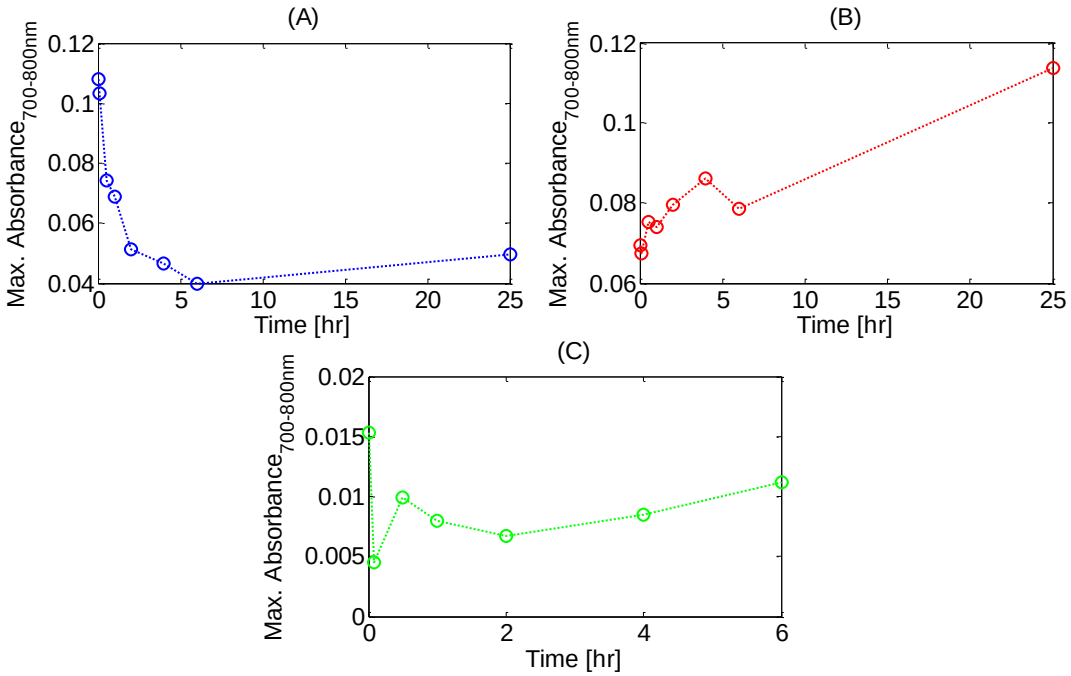

Figure 3.5: Maximum UV-vis absorbance between 700-800 nm as a function of time for (A) 1/1/2 $CuBr_2$/PMDETA/ascorbic acid molar ratio, (B) 1/10/2 $CuBr_2$/PMDETA/ascorbic acid molar ratio, and (C) 1/2/2 $CuBr_2$/bpy/ascorbic acid molar ratio; pH adjusted to ~12 in aqueous media.

The molar ratio 1/1/2 $CuBr_2$/PMDETA/ascorbic acid showed a decreasing peak height at 700-800 nm over time until 6 hours, which represents $CuBr_2$ reduction (Figure 3.5A) [56]. This was not observed when the PMDETA amount was increased tenfold (Figure 3.5B). It should be noted that excess amine is usually added to ensure that the catalyst is protected from side reactions during ARGET ATRP [63]. The excess amine seems to have impeded $CuBr_2$ reduction, as indicated by the increased maximum absorbance over time in the 700-800 nm region (Figure

3.5B). The exact reason for the increase is not understood, but the UV-vis maximum absorbance between 700-800 nm confirmed that a tenfold increase in PMDETA would not result in polymerization. The use of a ten times higher PMDETA to $CuBr_2$ molar ratio did not result in ARGET ATRP, as reported in the literature [57]. The ten times higher PMDETA to $CuBr_2$ molar ratio only allowed ARGET ATRP when a higher concentration of copper (i.e. 500 ppm vs. 153 ppm in this work) was used [57]. The explanation for the higher copper concentration needed was related to stability issues of PMDETA due to protonation: stability increased for less basic ligands [57]. Thus an alternative amine ligand for PMDETA, bpy, was tested (Figure 3.5C). For a molar ratio 1/2/2 of $CuBr_2$/bpy/ascorbic acid with the pH adjusted to ~12, a minimum was followed by a slight increase in the maximum UV-vis absorbance at 700-800 nm, representing $CuBr_2$ reduction immediately after ascorbic acid addition, followed by slight increase in $CuBr_2$ content. Thus the ascorbic acid consumed $CuBr_2$ instantaneously and continued to do so at a lower rate. A peak between 400-500 nm was observed which confirmed that an ascorbic acid + $CuBr_2$ charge transfer transition was present for 1/2/2 $CuBr_2$/bpy/ascorbic acid molar ratio (Appendix)[65]. The slight increase in $CuBr_2$ content after 2 hours in Figure 3.5C and the slight increase in $CuBr_2$ content after 6 hours in Figure 3.5A may have been attributed to the presence of oxygen which leaked into the system when taking aliquots for UV-vis sampling. Thus bpy is also a suitable amine ligand for $CuBr_2$ reduction, but the $CuBr_2$/bpy/ascorbic acid/immobilized BiBB molar ratio will need further investigation to improve control over the polymerization.

3.3.3.2 ARGET ATRP

ARGET ATRP was conducted with bpy as an amine ligand for the BiBB-modified membrane using 2.67 mmol of BiBB per membrane disc and soaked in DMF for at least two weeks before immobilization, with the 1/2/2 $CuBr_2$/bpy/ascorbic acid molar ratio. The $CuBr_2$/bpy/ascorbic acid/immobilized BiBB molar ratios were investigated in attempts to achieve linear polymerization behaviour, which is an indication of controlled polymerization (Table 3.9).

Table 3.9: ARGET ATRP experimental conditions

Entry	Immobilized BiBB/bpy/ascorbic acid/$CuBr_2$ molar ratio	NaBr [mM]	Sodium acrylate [M]	pH
I	1/0.25/0.25/0.125	1	1	8-9
II	1/0.25/0.25/0.125	5	1	8-9
III[a]	1/0.4/0.4/0.05	5	1	12
IV[a]	1/0.2/0.2/0.1	1/16 $CuBr_2$/NaBr molar ratio	1/3240 $CuBr_2$/sodium acrylate	8-9

[a] Membranes piece placed into individual vials under the same polymerization conditions, but for different polymerization times.

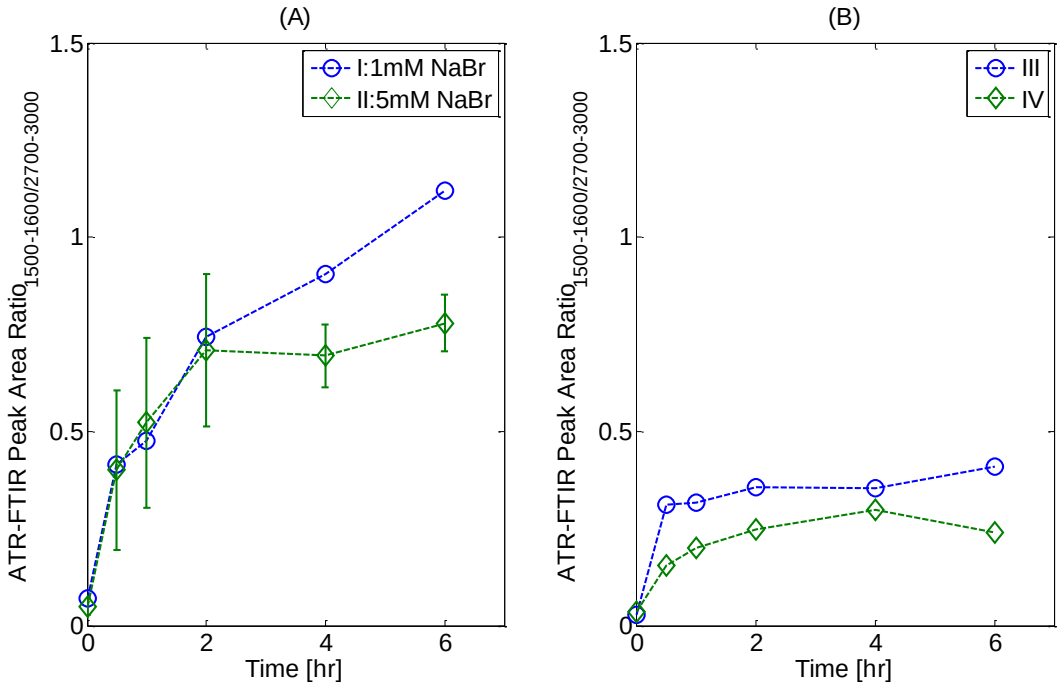

Figure 3.6: ATR – FTIR peak area ratio at 1500-1600 cm^{-1}/2700-3000 cm^{-1} over time for (A) varying NaBr concentrations with 1/0.25/0.25/0.125 immobilized BiBB/bpy/ascorbic acid/$CuBr_2$ molar ratio at pH 8-9 of conditions I and II (n=1 and n=2 for condition I and II respectively), and (B) parallel polymerization of membrane pieces in individual vials of conditions III and IV (n=1 for both conditions); unmodified membrane peak area ratio at 1500-1600 cm^{-1}/2700-3000 cm^{-1} is 0.016 ± 0.0017 (n=4).

When increasing the NaBr concentration from 1 mM to 5 mM (Figure 3.6A), there was no significant difference in peak area ratio for the first 2 hours. After four hours, there was

constant polymer content when using 5 mM NaBr concentration. In the literature, higher salt concentrations were used i.e. 10 mM, 30 mM, 100 mM, and 300 mM [59]. Increasing the salt concentration from 10 mM to 30 or 100 mM lowered the polymerization rate and more controlled polymerization was observed due to its promotion of higher $CuBr_2$ concentrations [59]. Perhaps adjusting to higher salt concentrations (i.e. 100 mM vs. 1 mM and 5 mM) would result in more linear polymer grafting evolution over time by decreasing the polymerization rate [59].

The peak area ratio-time profiles during polymerization (conditions I and II, Figure 3.6A) were compared with the UV-vis-time profile with the 1/2/2 $CuBr_2$/bpy/ascorbic acid molar ratio at pH 12 (Figure 3.5C). The increasing rate of polymerization with time was in general accordance with the decrease in maximum UV-vis peak absorbance at 700-800 nm, representing $CuBr_2$ reduction after ascorbic acid addition. As time progressed, the concentration of $CuBr_2$ slightly increased in the UV-vis experiment, indicating a lower amount of CuBr produced, which may explain the decrease in polymerization rate as time approached six hours. Again, the decrease in polymerization rate may be attributed to the presence of oxygen in the system oxidizing CuBr to $CuBr_2$. The result is in agreement with the generalized ATRP rate of polymerization equation (3.7), where the Cu(II) concentration is inversely proportional to the rate of polymerization. Although the experimental work demonstrated the inverse proportionality of Cu(II) concentrations to the rate of polymerization, the ATR-FTIR peak area ratio time profile demonstrated uncontrolled polymerization, with a plateau appearing after one or two hours of polymerization (Figure 3.6).

$$R_p = k_p[M][P^\bullet] = k_p K_{eq}[M][R-X]\frac{[Cu^I]}{[X-Cu^{II}]} \qquad (3.7)$$

where R_p = rate of polymerization [mol L^{-1} s^{-1}], k_p = polymerization rate constant [L mol^{-1} s^{-1}], [M] = monomer concentration [mol L^{-1}], [$P^\bullet$] = concentration of active radicals [mol L^{-1}], K_{eq} = equilibrium rate constant or ATRP rate constant [-], [R-X] = concentration of dormant chain ends [mol L^{-1}], [Cu^I] = concentration of copper(I) [mol L^{-1}], [Cu^{II}-X] = concentration of copper(II) [mol L^{-1}].

When conducting the polymerization with individual pieces of the BiBB-modified membranes having identical BiBB immobilization characteristics (conditions III and IV, Figure 3.6B), the polymerization was also uncontrolled, as illustrated by a plateau. The amount of polymer on the surface according to the ATR-FTIR peak area ratios was lowered as compared to polymerization on an intact membrane (Figure 3.6A vs. B). Gravimetry also confirmed the lower grafted polymer mass on the surface per milligram of BiBB modified membrane for conditions III and IV as compared to conditions I and II (i.e. negative mass data, which may have been affected by environmental humidity for condition III, and a mass five orders of magnitude lower, i.e. insignificant, for conditions IV as compared to conditions I and II). The plateau may be attributed to the oxygenation of the reaction medium during the addition of sodium acrylate solids into the vials and the low immobilized BiBB to $CuBr_2$ molar ratio (i.e. 1/0.05 and 1/0.1 for conditions III and IV respectively) leading to insufficient quantities of chain ends activated for propagation.

Hence, conditions I and II provided larger polymer quantities on the surface than conditions III and IV. The higher grafting content introduced significant swelling of the membrane when immersed in water, which was not previously reported in literature. These materials should therefore allow good levels of protein capture.

3.3.4 Lysozyme Static Binding Capacity

Preliminary static protein binding experiments with lysozyme were conducted for two types of poly(acrylic acid)-grafted membranes (PAA-*g*-RC), with a low poly(sodium acrylate) content (conditions III at 6 hours of polymerization) and a high poly(sodium acrylate) content (conditions II at 6 hours of polymerization).

Significant lysozyme static binding capacity was observed for 0.5 mg mL^{-1} initial lysozyme concentration in pH 5 phosphate citrate buffer, ~510 mg mL^{-1} and ~235 mg mL^{-1} for the PAA-*g*-RC membrane with high PAA and low PAA content respectively, after 24 hours of protein binding. This exceeds the reported literature value of 98.5 mg mL^{-1} by Singh *et al.* in 2008 [18] for weak cation exchange membrane adsorbers under static binding conditions of 2 mg mL^{-1} lysozyme in 10 mM potassium phosphate buffer at pH 7 for 16 hours.

3.4 Conclusions

The optimal conditions for BiBB immobilization were defined. The BiBB quantity used should be at least 0.74 mmol per membrane disc (~40 mg each) and the BiBB/TEA molar ratio should be 1/0.67. If membrane NaOH treatment is considered prior to BiBB immobilization, low NaOH concentrations should be employed (i.e. 0.5 M vs. 2 M). It is preferable to avoid NaOH treatment of the membrane to preserve its structural integrity, and DMF should be selected as solvent. This ensures a level of BiBB immobilization sufficient to be detectable by gravimetry and by ATR-FTIR. Uniformity/spatial distribution of the immobilized BiBB content across the membrane surface was improved when higher BiBB quantities (i.e. > 0.74 mmol) were used per membrane disc and with orbital shaking.

Successful poly(acrylic acid) grafting by ARGET ATRP was achieved. The polymer growth was not controlled, as the poly(sodium acrylate) content on the surface plateaued after the first one or two hours under all conditions. The highest grafting efficiency was achieved for a 1/0.25/0.25/0.125 immobilized BiBB/bpy/ascorbic acid/$CuBr_2$ molar ratio, 1 mM or 5 mM NaBr, and 1 M sodium acrylate at pH 8-9. Preliminary static protein binding capacity measurements for lysozyme was evaluated for the PAA-*g*-RC membrane with high and low PAA contents (510 vs. 235 mg mL^{-1} respectively). Hence, the PAA-*g*-RC membranes demonstrated good potential as weak cation exchange membrane adsorbers for protein capture, which will be further discussed in the next chapter.

4. Development of weak cation exchange membrane adsorbers for protein capture

4.1 Abstract

Weak cation exchange membrane adsorbers for the purification of human immunoglobin G were successfully developed via aqueous activator regenerated by electron transfer atom transfer radical polymerization (ARGET ATRP). The two-step process involved immobilization of the initiator, 2-bromoisobutyryl bromide (BiBB), on a regenerated cellulose (RC) membrane support layer (47 mm diameter disc) followed by grafting-from of poly(acrylic acid) by ARGET ATRP. The first step was studied by a 3^2 factorial design to determine the statistical effects of the RC membrane treatments (i.e. only methanol-washed RC membrane, 0nD; methanol-washed RC membrane and DMF storage for at least two weeks prior to immobilization, 0D; and methanol-washed RC membrane treated with 0.5 M NaOH followed by DMF storage, 0.5D) and the amount of BiBB used (i.e. 0, 0.74, and 2.67 mmol BiBB per membrane disc) on the relative and absolute immobilized BiBB amounts determined via ATR-FTIR and gravimetry, respectively. Storing the RC membranes in DMF for at least two weeks prior to immobilization, and treatment with 0.5 M NaOH followed by DMF storage gave statistically higher BiBB immobilization than only methanol-washed RC membranes (ANOVA, 95% confidence level). TGA and EDX also confirmed the presence of BiBB on the surface. Aqueous ARGET ATRP was then performed and there was a measurable increase in membrane diameter after polymerization. The calculated swelling factor for the poly(acrylic acid) grafted from the RC membrane (PAA-*g*-RC, 2 hr polymerization time) was 8. Finally, the dynamic protein binding capacity at 10% breakthrough ($DBC_{10\%}$) when employing 0.5 mg mL^{-1} IgG at a flow rate of 1 mL min^{-1} was measured. PAA-*g*-RC (2 hr) had the highest $DBC_{10\%}$ compared to 0D and 0D RC membranes using 2.67 mmol BiBB (0D 2.67) (30 vs. 4.4 and 6.1 mg mL^{-1}, respectively).

4.2 Introduction

Therapeutic proteins (e.g. monoclonal antibodies, mAbs) have increasingly been used for the treatment of cancers, autoimmune diseases, and other ailments [1]. To improve access to these indispensable products, production needs to be optimized for lower cost and higher protein

throughput. The inefficiency of production stems from the advances of increased cell titers in upstream bioprocessing for protein production [1], leading to a bottleneck in the downstream bioprocess. More specifically, chromatographic purification has become the limiting step in the process, where resins functionalized with binding sites for protein capture are used [4]. The resins are limited by the diffusion of proteins into their pores towards the binding sites and can result in pressure build-up along the column, which lowers the throughput. Moreover, labour is required for the loading/unloading, cleaning and packing of the resins, and is prone to inefficient column packing leading to lower separation resolution. As such, alternatives such as membrane adsorbers that are disposable, easy to handle, and not diffusion limited, leading to higher protein throughput, can be used. The major challenge facing membrane adsorbers is the need for higher protein binding capacities at high flow rates. Thus, the development of membrane adsorbers with higher protein binding capacity is required.

The preparation of cation exchange membrane adsorbers for protein capture via surface initiated atom transfer radical polymerization techniques on regenerated cellulose (RC) membranes is a two-step process whereby the initiator is first immobilized on the membrane, and followed by the polymerization of monomers with protein binding capabilities via electrostatic interactions. It was reported that the initiator immobilization level was low [13,14,40,42,44,47,48,50,69,104,118,119], often below the detection level of ATR-FTIR analysis [13,40]. Yet the subsequent polymerization step was successful, with detection achievable by ATR-FTIR.

In this investigation, BiBB immobilization factors such as RC membrane treatment with NaOH, storage in DMF, and the amount of BiBB used per membrane disc were optimized. This approach enabled an increase in the grafting of poly(acrylic acid) via ARGET ATRP, an ATRP method using less catalyst than traditional ATRP and able to proceed even under limited oxygen contamination in aqueous solution, to obtain membranes with high dynamic protein binding capacities for human immunoglobinG (IgG).

4.3 Materials and methods

4.3.1 Materials

Regenerated cellulose (RC) membranes from Whatman Inc. (RC60, pore size 1 μm, 47 mm diameter) were selected for use as the support layer and were purchased from VWR International (Mississauga, ON, Canada). *N*,*N*-Dimethylformamide (DMF; 99.8%, Sigma Aldrich, Oakville, ON, Canada) was dried over CaH_2 overnight, followed by vacuum distillation. Triethylamine (TEA; 99.5%, EMD Millipore Canada) was kept dry over 4Å molecular sieves. 2-Bromoisobutyryl bromide (BiBB; 98%, Sigma Aldrich, Oakville, ON, Canada), copper (II) bromide (99.999%, Sigma Aldrich, Oakville, ON, Canada), sodium acrylate (97%, Sigma Aldrich, Oakville, ON, Canada), 2,2′-bipyridine (bpy; 99%, Sigma Aldrich, Oakville, ON, Canada), Milli-Q water, ascorbic acid (Food grade, J.T. Baker Chemical Co., Center Valley, PA, USA), sodium bromide (ACS grade, BDH Chemicals, Toronto, ON, Canada), sodium hydroxide pellets (NaOH; 97%, Sigma Aldrich, Oakville, ON, Canada), ethanol, methanol, potassium chloride (Fisher Scientific, Canada), human IgG (Equitech-Bio, Inc. Kerrville, Texas, USA), sodium acetate (EMD Chemicals Inc., Gibbstown, USA), and glacial acetic acid (EMD Chemicals Inc., Gibbstown, USA) were used as is unless otherwise specified.

4.3.2 Membrane treatment

Prior to immobilization the RC membranes were soaked in methanol for 10 minutes, rinsed thoroughly with water and then THF, and dried in a vacuum oven overnight. These membranes were then either dipped into 0.5 M NaOH for ten seconds or were used as is. All the NaOH-treated membranes were subsequently rinsed with ethanol until neutral pH, rinsed in dry DMF once, and directly stored in dry DMF until immobilization. Membranes that were not treated with NaOH (i.e. 0 M NaOH treatment) were dried in the vacuum oven overnight prior to immobilization, or were stored in dry DMF for at least two weeks prior to immobilization.

4.3.3 Immobilization of initiator

2-Bromoisobutyryl bromide (BiBB) was used as the initiator. One Whatman RC60 membrane disc (47 mm diameter) was placed into a 250 mL glass jar with a plastic screw cap cover in ~12.5 mL of dry DMF. All the immobilization reactions were agitated on an orbital shaker (Thermo Scientific 2309 lab rotator, Canada) at 167 rpm immediately after adding the reagents. It should be noted that the volume of the solvent and the diameter of the container (~58

mm) prevented the membrane from flipping over during agitation of the reaction medium. Two BiBB quantities per membrane disc were considered with a BiBB/TEA molar ratio of ~1/0.67 in all cases (the average mass of the membrane was 40 mg):

i. Stoichiometric BiBB (0.74 mmol per membrane disc) - based on a degree of substitution (DS) of three for the RC membrane, and assuming 100% accessibility.
ii. Excess BiBB (2.67 mmol per membrane disc) - arbitrary value.

The jar containing one RC membrane disc and solvent was placed in an ice bath while the BiBB was added drop-wise. After 30 minutes, the ice bath was removed and the reaction medium was maintained at room temperature for at least 22 hours. All the immobilization reactions were performed under these conditions except for (ii) where TEA and BiBB were added in the following sequence: 0.1mL TEA + 0.125 mL BiBB drop-wise in an ice bath, 0.15 mL of TEA 15 minutes after the beginning of the immobilization, and then 0.2 mL of BiBB one hour after the first BiBB addition. This sequence allowed the consumption of impurities in the medium for improved immobilization. For conditions (ii), the ice bath was removed ~45 minutes after the second addition of BiBB. Subsequently, the heterogeneous reaction conditions of (ii) were maintained at room temperature for at least 22 hours after the first addition of BiBB. All the BiBB-modified membranes were then washed with THF three times (10 minute soak, 5 second soak, 45 minute soak), rinsed with methanol three times, and dried in a vacuum oven overnight. Mass and ATR-FTIR measurements were then completed for the RC membrane discs dried in a vacuum oven (30 in Hg, Fisher Scientific vacuum oven 280, Canada) at least overnight.

The BiBB density on RC membrane surface was calculated from gravimetry data by (4.1). A sample calculation can be found in the Appendix.

$$\text{BiBB density}\,[\text{BiBB molecules g RC}^{-1}] = \frac{\text{moles of immobilized BiBB} \times N_A}{\text{grams of regenerated cellulose}} \qquad (4.1)$$

where N_A = Avogadro's number.

4.3.4 ARGET ATRP

Deoxygenated Milli-Q water was sparged with N_2 for at least 30 minutes. The $CuBr_2$, 2,2′-bipyridine (bpy), and ascorbic acid quantities used were determined based on the quantity of

immobilized BiBB with a molar ratio 1/0.25/0.25/0.125 of immobilized BiBB/bpy/ascorbic acid/$CuBr_2$ with 1 or 100 mM sodium bromide, and 1 M sodium acrylate in 35 mL of deoxygenated Milli-Q water. The reagents were added in the following sequence under N_2 purge in a three-neck round bottom flask: $CuBr_2$, bpy, NaBr, 35 mL Milli-Q water, sodium acrylate, ascorbic acid, and finally the BiBB-modified membrane (0D 2.67). The pH was adjusted to ~8-9 with 1 M NaOH and the solution was agitated on an orbital shaker at ~167 rpm (Thermo Scientific 2309 lab rotator, Canada).

Immediately after the specified polymerization time (either 2 or 6 hours) the membrane samples were rinsed in Milli-Q water thrice, soaked in Milli-Q water (~35 mL) for at least 30 minutes, rinsed, soaked for 40 minutes, rinsed, soaked for 30 minutes, and rinsed with Milli-Q water again. Samples of the rinsing water were taken for UV-vis spectroscopy to detect any residual sodium acrylate, $CuBr_2$, bpy, or ascorbic acid after each washing step. The washing procedure was thus determined to be sufficient according to UV-vis spectra approaching the baseline of zero (Figure B1, Appendix). The washed poly(acrylic acid)-grafted RC membranes (PAA-*g*-RC) were then placed on Petri dishes for drying overnight under ambient conditions. Afterwards, the membranes were placed into a vacuum oven at room temperature (30 in Hg, Fisher Scientific vacuum oven 280, Canada) at least overnight prior to the mass and ATR-FTIR measurements. The grafting ratio and theoretical molecular weight were calculated according to the following equations. The sample calculations can be found in the Appendix.

$$\text{Grafting ratio}\,[\%] = \frac{W_p - W_i}{W_i} \times 100\% \qquad (4.2)$$

where W_p = mass of PAA-*g*-RC membrane [mg], W_i = mass of BiBB immobilized membrane [mg].

$$M_{n,theo} = \frac{n_{m0}}{n_{BiBB}} \times MW_{monomer} \times conversion \qquad (4.3)$$

where $M_{n,theo}$ = theoretical number-average molecular weight of polymer [g mol^{-1}], n_{m0} = quantity of monomer initially added [mol], n_{BiBB} = quantity of BiBB immobilized [mol], $MW_{monomer}$ = molecular weight of monomer [g mol^{-1}].

Monomer conversion was determined gravimetrically by converting the known polymer mass grafted on the membrane to moles and dividing it by the initial moles of monomer used at the start of polymerization.

4.3.5 ATR-FTIR

A Bruker Tensor 27 FTIR spectrometer (Billerica, MA, USA) with a PIKE MiRacle ATR accessory (Madison, WI, USA) single point reflection with a ZnSe crystal and an angle of incidence of 45° (64 scans, 4 cm^{-1} resolution) was used. Baseline correction and atmospheric correction for CO_2 were applied by OPUS software. Twenty four points were measured across the membrane in a 4x6 grid. Thus, 48 measurements were taken for each membrane sample unless otherwise specified.

The BiBB immobilization was estimated by taking the peak area ratios between 1680-1800 cm^{-1} and 2700-3000 cm^{-1}, corresponding to the carbonyl [124] and C-H groups respectively, using a baseline of zero. Polymer grafting was evaluated from the peak areas ratios between 1500-1600 cm^{-1} and 2700-3000 cm^{-1} for the ionized carboxylic groups [18] and C-H groups, respectively, using a baseline of zero for semi-quantitative analysis.

4.3.6 Environmental scanning electron microscopy and energy dispersive x-ray spectroscopy

An environmental scanning electron microscope (ESEM Leo 1530, Carl Zeiss AG, Germany) was used to observe the surface morphology of BiBB-modified samples at 1000x magnification. Membrane samples were coated with gold prior to the analysis (ESEM gold coating unit Desk II, Denton Vacuum, USA). Energy dispersive x-ray spectroscopy (EDX) was also used to obtain estimated weight percentages of the surface elements.

4.3.7 Thermogravimetric analysis

Thermogravimetric analysis (TGA) was conducted on the BiBB-modified samples (Q500, TA Instruments, USA). The samples (~3-4 mg) were first equilibrated at 25°C, heated to 50°C at 10°C min^{-1}, equilibrated at 50°C, and then the temperature was increased to 600°C at 10°C min^{-1}. The first derivative of the recorded mass over temperature curve was calculated and plotted.

4.3.8 RC membrane swelling tests

Membranes were cut with a 19 mm die and only the polymer-grafted RC membranes were cut while they were wet. The samples were left to dry at room temperature for 24 hours and their mass was measured. The membranes were then soaked for 6 hours into pH 5 acetate buffer made from 0.2 M sodium acetate and 0.2 M acetic acid on an orbital shaker (Thermo Scientific 2309 lab rotator, Canada). Subsequently, the membranes were placed on a plastic mesh with a Kimwipe underneath for 5 minutes for each side of the membrane. This was done to remove the water on the surface of the membrane. The mass of the swollen membrane was then measured. The swelling factor was calculated by taking the ratio of the swollen mass to the dry mass.

4.3.9 Dynamic protein binding capacity for human IgG

The wet PAA-*g*-RC membranes were cut into 25 or 47 mm diameter pieces using a die. An ÄKTA Prime system (GE Healthcare BioSciences, Uppsala, Sweden) was used for the dynamic protein binding capacity tests. The system was first flushed with 20% ethanol and deionized water for ten minutes each. An equilibration buffer was made by mixing 0.2 M sodium acetate and 0.2 M acetic acid to obtain a pH of 5. A binding buffer was made consisting of 0.5 mg mL^{-1} of IgG in the equilibration buffer. An elution buffer was made consisting of 1 M KCl in the equilibration buffer. Depending on the size of the PAA-*g*-RC membrane, it was placed into a 25 or 47 mm stainless steel Natrix membrane holder (Burlington, ON, Canada) and connected to the ÄKTA system. The equilibration lasted 10 minutes at a flow rate of 1 mL min^{-1}. Binding lasted for 50 minutes at the same flow rate. The membranes were then washed with the equilibration buffer for 20 minutes, or 40 minutes at 1 mL min^{-1}. Then the proteins were eluted with the elution buffer for 20 minutes at a flow rate of 2 mL min^{-1}. The UV absorbance at 280 nm was used for protein binding and for elution detection. Single point calibration was conducted for a 0.5 mg mL^{-1} IgG standard. The dynamic binding capacities at 10% breakthrough were computed by integration of the concentration versus retention volume as mentioned in [128] (4.4). Outliers on the breakthrough curves were removed using the MATLAB code found in the Appendix.

$$\text{Dynamic binding capacity (DBC)}\,[\text{mg mL}^{-1}] = \frac{\int_0^{V_p} (c_0 - c)\,dV - c_0 V_0}{V_m} \qquad (4.4)$$

where V_p = loading volume of protein solution at 10% breakthrough [mL], V_0 = dead volume of set-up in breakthrough mode [mL], V_m = membrane volume [mL], c_0 = feed protein concentration [mg mL^{-1}] (i.e. 0.5 mg mL^{-1} IgG), c = protein concentration measured at outlet [mg mL^{-1}].

4.3.10 Statistical analysis

A 3^2 factorial design was employed to observe the effects of the BiBB quantity used per membrane disc (0, 0.74, 2.67 mmol) and the RC membrane treatments prior to immobilization (methanol-washed RC membrane, 0nD; methanol-washed RC membrane stored in DMF for at least two weeks prior to BiBB immobilization, 0D; and methanol-washed RC membrane treated with 0.5M NaOH and subsequent DMF storage prior to immobilization, 0.5D) on the ATR-FTIR peak area ratio (i.e. the peaks at 1600-1800 cm^{-1}/2700-3000 cm^{-1}) and the degree of substitution. These factors were analyzed using ANOVA (95% confidence level) for statistical significance. Each condition was replicated 3 times with 48 repeated measurement on each sample for ATR-FTIR. T-tests were also used with a confidence level of 95%. The error bars represent the standard error on the mean unless otherwise specified.

4.4 Results and Discussion

4.4.1 Immobilization of initiator

In order to optimize the amount of BiBB immobilized on the surface, milder conditions achieving the same level of BiBB immobilization as for the NaOH-treated membranes were required in order to preserve the structural integrity of the membrane. The working hypothesis was that NaOH allowed for better accessibility of BiBB to the hydroxyl sites in the cellulose fibres. Similarly, the membrane can be swollen such that intermolecular interactions among cellulose chains are disrupted by the solvent to improve the accessibility of the hydroxyl groups for the reaction. The experimental conditions used for this study with a 3^2 factorial design are listed in Table 4.1.

Table 4.1: 3^2 factorial design of BiBB quantity used per membrane disc and RC membrane treatment with agitation by shaker

Name	BiBB quantity used per membrane disc [mmol]	RC membrane treatment
0nD	0 (0)	0 (MeOH)
0nD 0.74	1 (0.74)	0 (MeOH)
0nD 2.67	2 (2.67)	0 (MeOH)
0D	0 (0)	1 (MeOH + DMF)
0D 0.74	1 (0.74)	1 (MeOH + DMF)
0D 2.67	2 (2.67)	1 (MeOH + DMF)
0.5D	0 (0)	2 (MeOH + 0.5M NaOH + DMF)
0.5D 0.74	1 (0.74)	2 (MeOH + 0.5M NaOH + DMF)
0.5D 2.67	2 (2.67)	2 (MeOH + 0.5M NaOH + DMF)

MeOH = methanol-washed and dried; MeOH + DMF = methanol-washed and dried + DMF storage for at least 2 weeks; MeOH + DMF + 0.5M NaOH = methanol-washed and dried + DMF storage + 0.5M NaOH treatment.

4.4.1.1 ESEM and EDX for the 3^2 factorial design treatment conditions

ESEM images for the 9 initiator immobilization conditions were recorded with 1K magnification. Although there were no visible differences amongst the samples according to ESEM images (Figure 4.1), EDX analysis demonstrated differences in their surface elemental composition (Figure 4.2).

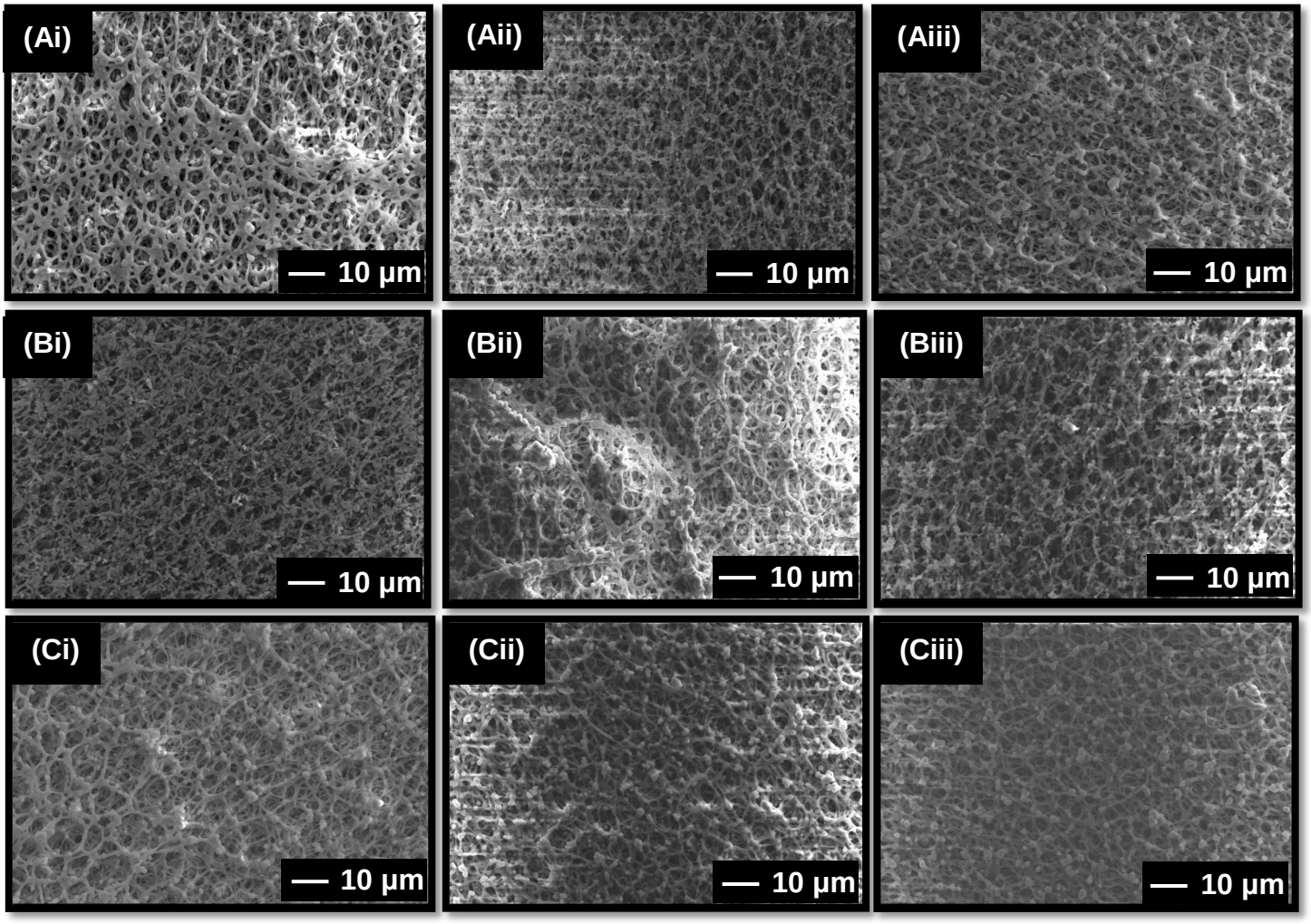

Figure 4.1: ESEM images for (Ai) 0nD, (Aii) 0nD 0.74, (Aiii) 0nD 2.67, (Bi) 0D, (Bii) 0D 0.74, (Biii) 0D 2.67, (Ci) 0.5D, (Cii) 0.5D 0.74, and (Ciii) 0.5D 2.67 BiBB immobilization conditions at 1K magnification; Note: No distinction was made whether the surfaces were from the top or bottom of the membrane for ESEM analysis.

Six different elements were detected on the membrane samples. The high carbon and oxygen content confirmed the presence of regenerated cellulose from the support layer, the major component. Next, it was observed that with the addition of both 0.74 and 2.67 mmol BiBB per membrane disc there was bromine detected, which confirmed the presence of immobilized BiBB. EDX also detected nitrogen on 0D 2.67, 0.5D 0.74, and 0.5D 2.67, which may have come from residual DMF. Moreover, there were some salts (NaCl) on the 0.5D membrane sample, possibly due to impurities on the surface of the membrane.

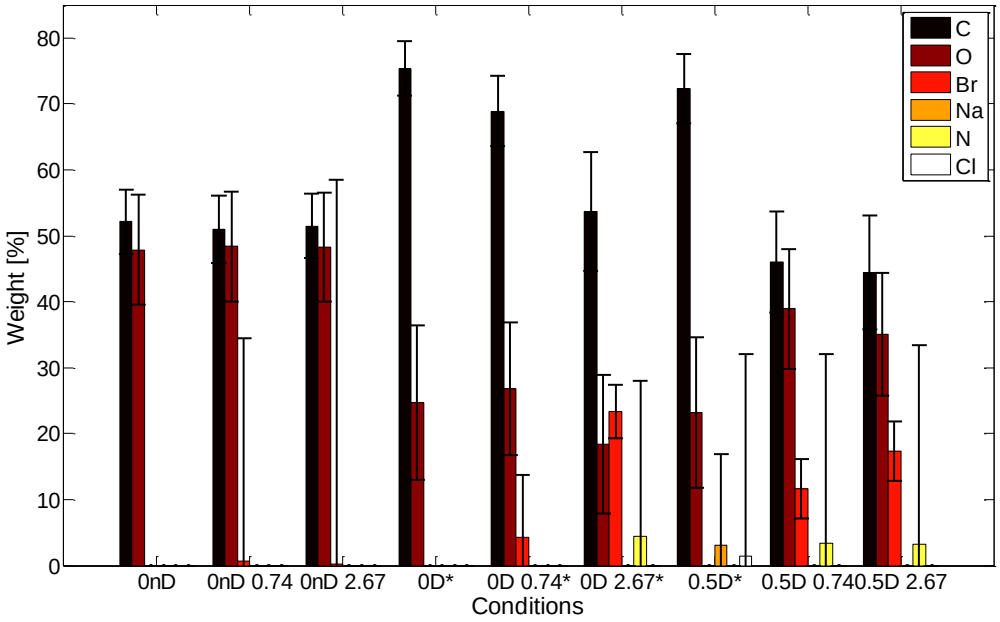

Figure 4.2: Carbon, oxygen, bromine, sodium, nitrogen, chlorine weight percentages for the 9 initiator immobilization conditions; The error bars represents the fitting errors; *Spot measurement as opposed to full sample area measurement; A table of the weight % values can be found in the Appendix.

When comparing the samples amongst each other, the higher carbon content of samples 0D, 0D 0.74, 0D 2.67 and 0.5D may have been due to sampling errors, as only one spot of the membrane was measured as opposed to a full area scan for the elemental composition measurements. Furthermore, as expected, the storage in DMF and the use of 0.5 M NaOH treatment yielded higher bromine contents on the surface than only methanol-washed RC membranes (0D 0.74, 0D 2.67, 0.5D 0.74, and 0.5D 2.67 vs. 0nD 0.74 and 0nD 2.67, Figure 4.2). The storage of RC into DMF prior to immobilization helped to swell the cellulose [83,99]. Similarly, the NaOH treatment was able to swell and activate the hydroxyl groups for more substitution of BiBB on the RC membrane. When comparing the 0.5 M NaOH-treated, methanol-washed RC membranes and the DMF-stored, methanol-washed RC membranes using 2.67 mmol BiBB per membrane disc (i.e. 0.5D 2.67 vs. 0D 2.67), 0D 2.67 had a higher bromine content than 0.5D 2.67. However, if replicates were taken for EDX analysis, the standard errors may demonstrate that the two conditions yielded very similar bromine contents. Furthermore, the fitting errors (represented by the error bars in Figure 4.2) for the bromine element for 0nD 0.74

and 0nD 2.67 were large, which may mean that the BiBB contents for those conditions were negligible.

4.4.1.2 Thermal degradation studies on unmodified and BiBB-modified RC membrane samples

Thermogravimetric analysis complemented EDX analysis in confirming the presence of immobilized BiBB on the RC membranes after DMF storage and NaOH treatment (0D vs. 0.5D, respectively).

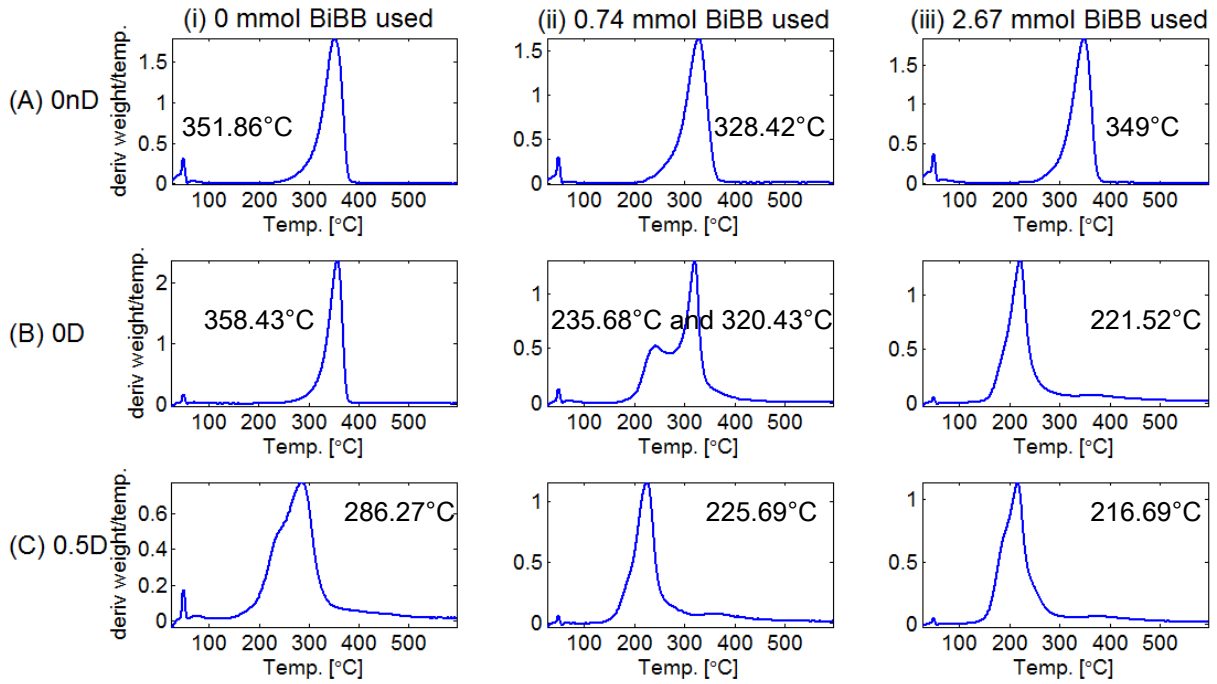

Figure 4.3: First derivative TGA plots for (Ai) 0nD, (Aii) 0nD 0.74, (Aiii) 0nD 2.67, (Bi) 0D, (Bii) 0D 0.74, (Biii) 0D 2.67, (Ci) 0.5D, (Cii) 0.5D 0.74, and (Ciii) 0.5D 2.67 BiBB immobilization conditions.

In the literature, the microcrystalline cellulose (MCC) degradation temperature was reported as 368°C, whereas MCC-BiBB (DS = 0.92) degraded at 267°C [111]. Although MCC is structurally different from the RC membranes, the degradation temperatures were within the

same order of magnitude as the results in Figure 4.3 and a lower degradation temperature was also observed when BiBB was immobilized onto the surface.

For example, when comparing rows (B) and (C) in Figure 4.3, the maximum degradation temperature decreased when the BiBB quantity used per membrane disc was increased for the immobilization reaction. With increased BiBB immobilized, more hydrogen bromide is formed in the degradation of BiBB-modified RC membrane, leading to degradation at lower temperatures especially for 0D and 0.5D-treated membranes [111]. Thus, the fairly constant degradation temperature for 0nD RC membranes as BiBB quantities per membrane disc increased for the reaction (Figure 4.3 row A), may have demonstrated the lack of BiBB immobilized for the 0nD conditions.

When comparing columns (ii) and (iii) in Figure 4.3, the degradation temperature also decreased with each treatment. This demonstrates the increasing BiBB immobilization on the RC membrane with the 0D and 0.5D treatment, since more BiBB immobilized means more hydrogen bromide produced and faster degradation. When comparing the 0D and 0.5D treatments to 0nD (Figure 4.3, column i), the maximum degradation temperature decreased significantly with the application of the 0.5 M NaOH treatment. This may be related to lower structural stability of the cellulose after the 0.5 M NaOH treatment.

4.4.1.3 Effects of RC membrane treatment and BiBB quantities used per membrane quantity on ATR-FTIR peak area ratios and the degree of substitution of immobilized BiBB

From the ATR-FTIR peak area ratios and the degree of substitution calculated by gravimetry, a higher amount of BiBB used per membrane disc and RC membrane treatment, whether by storage in DMF for two weeks prior to immobilization or with 0.5 M NaOH, gave higher immobilized BiBB contents (Figure 4.4A). The highest DS obtained was ~0.45 for the 0.5 M NaOH-treated, methanol-washed RC membrane and using the highest BiBB quantity of 2.67 mmol per membrane disc (Figure 4.4B). The tables of the ATR-FTIR peak area ratios and DS values are shown in the Appendix.

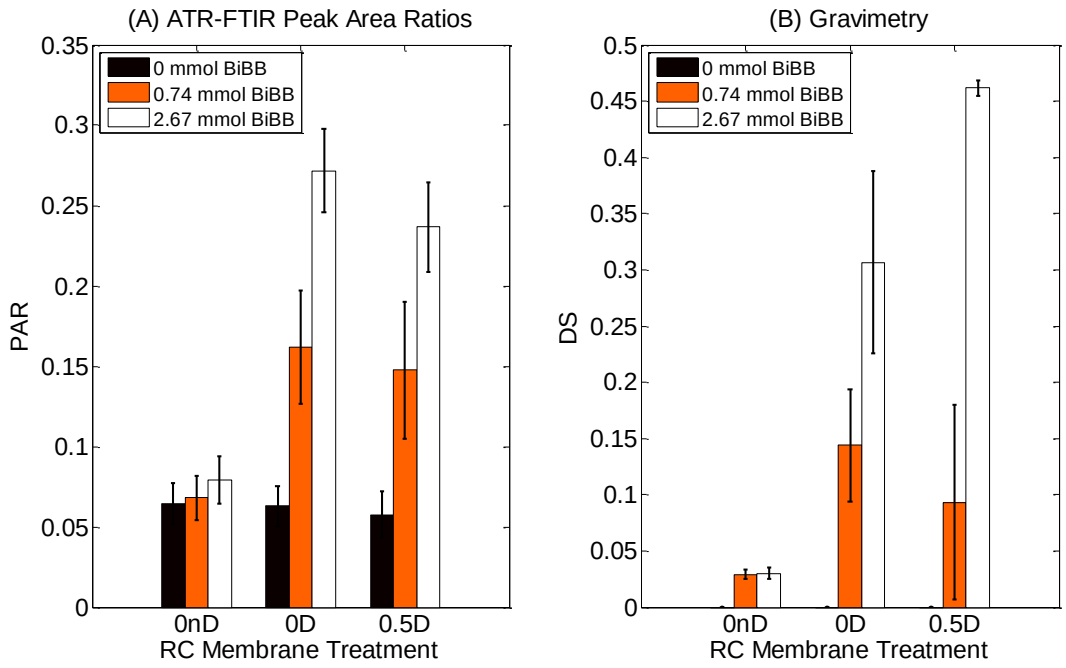

Figure 4.4: Effect of BiBB quantity used per membrane disc and RC membrane treatment on (A) ATR-FTIR peak area ratios (PAR) at 1680-1800 cm^{-1}/2700-3000 cm^{-1} (n=3 for each bar) and (B) DS of BiBB-modified RC membrane from gravimetry (n=3 for each bar).

Table 4.2: ANOVA analysis of BiBB quantity used per membrane disc, DMF storage, replication and membrane surface for the ATR-FTIR peak area ratios at 1680-1800 cm^{-1}/2700-3000 cm^{-1}

	SS	DF	MS	F	F_{crit}	
Membrane surface (i.e. top or bottom)	0.0087	1	0.0087	0.087	4.54	Not significant
Replication	0.0074	2	0.0037	0.037	3.68	Not significant
RC membrane treatments	2.19	2	1.09	10.95	3.68	Significant
BiBB quantity used per membrane disc	3.90	2	1.95	19.51	3.68	Significant
RC membrane treatments x BiBB quantity used per membrane disc Interaction	1.57	4	0.39	3.93	3.06	Significant
Experimental error	1.50	15	0.10			
Sampling error	0.81	1269	0.00060			
Total	9.98	1295				

SS = sum of squares; DF = degree of freedom; MS = mean squares; F = f-value; F_{crit} = critical f-value.

ANOVA analysis of the ATR-FTIR peak area ratios for the 3^2 factorial conditions is presented in Table 4.2. In the ANOVA analysis (Table 4.2), blocking was first applied and indicated that the experiments were reproducible and that there were no differences in relative BiBB content between the top or bottom membrane surfaces based on ATR-FTIR peak area ratios (PAR). There were no differences in relative BiBB content between the top or bottom membrane surface as compared to the ANOVA analysis in Chapter 3.3.2 due to the use of the orbital shaker and higher amounts of BiBB quantity used per membrane disc (i.e. > 0.74 mmol BiBB) in the present chapter rather than stir bar agitation (Chapter 3.3.2). As for the RC membrane treatments, the influence of the treatments towards the ATR-FTIR peak area ratios was statistically significant. Thus, it can be concluded that DMF storage and the 0.5 M NaOH treatment yielded higher ATR-FTIR peak area ratios than the 0nD conditions, confirming a higher quantity of initiator. Moreover, consistently with the results in [14] and the preliminary results observed in this thesis, increasing the BiBB quantity used per membrane disc increased the amount of initiator immobilized on the surface. Lastly, there were interactions of the treatments and the BiBB quantity used per membrane disc that influenced the ATR-FTIR peak area ratios. Similarly, ANOVA analysis was applied to the DS values determined by gravimetry (Table 4.3). Again, the RC membrane treatments and BiBB quantity used per membrane disc had an effect on the quantity of immobilized initiator and the experiments were reproducible.

Table 4.3: ANOVA analysis of BiBB quantity used, DMF storage, and replication for the gravimetry (DS) results, excluding the 0 mmol BiBB quantity used data

	SS	DF	MS	F	F_{crit}	
Replication	0.011	2	0.0057	0.64	3.52	Not significant
RC membrane treatments	0.20	2	0.10	11.57	3.52	Significant
BiBB quantity used per membrane disc	0.14	1	0.14	15.98	4.38	Significant
RC membrane treatments x BiBB quantity used per membrane disc Interaction	0.10	2	0.051	5.75	3.52	Significant
Experimental error	0.089	10	0.0089			
Total	0.55	17				

SS = sum of squares; DF = degree of freedom; MS = mean squares; F = f-value; F_{crit} = critical f-value.

From gravimetry, the estimated initiator density (BiBB molecules per gram of RC) was also calculated for comparison of the present immobilization method (Table 4.4) with the literature.

Table 4.4: Estimated BiBB density (molecules g RC^{-1}, n=3)

Immobilization conditions	BiBB density [molecules x 10^{-19} g^{-1} RC]
0nD 0.74	11 ± 2
0nD 2.67	11 ± 2
0D 0.74	54 ± 19
0D 2.67	144 ± 35
0.5D 0.74	35 ± 32
0.5 2.67	172 ± 3

The BiBB density, estimated as the number molecules of BiBB per gram of RC membrane, was lower than reported in [14], which used the same RC membrane. The highest reported BiBB density in the literature was 246 x 10^{19} molecules BiBB per gram of RC membrane when using an initial BiBB concentration of 21.5 mM per ten RC membranes [14]. The lowest reported initiator density was 103 x 10^{19} molecules BiBB per gram of RC membrane for an initial BiBB concentration of 1.79 mM for ten RC membranes [14]. In comparison, the

highest BiBB density in Table 4.4 was 171 x 10^{19} molecules BiBB per gram of RC membrane for an initial BiBB concentration of 214 mM per membrane disc. ATR-FTIR was able to detect the carbonyl groups on the surface in the present case, whereas the BiBB in [14] was undetectable by ATR-FTIR, in spite of the higher initiator density calculated. The present work demonstrated that initiator densities as low as ~11 x 10^{19} molecules g^{-1} RC can be detected by ATR-FTIR, and that low concentrations of BiBB per ten RC membranes used in [14] may not yield high immobilization levels. Moreover, the usefulness of the method to calculate the BiBB density by HPLC analysis, to measure BiBB concentration in the reaction medium before and after the immobilization in [14] may have been limited.

4.4.2 Activator regenerated by electron transfer atom transfer radical polymerization (ARGET ATRP)

The immobilization conditions under which the RC membranes were able to best resist physical disintegration during the polymerization were determined to be 0D 2.67.

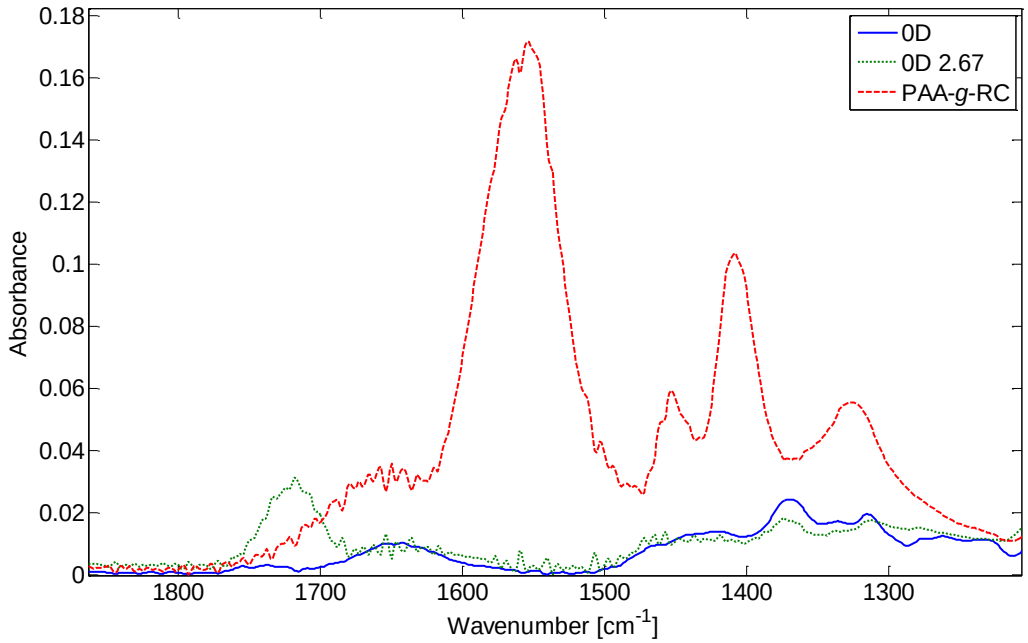

Figure 4.5: ATR-FTIR spectra for 0D, 0D 2.67, and PAA-*g*-RC (2 hours polymerization time) membrane.

The poly(acrylic acid)-modified membranes, PAA-*g*-RC (2 hr), were characterized by ATR-FTIR (Figure 4.5). The appearance of a peak between 1500-1600 cm^{-1} and an increase in intensity for a peak around 1400-1500 cm^{-1} confirmed the presence of ionized carboxylic acid groups characteristic for poly(acrylic acid) as reported in [18].

Gravimetry was also used to estimate the polymerization yield (Table 4.5). The monomer conversion was low but the grafting ratios were consistently above 100%, which may be due to the excess monomer used in comparison to the BiBB-modified RC membrane mass (i.e. 3.29 g sodium acrylate vs. ~ 48-54 mg BiBB-modified RC membrane). PAA quantification was also attempted by cleaving off the chains via acid hydrolysis. SEC and NMR analyses were then attempted. Unfortunately, the amounts of material recovered by that procedure were insufficient, so a better protocol will need to be investigated to remove any impurities in the system and to ensure that the recovered material is indeed PAA. Thus, theoretical number-average molecular weight ($M_{n,theo}$) were rather determined by gravimetry, which suggests that oligomers were grafted from the surface. Longer polymerization times and lower NaBr concentrations could be used to increase the conversion for higher $M_{n,theo}$ as observed in Table 4.5 (t-tests, 95% confidence level).

Table 4.5: Monomer conversion, theoretical number-average molecular weight, and grafting ratio of PAA-*g*-RC membrane corresponding to ARGET ATRP conditions of 1/0.25/0.25/0.125 immobilized BiBB/bpy/ascorbic acid/$CuBr_2$ molar ratio with 1 or 100mM NaBr and 2 or 6 hours polymerization

Entry	NaBr [mM]	Time [hr]	Conversion[%][a]	$M_{n,theo}$ [g mol^{-1}][a]	Grafting ratio [%] [a]
I	100	2	1.8 ± 0.5 (n=4)	682 ± 86 (n=4)	109 ± 28 (n=4)
II	1	6	3.4 ± 0.4 (n=2)	1052 ± 17 (n=2)	202 ± 20 (n=2)

[a] Calculated by gravimetry; sample calculations can be found in the Appendix.

Even though the estimated molecular weights obtained were low, the wet membrane significantly increased in diameter after polymerization (i.e. from a 47 mm diameter circle to an ellipse with 60 mm at its major axis and 50 mm at its minor axis). Images comparing the unmodified 47 mm RC membrane, wet PAA-*g*-RC (2 hr) membrane, and dried PAA-*g*-RC (2 hr)

membrane are shown in Figure 4.6. Note: PAA-*g*-RC (2 hr) membrane can either shrivel when dried or maintain the shape of its wet form depending on which side of the membrane's surface dries on the glass surface.

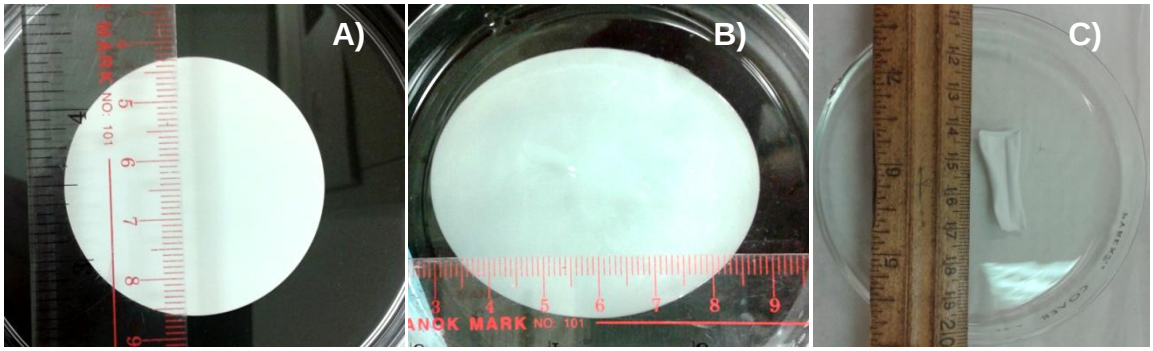

Figure 4.6: Appearance of (A) unmodified 47 mm RC membrane, (B) wet PAA-*g*-RC (2 hr) membrane, and (C) dried PAA-*g*-RC (2 hr) membrane.

The swelling factors for the 0D, 0D 2.67, and PAA-*g*-RC (2 hr) membrane were calculated (Table 4.6). The PAA-*g*-RC (2 hr) membrane swelled to eight times its dry mass after soaking into a pH 5 acetate buffer solution.

Table 4.6: Swelling factor of 0D, 0D 2.67, and PAA-*g*-RC (2 hr) membrane in pH 5 acetate buffer solution

Membrane	Swelling factor [-]
0D	6.26 ± 0.67[a]
0D 2.67	4.18 ± 0.33[b]
PAA-*g*-RC (2 hr)	8.00 ± 0.51[a]

[a] n=2; [b] n=3.

4.4.3 Dynamic protein binding capacity for IgG

The breakthrough curves for 0D, 0D 2.67, and PAA-*g*-RC (2 hr) membranes each with three replicates are presented in Figure 4.7. The corresponding average dynamic binding capacity at 10% breakthrough for the IgG on 0D, 0D 2.67, and PAA-*g*-RC (2 hr) membranes are shown in Table 4.7. When comparing the breakthrough curves for the 0D and 0D 2.67 replicates with the

PAA-*g*-RC (2 hr) membrane replicates, initial breakthrough was fast for 0D and 0D 2.67, indicating negligible protein binding on these membranes as reflected by their low $DBC_{10\%}$ (Figure 4.7 and Table 4.7).

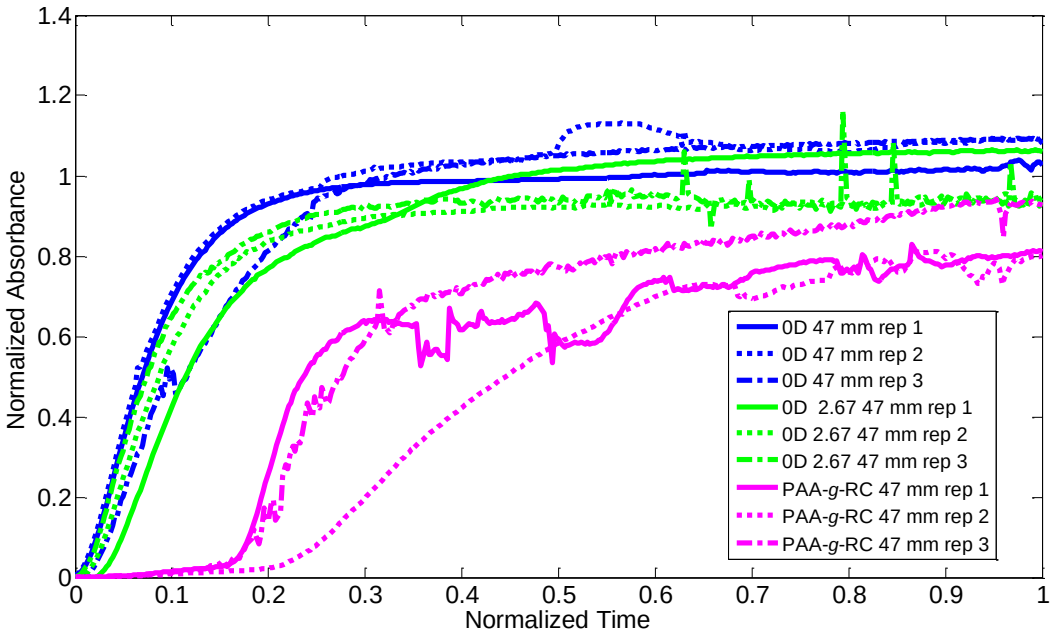

Figure 4.7: Normalized breakthrough curves of 0D, 0D 2.67, and PAA-*g*-RC (2 hr) 47 mm diameter membranes with three replicates (rep) for each condition; The breakthrough curves were normalized against the maximum possible absorbance from feed IgG with concentration of 0.5 mg mL^{-1} and time was normalized with the time at which the binding step ended; All the outliers in the curves were removed using the MATLAB code in the Appendix.

As a result, the 0D and 0D 2.67 RC membranes both yielded the same dynamic binding capacity for IgG at 10% breakthrough according to the t-test when using a 47 mm diameter membrane holder (95% confidence level). With the PAA-*g*-RC (2 hr) membrane, a statistically higher $DBC_{10\%}$ of 30 mg mL^{-1} was achieved using the 47 mm diameter membrane (t-test, 95% confidence level, Table 4.7). Its $DBC_{10\%}$ was on the same order of magnitude as the Repligen commercially available protein A resins (i.e. $DBC_{10\%}$ 15-33 mg mL^{-1} IgG at flow rates greater than 1 mL min^{-1}) [129]. Similarly, UV-initiated PAA grafting-from two different Sartorius RC

membranes yielded $DBC_{10\%}$ values of 34.6 and 37.2 mg mL^{-1} IgG at a 1mL min^{-1} flowrate of 20 mM sodium acetate buffer (pH 5) using an Äkta Purifier system [130].

Table 4.7: DBC at 10% breakthrough for 0D, 0D 2.67, and PAA-*g*-RC (2 hr) membrane, (n=3 unless otherwise specified)

Type of RC membrane	Membrane diameter [mm]	Dry thickness [μm]	$DBC_{10\%}$ [mg mL^{-1}]
0D	47	74 ± 3	4.4 ± 0.9[c]
0D 2.67	47	78 ± 5[b]	5.7 ± 1.3[c]
PAA-*g*-RC (2 hr)[a]	25	93 ± 0.5	141.5[d]
PAA-*g*-RC (2 hr)[a]	25	93 ± 0.5	11.9[d]
PAA-*g*-RC (2 hr)	47	93 ± 0.5	30 ± 2.9

[a] From the same RC sample; [b] n=2;[c] Statistically the same; [d] n=1.

However, the polymer grafting seems to be non-uniform: the dynamic protein binding capacities of two 25 mm membrane samples cut from the same piece of PAA-*g*-RC (2 hr) membrane were compared and shown to be very different (11.9 vs. 141.5 mg mL^{-1}, Table 4.7). This suggests that on an intact PAA-*g*-RC (2 hr) membrane, there were regions on the surface with varying polymer quantities since the immobilized BiBB was not distributed uniformly across the membrane surface prior to polymerization (Figure 4.8).

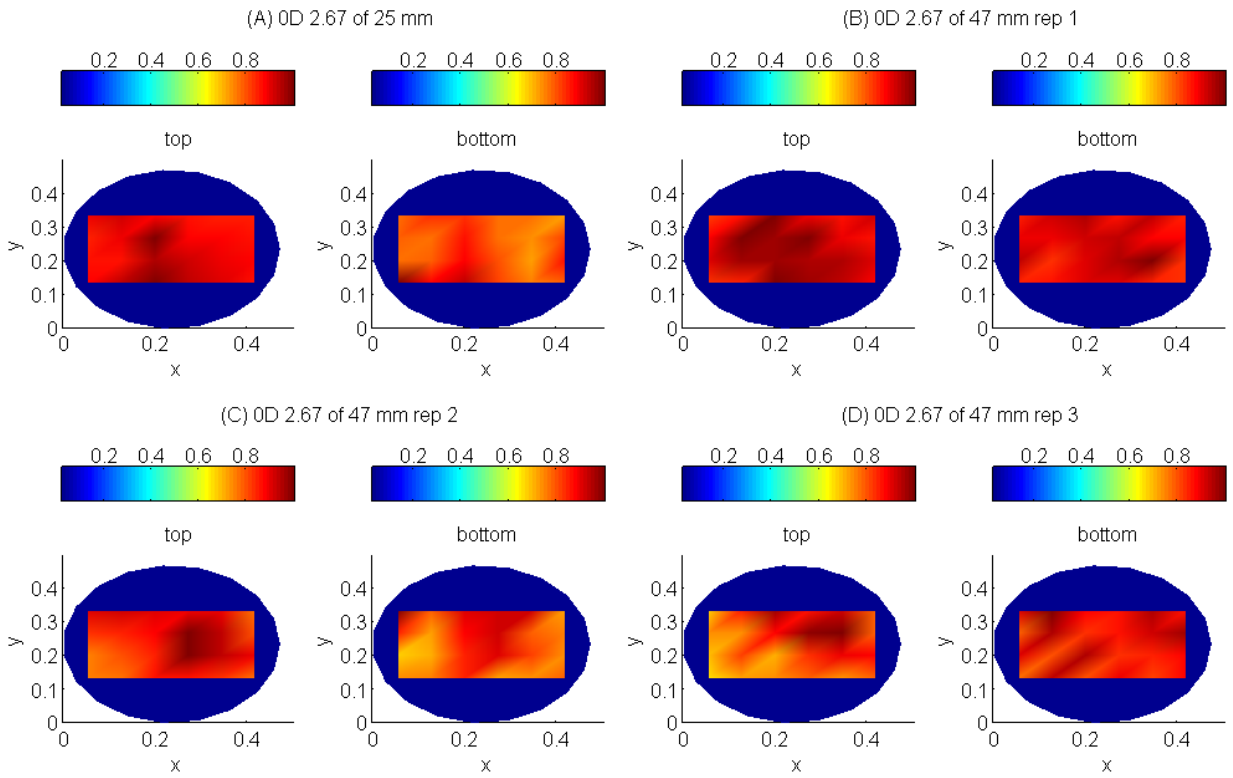

Figure 4.8: Normalized ATR-FTIR peak area ratios at 1680-1800 cm^{-1}/2700-3000 cm^{-1} (coloured surface) for the (A) surfaces of 0D 2.67 RC membrane used for subsequent polymerization and the resultant PAA-*g*-RC (2 hr) membrane was tested for DBC in a 25 mm diameter membrane holder, (B) surfaces of 0D 2.67 RC membrane used for subsequent polymerization and the resultant PAA-*g*-RC (2 hr) membrane was tested for DBC in a 47 mm membrane holder first replicate (rep), (C) surfaces of 0D 2.67 RC membrane used for subsequent polymerization and the resultant PAA-*g*-RC (2 hr) membrane was tested for DBC in a 47 mm diameter membrane holder second replicate (rep), and (D) surfaces of 0D 2.67 RC membrane used for subsequent polymerization and the resultant PAA-*g*-RC (2 hr) membrane was tested for DBC in a 47 mm diameter membrane holder third replicate (rep); Blue disc represents unmodified RC membrane peak area ratio; Peak area ratios were normalized according to the maximum peak area ratio on each surface.

Although the ANOVA analysis in the previous section indicated that the top and bottom membrane surfaces had the same relative amount of BiBB immobilized, it did not specify whether the BiBB were evenly dispersed across the membrane surface. Moreover, in the previous chapter, the influence of agitation on BiBB immobilization was discussed. It was determined that choosing higher BiBB quantities (i.e. > 0.74 mmol BiBB) per membrane disc and using the orbital shaker resulted in more uniform BiBB immobilization, as opposed to using

0.41 mmol BiBB per membrane disc with stir bar agitation. The present results indicated that the recorded distribution of immobilized BiBB across the membrane surface may have been insufficient to ensure uniform polymer grafting across the surface. Each 0D 2.67 (Figure 4.8A, B, C, and D) for subsequent polymerization displayed regions where there were high and low BiBB density immobilized across the membrane surface, as determined by the high and low ATR-FTIR peak area ratios respectively. The resulting non-uniform BiBB immobilized surface would lead to regions of high and low polymer grafting across the membrane surface and would affect $DBC_{10\%}$ of the PAA-*g*-RC membranes.

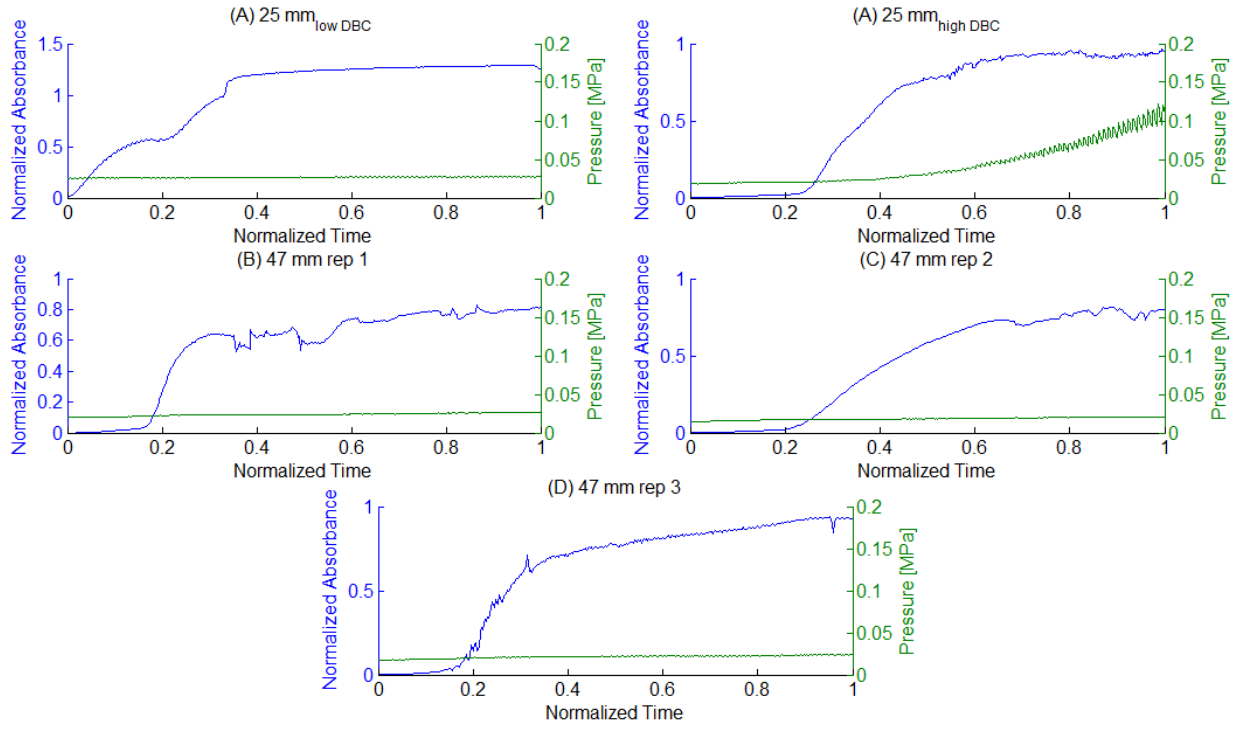

Figure 4.9: Normalized breakthrough curves and corresponding pressure of 0.5 mg mL^{-1} IgG in pH 5 acetate buffer at 1 mL min^{-1} (A) through the PAA-*g*-RC (2 hr) membranes in a 25 mm membrane holder resulting in low and high $DBC_{10\%}$ values and (B)-(D) through the three replicates (rep) of PAA-*g*-RC (2 hr) membranes in a 47 mm membrane holder. Outliers were removed by the MATLAB code found in the Appendix.

Thus, when a 47 mm diameter piece was cut from an intact PAA-*g*-RC (2 hr) membrane, there may have been regions of low and high polymer contents due to the regions of low and

high BiBB contents (Figure 4.8B, C, and D). Breakthrough may thus have started earlier for the 47 mm membranes as compared to the higher protein capacity 25 mm PAA-*g*-RC (2 hr) membrane, due to the IgG buffer solution preferentially going through the paths of least resistance, i.e. the regions of low polymer content or low polymer density (Figure 4.9). As a result of these paths of least resistance, it resulted in lower recorded pressure in the ÄKTA Prime system for the 47 mm membranes compared to the higher protein capacity 25 mm PAA-*g*-RC (2 hr) membrane (Figure 4.9). On the other hand, another region of the 47 mm membrane was responsible for the bulk of the dynamic protein binding. Here it was observed that the region responsible for the bulk of protein binding for all the 47 mm PAA-*g*-RC (2 hr) membrane replicates should have similar binding properties as the high capacity 25 mm PAA-*g*-RC (2 hr) membrane, as the quantities of IgG bound in those membranes were in the same order of magnitude (Table 4.8).

Table 4.8: Mass of protein bounded on PAA-*g*-RC (2hr) membrane at 10% breakthrough

Membrane diameter [mm]	Mass of protein bounded on PAA-*g*-RC membrane (2 hr) at 10% breakthrough [mg]
25 low $DBC_{10\%}$[a]	0.5
25 high $DBC_{10\%}$[a]	6.4
47 rep 1	4.4
47 rep 2	5.7
47 rep 3	4.3

[a] Cut from the same RC sample; rep = replicate.

Accordingly, the 25 mm diameter PAA-*g*-RC (2 hr) membrane which yielded higher $DBC_{10\%}$ may have been cut from the region where there were more immobilized BiBB for higher polymer grafting to bound the similar quantities of IgG as all the 47 mm PAA-*g*-RC (2 hr) membrane replicates (i.e. based on 0D 2.67 in Figure 4.8A). Polymerization uniformity across the membrane surface will need to be further investigated and improvement of distribution of polymer grafting may involve the improvement of the BiBB immobilization step for better BiBB distribution across the membrane surface.

4.5 Conclusions

Storing methanol-washed RC membranes in DMF for two weeks prior to immobilization (0D) and 0.5 M NaOH treatment on methanol-washed RC membranes with subsequent DMF storage yielded higher BiBB immobilization than the methanol-washed RC membranes (0nD) according to ANOVA analysis (95% confidence level). Moreover, for higher BiBB quantities used per membrane disc, there was more BiBB immobilized (ANOVA 95% confidence level). The final immobilization conditions of 0D 2.67 were used for subsequent ARGET ATRP due to the high levels of immobilized BiBB achieved (DS ~0.40) without the need for the extra 0.5 M NaOH treatment step.

In ARGET ATRP, PAA was successfully grafted but had oligomeric molecular weights ($M_{n,theo}$ = 682 g mol^{-1}) according to gravimetry. However, this led to significant RC membrane swelling and the 47 mm diameter circular membrane became an ellipse with a major axis of 60 mm and a minor axis of 50 mm. The swelling factor, the ratio between the swollen mass and the dry mass, described swelling of the PAA-*g*-RC (2 hr) membrane by eight times its dry weight. Dynamic protein binding capacities at 10% breakthrough yielded ~30 mg mL^{-1} for IgG with PAA-*g*-RC (2 hr) membrane. Thus, the weak cation exchange membrane adsorbers demonstrated promise in mAbs capture. Suggestions for further investigation on the grafted polymer distribution across the membrane surface are given in Chapter 6.

5. Conclusions

Weak cation exchange membrane adsorbers using regenerated cellulose (RC) support have thus been successfully developed and have demonstrated promise for mAbs purification in downstream bioprocessing. The development of weak cation exchange membrane adsorbers was a two-step process with initiator immobilization followed by polymerization. The immobilization of the initiator, 2-bromoisobutyryl bromide (BiBB), was optimized. A polynomial regression curve on preliminary data found that a BiBB/TEA molar ratio of 1/0.67 would yield higher BiBB immobilization according to the ATR-FTIR peak area ratios. A higher BiBB quantity used per membrane disc (i.e. 0.74 or 2.67 mmol BiBB), DMF as solvent medium, RC membrane storage in DMF for two weeks prior to immobilization reaction, and NaOH treatment of the RC membrane and DMF storage gave statistically higher immobilized BiBB contents according to ANOVA analysis (95% confidence level). The distribution of immobilized BiBB was found to be more uniform across the membrane surface when larger amounts of BiBB per membrane disc (i.e. 0.74 or 2.67 mmol) and orbital shaking were used for agitation, but may not be sufficient to ensure uniform polymer grafting.

ARGET ATRP was then performed at various molar ratios of immobilized BiBB/2,2′-bipyridine (bpy)/ascorbic acid/$CuBr_2$, and two samples with high and low amounts of PAA grafted from the BiBB-modified RC membranes were tested with lysozyme for their static protein binding capacity. The high and low PAA-grafted membranes had lysozyme static protein binding capacities of 510 mg mL^{-1} and 235 mg mL^{-1}, respectively. ARGET ATRP conditions enabling high PAA grafting with increased NaBr concentration during polymerization were tested for their dynamic protein binding capacity of IgG. Properties of the PAA were also determined. From gravimetry, the $M_{n,theo}$ of PAA was determined to be 682 g mol^{-1} which was sufficient to increase the diameter of the membrane from a 47 mm circle to an ellipse with a major axis of 60 mm and a minor axis of 50 mm. The swelling factor, the ratio of the swollen mass and the dry mass, was determined to be 8. The dynamic protein binding capacity for IgG at 10% breakthrough ($DBC_{10\%}$) was then determined. DMF-stored RC membranes (0D) and BiBB-modified DMF-stored RC membranes using 2.67 mmol BiBB per membrane disc (0D 2.67) had

statistically the same $DBC_{10\%}$ according to t-tests (95% confidence level). Finally, the poly(acrylic acid)-grafted RC membrane (PAA-*g*-RC 47 mm in diameter) achieved the highest $DBC_{10\%}$ of ~30 mg mL^{-1} (t-tests, 95% confidence level). Further work on the characterization of the grafted PAA will need to be performed to improve the uniformity of grafted polymer across the surface for efficient protein binding.

6. Recommendations

The following recommendations are proposed for future work.

i. The issue of polymer grafting distribution uniformity across the membrane surfaces was brought to attention in Chapter 4. A solution to improve polymer grafting distribution uniformity would be to change the immobilization method. Perhaps cellulose can be solubilized, substituted with BiBB, and subsequently crosslinked prior to surface-initiated aqueous ARGET ATRP. The process would ensure uniformly substituted BiBB. The agitation method during polymerization should also be looked into as the membrane was pressed towards the bottom of the three neck round bottom flask when agitated with the shaker.

ii. Subsequently, it is important to understand the structure of PAA so that it is understood where protein units are being bound to and whether the structure (e.g. cross-linked, brush etc.) would affect mass transfer. To elucidate the structure of PAA, it should be cleaved from the RC membrane surface. The entire PAA-*g*-RC membrane should be used for PAA cleavage, to ensure that more PAA is obtained rather than using bits and pieces left over from DBC tests. Furthermore, purification methods should be devised to ensure that no impurities remain in the cleaved polymer. Finally, for NMR analysis, deuterated DMSO could be used to better solubilize the PAA for the ^{1}H NMR and ^{13}C NMR spectra. Adding a drop of trifluoroacetic acid could then be used to identify the hydroxyl groups.

ESEM images of the PAA-*g*-RC samples would also help to visualize the structure of the RC membrane before and after the polymerization and help to visualize changes in the structure due to swelling. Moreover, it may confirm the non-uniformity of PAA grafted across the membrane surface and also would be needed to confirm the non-uniformity/heterogeneity of the top and bottom sides of the unmodified membrane surfaces.

Streaming potential measurements for the membrane material would help identify the charge characteristic of the membrane surface by obtaining the zeta potential profile

with increasing pH for protein purification optimization. Changing the ionic strength instead of the pH should also be carried out to measure the resulting zeta potential. By fitting the data to the Eversole and Boardman equation, the electrokinetic thickness of the polymer layer on the surface can also be estimated as in [131].

iii. One of the main issues with PAA-g-RC membranes was its physical strength. Many of the same ARGET ATRP conditions had to be performed repeatedly due to the brittleness of the material when dry, and the gel-like behaviour when wet, which needed to be treated with utmost care to preserve a 47 mm diameter PAA-*g*-RC membrane piece intact for subsequent DBC characterization. Modifying and grafting-from a polypropylene (PP) support would improve the strength of the material. Moreover, it would allow for easier isolation of the cleaved PAA from the PP support layer.

iv. Further DBC tests should also be performed to elucidate whether the developed membranes would enable for selectivity of the monoclonal antibodies (mAbs) over other proteins present in the mAbs upstream production process.

References

[1] S.S. Farid, Process economics of industrial monoclonal antibody manufacture, J. Chromatogr. B Anal. Technol. Biomed. Life Sci. 848 (2007) 8–18. doi:10.1016/j.jchromb.2006.07.037.

[2] E. Müller, Properties and Characterization of High Capacity Resins for Biochromatography, Chem. Eng. Technol. 28 (2005) 1295–1305. doi:10.1002/ceat.200500161.

[3] K.A. Thiel, Biomanufacturing, from bust to boom...to bubble?, Nat. Biotechnol. 22 (2004) 1365–1372. doi:10.1038/nbt1104-1365.

[4] E. Langer, Trends in downstream processing, BioPharm Int. (2013) 32–35.

[5] N. Hammerschmidt, A. Tscheliessnig, R. Sommer, B. Helk, A. Jungbauer, Economics of recombinant antibody production processes at various scales: Industry-standard compared to continuous precipitation, Biotechnol. J. 9 (2014) 766–775. doi:10.1002/biot.201300480.

[6] X. Han, A. Hewig, G. Vedantham, Recovery and Purification of Antibody, in: M. Al-Rubeai (Ed.), Antib. Expr. Prod., Springer, New York, 2011: pp. 25–52. doi:10.1007/978-94-007-1257-7.

[7] A.A. Shukla, B. Hubbard, T. Tressel, S. Guhan, D. Low, Downstream processing of monoclonal antibodies-Application of platform approaches, J. Chromatogr. B Anal. Technol. Biomed. Life Sci. 848 (2007) 28–39. doi:10.1016/j.jchromb.2006.09.026.

[8] C. Charcosset, Membrane chromatography, in: Membrane Processes in Biotechnology and Pharmaceutics, Elsevier B.V., New York, 2012.

[9] S. Hofer, A. Ronacher, J. Horak, H. Graalfs, W. Lindner, Static and dynamic binding capacities of human immunoglobulin G on polymethacrylate based mixed-modal, thiophilic and hydrophobic cation exchangers, J. Chromatogr. A. 1218 (2011) 8925–8936. doi:10.1016/j.chroma.2011.06.012.

[10] A.M. Lenhoff, Protein adsorption and transport in polymer-functionalized ion-exchangers, J. Chromatogr. A. 1218 (2011) 8748–8759. doi:10.1016/j.chroma.2011.06.061.

[11] W. Guo, Z. Shang, Y. Yu, L. Zhou, Membrane affinity chromatography of alkaline phosphatase, J. Chromatogr. A. 685 (1994) 344–348. doi:10.1016/0021-9673(94)00725-X.

[12] Z. Liu, H. Du, S.R. Wickramasinghe, X. Qian, Membrane Surface Engineering for Protein Separations: Experiments and Simulations, Langmuir. 30 (2014) 10651–10660. doi:10.1021/la5026119.

[13] B. V. Bhut, S.R. Wickramasinghe, S.M. Husson, Preparation of high-capacity, weak anion-exchange membranes for protein separations using surface-initiated atom transfer radical polymerization, J. Memb. Sci. 325 (2008) 176–183. doi:10.1016/j.memsci.2008.07.028.

[14] B. V. Bhut, S.M. Husson, Dramatic performance improvement of weak anion-exchange membranes for chromatographic bioseparations, J. Memb. Sci. 337 (2009) 215–223. doi:10.1016/j.memsci.2009.03.046.

[15] B. V. Bhut, K.A. Conrad, S.M. Husson, Preparation of high-performance membrane adsorbers by surface-initiated AGET ATRP in the presence of dissolved oxygen and low catalyst concentration, J. Memb. Sci. 390-391 (2012) 43–47. doi:10.1016/j.memsci.2011.10.057.

[16] N. Singh, S.M. Husson, B. Zdyrko, I. Luzinov, Surface modification of microporous PVDF membranes by ATRP, J. Memb. Sci. 262 (2005) 81–90. doi:10.1016/j.memsci.2005.03.053.

[17] H.C.S. Chenette, J.R. Robinson, E. Hobley, S.M. Husson, Development of high-productivity, strong cation-exchange adsorbers for protein capture by graft polymerization from membranes with different pore sizes, J. Memb. Sci. 423-424 (2012) 43–52. doi:10.1016/j.memsci.2012.07.040.

[18] N. Singh, J. Wang, M. Ulbricht, S.R. Wickramasinghe, S.M. Husson, Surface-initiated atom transfer radical polymerization: A new method for preparation of polymeric membrane adsorbers, J. Memb. Sci. 309 (2008) 64–72. doi:10.1016/j.memsci.2007.10.007.

[19] N. Singh, Z. Chen, N. Tomer, S.R. Wickramasinghe, N. Soice, S.M. Husson, Modification of regenerated cellulose ultrafiltration membranes by surface-initiated atom transfer radical polymerization, J. Memb. Sci. 311 (2008) 225–234. doi:10.1016/j.memsci.2007.12.036.

[20] J. Wang, R.T. Sproul, L.S. Anderson, S.M. Husson, Development of multimodal membrane adsorbers for antibody purification using atom transfer radical polymerization, Polym. (United Kingdom). 55 (2014) 1404–1411. doi:10.1016/j.polymer.2013.12.023.

[21] Y.L. Wu, Y.S. Yan, J.M. Pan, X.H. Dai, W.D. Shi, M.J. Meng, Fabrication and evaluation of molecularly imprinted regenerated cellulose composite membranes via atom transfer radical polymerization, Chinese Chem. Lett. 25 (2014) 273–278. doi:10.1016/j.cclet.2013.11.019.

[22] X. Qian, H. Fan, C. Wang, Y. Wei, Preparation of high-capacity, weak anion-exchange membranes by surface-initiated atom transfer radical polymerization of poly(glycidyl methacrylate) and subsequent derivatization with diethylamine, Appl. Surf. Sci. 271 (2013) 240–247. doi:10.1016/j.apsusc.2013.01.167.

[23] A.H. Mohd Yusof, M. Ulbricht, Polypropylene-based membrane adsorbers via photo-initiated graft copolymerization: Optimizing separation performance by preparation conditions, J. Memb. Sci. 311 (2008) 294–305. doi:10.1016/j.memsci.2007.12.027.

[24] Y. Zheng, H. Liu, P. V. Gurgel, R.G. Carbonell, Polypropylene nonwoven fabrics with conformal grafting of poly(glycidyl methacrylate) for bioseparations, J. Memb. Sci. 364 (2010) 362–371. doi:10.1016/j.memsci.2010.08.037.

[25] R. Arshady, Beaded polymer supports and gels. II. Physico-chemical criteria and functionalization, J. Chromatogr. 586 (1991) 199–219. doi:10.1016/0021-9673(91)85125-Y.

[26] B. Slaughter, S. Khurshid, O. Fisher, O. Khademhosseini, N. Peppas, Hydrogels in Regenerative Medicine, Adv. Mater. 21 (2009) 3307–3329. doi:10.1002/adma.200802106.

[27] Y. Wei, J. Ma, C. Wang, Preparation of high-capacity strong cation exchange membrane for protein adsorption via surface-initiated atom transfer radical polymerization, J. Memb. Sci. 427 (2013) 197–206. doi:10.1016/j.memsci.2012.09.053.

[28] S. Hansson, V. Trouillet, T. Tischer, A.S. Goldmann, A. Carlmark, C. Barner-Kowollik, E. Malmström, Grafting efficiency of synthetic polymers onto biomaterials: A comparative study of grafting- from versus grafting- to, Biomacromolecules. 14 (2013) 64–74. doi:10.1021/bm3013132.

[29] J. Yu, Y. Liu, X. Liu, C. Wang, J. Wang, F. Chu, C. Tang, Integration of renewable cellulose and rosin towards sustainable copolymers by “grafting from” ATRP, Green Chem. 16 (2014) 1854–1864. doi:10.1039/c3gc41550c.

[30] O. Roling, A. Mardyukov, J.A. Krings, A. Studer, B.J. Ravoo, Polymer Brushes Exhibiting Versatile Supramolecular Interactions Grown by Nitroxide-Mediated Polymerization and Structured via Microcontact Chemistry, Macromolecules. 47 (2014) 2411–2419. doi:10.1021/ma500043b.

[31] R. Barbey, L. Lavanant, D. Paripovic, N. Schüwer, C. Sugnaux, S. Tugulu, H.A. Klok, Polymer brushes via surface-initiated controlled radical polymerization: synthesis, characterization, properties, and applications, Chem. Rev. 109 (2009) 5437–5527. doi:10.1021/cr900045a.

[32] S. Tugulu, R. Barbey, M. Harms, M. Fricke, D. Volkmer, A. Rossi, H.A. Klok, Synthesis of poly(methacrylic acid) brushes via surface-initiated atom transfer radical polymerization of sodium methacrylate and their use as substrates for the mineralization of calcium carbonate, Macromolecules. 40 (2007) 168–177. doi:10.1021/ma060739e.

[33] J. Lindqvist, E. Malmström, Surface modification of natural substrates by atom transfer radical polymerization, J. Appl. Polym. Sci. 100 (2006) 4155–4162. doi:10.1002/app.23457.

[34] L. Carlsson, T. Ingverud, H. Blomberg, A. Carlmark, P.T. Larsson, E. Malmström, Surface characteristics of cellulose nanoparticles grafted by surface-initiated ring-opening polymerization of ε-caprolactone, Cellulose. 22 (2015) 1063–1074. doi:10.1007/s10570-014-0510-1.

[35] A. Carlmark, E.E. Malmström, ATRP grafting from cellulose fibers to create block-copolymer grafts, Biomacromolecules. 4 (2003) 1740–1745. doi:10.1021/bm030046v.

[36] J. Lindqvist, D. Nyström, E. Östmark, P. Antoni, A. Carlmark, M. Johansson, A. Hult, E. Malmström, Intelligent Dual-responsive cellulose surfaces via surface-initiated ATRP, Biomacromolecules. 9 (2008) 2139–2145. doi:10.1021/bm800193n.

[37] S. Hansson, P. Antoni, H. Bergenudd, E. Malmström, Selective cleavage of polymer grafts from solid surfaces: assessment of initiator content and polymer characteristics, Polym. Chem. 2 (2011) 556. doi:10.1039/c0py00388c.

[38] D. Nyström, J. Lindqvist, E. Ostmark, A. Hult, E. Malmström, Superhydrophobic bio-fibre surfaces via tailored grafting architecture., Chem. Commun. (Camb). (2006) 3594–3596. doi:10.1039/b607411a.

[39] E. Larsson, S.A. Pendergraph, T. Kaldéus, E. Malmström, A. Carlmark, Cellulose grafting by photoinduced controlled radical polymerisation, Polym. Chem. (2014) 1865–1874. doi:10.1039/C4PY01618A.

[40] S. Hansson, A. Carlmark, E. Malmström, L. Fogelström, Toward industrial grafting of cellulosic substrates via ARGET ATRP, J. Appl. Polym. Sci. 132 (2015) 41434. doi:10.1002/app.41434.

[41] C. Porsch, S. Hansson, N. Nordgren, E. Malmström, Thermo-responsive cellulose-based architectures: tailoring LCST using poly(ethylene glycol) methacrylates, Polym. Chem. 2 (2011) 1114. doi:10.1039/c0py00417k.

[42] S. Hansson, E. Östmark, A. Carlmark, E. Malmström, ARGET ATRP for versatile grafting of cellulose using various monomers, ACS Appl. Mater. Interfaces. 1 (2009) 2651–2659. doi:10.1021/am900547g.

[43] R. Westlund, A. Carlmark, A. Hult, E. Malmström, I.M. Saez, Grafting liquid crystalline polymers from cellulose substrates using atom transfer radical polymerization, Soft Matter. 3 (2007) 866–871. doi:10.1039/b700630f.

[44] A. Carlmark, E. Malmström, Atom Transfer Radical Polymerization from Cellulose Fibers at Ambient Temperature, J. Am. Chem. Soc. 124 (2002) 900–901. T:\Gruppe\Literatur\Originale\Calmark2001.pdf.

[45] E. Malmström, A. Carlmark, Controlled grafting of cellulose fibres – an outlook beyond paper and cardboard, Polym. Chem. 3 (2012) 1702. doi:10.1039/c1py00445j.

[46] M. Xiao, S. Li, W. Chanklin, A. Zheng, H. Xiao, Surface-initiated atom transfer radical polymerization of butyl acrylate on cellulose microfibrils, Carbohydr. Polym. 83 (2011) 512–519. doi:10.1016/j.carbpol.2010.08.011.

[47] M. Wang, J. Yuan, X. Huang, X. Cai, L. Li, J. Shen, Grafting of carboxybetaine brush onto cellulose membranes via surface-initiated ARGET-ATRP for improving blood compatibility, Colloids Surfaces B Biointerfaces. 103 (2013) 52–58. doi:10.1016/j.colsurfb.2012.10.025.

[48] Y.T. Wei, Y.M. Zheng, J.P. Chen, Functionalization of regenerated cellulose membrane via surface initiated atom transfer radical polymerization for boron removal from aqueous solution, Langmuir. 27 (2011) 6018–6025. doi:10.1021/la200154y.

[49] K. Pan, X. Zhang, R. Ren, B. Cao, Double stimuli-responsive membranes grafted with block copolymer by ATRP method, J. Memb. Sci. 356 (2010) 133–137. doi:10.1016/j.memsci.2010.03.044.

[50] K. Pan, X. Zhang, J. Zhu, B. Cao, Grafting of regenerated cellulose membrane by surface-initiated atom transfer radical polymerization and its pH-resposive behavior, Polym. Adv. Technol. 22 (2011) 1948–1952. doi:10.1002/pat.1699.

[51] K. Matyjaszewski, Atom Transfer Radical Polymerization (ATRP): Current Status and Future Perspectives, (2012).

[52] T.B. Silva, M. Spulber, M.K. Kocik, F. Seidi, H. Charan, M. Rother, S.J. Sigg, K. Renggli, G. Kali, N. Bruns, Hemoglobin and red blood cells catalyze atom transfer radical polymerization, Biomacromolecules. 14 (2013) 2703–2712. doi:10.1021/bm400556x.

[53] S.J. Sigg, F. Seidi, K. Renggli, T.B. Silva, G. Kali, N. Bruns, Horseradish peroxidase as a catalyst for atom transfer radical polymerization, Macromol. Rapid Commun. 32 (2011) 1710–1715. doi:10.1002/marc.201100349.

[54] N. V. Tsarevsky, W.A. Braunecker, K. Matyjaszewski, Electron transfer reactions relevant to atom transfer radical polymerization, J. Organomet. Chem. 692 (2007) 3212–3222. doi:10.1016/j.jorganchem.2007.01.051.

[55] A. Anastasaki, V. Nikolaou, Q. Zhang, J. Burns, S.R. Samanta, C. Waldron, A.J. Haddleton, R. McHale, D. Fox, V. Percec, P. Wilson, D.M. Haddleton, Copper(II)/tertiary amine synergy in photoinduced living radical polymerization: Accelerated synthesis of ω-functional and α,ω-heterofunctional poly(acrylates), J. Am. Chem. Soc. 136 (2014) 1141–1149. doi:10.1021/ja411780m.

[56] Y. Kwak, K. Matyjaszewski, ARGET ATRP of methyl methacrylate in the presence of nitrogen-based ligands as reducing agents, Polym. Int. 58 (2009) 242–247. doi:10.1002/pi.2530.

[57] K. Matyjaszewski, W. Jakubowski, K. Min, W. Tang, J. Huang, W.A. Braunecker, N. V Tsarevsky, Diminishing catalyst concentration in atom transfer radical polymerization with reducing agents., Proc. Natl. Acad. Sci. U. S. A. 103 (2006) 15309–15314. doi:10.1073/pnas.0602675103.

[58] K. Matyjaszewski, D. Hongchen, W. Jakubowski, J. Pietrasik, A. Kusumo, Grafting from surfaces for "everyone": ARGET ATRP in the presence of air, Langmuir. 23 (2007) 4528–4531. doi:10.1021/la063402e.

[59] A. Simakova, S.E. Averick, D. Konkolewicz, K. Matyjaszewski, Aqueous ARGET ATRP, Macromolecules. 45 (2012) 6371–6379. doi:10.1021/ma301303b.

[60] S.R. Woodruff, B.J. Davis, N. V. Tsarevsky, Selecting the optimal reaction conditions for copper – mediated atom transfer radical polymerization at low catalyst concentration, in: K. Matyjaszewski, B.S. Sumerlin, N.V. Tsarevsky (Eds.), ACS Symp. Ser., American Chemical Society, Washington D.C., 2012: pp. 99–113. doi:10.1021/bk-2012-1100.ch007.

[61] A.Y. Sankhe, S.M. Husson, S.M. Kilbey, Direct polymerization of surface-tethered polyelectrolyte layers in aqueous solution via surface-confined atom transfer radical polymerization, J. Polym. Sci. Part A Polym. Chem. 45 (2007) 566–575. doi:10.1002/pola.21817.

[62] R. Dong, S. Krishnan, B.A. Baird, M. Lindau, C.K. Ober, Patterned biofunctional poly(acrylic acid) brushes on silicon surfaces, Biomacromolecules. 8 (2007) 3082–3092. doi:10.1021/bm700493v.

[63] N. Chan, M.F. Cunningham, R.A. Hutchinson, ARGET ATRP of methacrylates and acrylates with stoichiometric ratios of ligand to copper, Macromol. Chem. Phys. 209 (2008) 1797–1805. doi:10.1002/macp.200800328.

[64] E.J. Ashford, V. Naldi, R. O'Dell, N.C. Billingham, S.P. Armes, First example of the atom transfer radical polymerisation of an acidic monomer: direct synthesis of methacrylic acid copolymers in aqueous media, Chem. Commun. (1999) 1285–1286. doi:10.1039/a903773j.

[65] Y.K. Jhon, S. Arifuzzaman, A.E. Özçam, D.J. Kiserow, J. Genzer, Formation of polyampholyte brushes via controlled radical polymerization and their assembly in solution, Langmuir. 28 (2012) 872–882. doi:10.1021/la203697a.

[66] W.T. Eckenhoff, A.B. Biernesser, T. Pintauer, Kinetic and mechanistic aspects of atom transfer radical addition (ATRA) catalyzed by copper complexes with tris(2-pyridylmethyl)amine, Inorg. Chem. 51 (2012) 11917–11929. doi:10.1021/ic3018198.

[67] F. Tomicki, D. Krix, H. Nienhaus, M. Ulbricht, Stimuli-responsive track-etched membranes via surface-initiated controlled radical polymerization: Influence of grafting

density and pore size, J. Memb. Sci. 377 (2011) 124–133. doi:10.1016/j.memsci.2011.04.028.

[68] S.B. Lee, R.R. Koepsel, S.W. Morley, K. Matyjaszewski, Y. Sun, A.J. Russell, Permanent, nonleaching antibacterial surfaces, 1. Synthesis by atom transfer radical polymerization, Biomacromolecules. 5 (2004) 877–882. doi:10.1021/bm034352k.

[69] G. Zampano, M. Bertoldo, S. Bronco, Poly(ethyl acrylate) surface-initiated ATRP grafting from wood pulp cellulose fibers, Carbohydr. Polym. 75 (2009) 22–31. doi:10.1016/j.carbpol.2008.06.005.

[70] S. Yamamoto, M. Ejaz, Y. Tsujii, T. Fukuda, Surface interaction forces of well-defined, high-density polymer brushes studied by atomic force microscopy. 2. Effect of graft density, Macromolecules. 33 (2000) 5608–5612. doi:10.1021/ma991988o.

[71] E. Ruckenstein, W. Guo, Crosslinked mercerized cellulose membranes and their application to membrane affinity chromatography, J. Memb. Sci. 187 (2001) 277–286. doi:10.1016/S0376-7388(01)00357-X.

[72] W. Guo, E. Ruckenstein, A new matrix for membrane affinity chromatography and its application to the purification of concanavalin A, J. Memb. Sci. 182 (2001) 227–234. doi:10.1016/S0376-7388(00)00574-3.

[73] F. Cattoli, G.C. Sarti, Separation of MBP fusion proteins through affinity membranes, Biotechnol. Prog. 18 (2002) 94–100. doi:10.1021/bp010119r.

[74] E. Sada, Engineering aspects of bioaffinity separation, J. Chem. Eng. Japan. 23 (1990) 259–269. doi:10.1252/jcej.23.259.

[75] D. Roy, M. Semsarilar, J.T. Guthrie, S. Perrier, Cellulose modification by polymer grafting: a review., Chem. Soc. Rev. 38 (2009) 2046–2064. doi:10.1039/b808639g.

[76] H.A. Kraessig, Cellulose : structure, accessibility, and reactivity, Gordon and Breach Science Publishers, Philadelphia, 1993.

[77] A. O'sullivan, Cellulose: the structure slowly unravels, Cellulose. 4 (1997) 173–207. doi:Chemistry and Materials Science.

[78] F.J. Kolpak, J. Blackwell, Determination of the structure of cellulose II., Macromolecules. 9 (1976) 273–278. doi:10.1021/ma60050a019.

[79] D. Roy, J.T. Guthrie, Graft Polymerization : Grafting Poly (styrene) from Cellulose via Reversible Addition-Fragmentation Chain Transfer (RAFT) Polymerization, Macromolecules. 38 (2005) 10363–10372.

[80] D. Klemm, B. Heublein, H.P. Fink, A. Bohn, Cellulose: Fascinating biopolymer and sustainable raw material, Angew. Chemie - Int. Ed. 44 (2005) 3358–3393. doi:10.1002/anie.200460587.

[81] S.H. Kim, C.M. Lee, K. Kafle, Characterization of crystalline cellulose in biomass: Basic principles, applications, and limitations of XRD, NMR, IR, Raman, and SFG, Korean J. Chem. Eng. 30 (2013) 2127–2141. doi:10.1007/s11814-013-0162-0.

[82] J.A. Howsmon, Water Sorption and the Poly-Phase Structure of Cellulose Fibers, Text. Res. J. 19 (1949) 152–162. doi:10.1177/004051754901900303.

[83] L.C. Fidale, N. Ruiz, T. Heinze, O.A. El Seoud, Cellulose swelling by aprotic and protic solvents: What are the similarities and differences?, Macromol. Chem. Phys. 209 (2008) 1240–1254. doi:10.1002/macp.200800021.

[84] S.N. Bhattacharyya, D. Maldas, Graft copolymerization onto cellulosics, Prog. Polym. Sci. 10 (1984) 171–270. doi:10.1016/0079-6700(84)90002-9.

[85] K. Negishi, Y. Mashiko, E. Yamashita, A. Otsuka, T. Hasegawa, Cellulose Chemistry Meets Click Chemistry: Syntheses and Properties of Cellulose-Based Glycoclusters with High Structural Homogeneity, Polymers (Basel). 3 (2011) 489–508. doi:10.3390/polym3010489.

[86] S.H. Zeronian, Cellulose Chemistry and its Application, Ellis Horwood Limited, New York, 1985.

[87] C.E. Carraher Jr, Seymour/Carraher's Polymer Chemistry, 6th ed., Marcel Dekker Inc., New York, 2003.

[88] K.L. Kato, R.E. Cameron, A review of the relationship between thermally-accelerated ageing of paper and hornification, Cellulose. 6 (1999) 23–40. doi:10.1023/A:1009292120151.

[89] M. Granström, J. Kavakka, A. King, J. Majoinen, V. Mäkelä, J. Helaja, S. Hietala, T. Virtanen, S.L. Maunu, D.S. Argyropoulos, I. Kilpeläinen, Tosylation and acylation of cellulose in 1-allyl-3-methylimidazolium chloride, Cellulose. 15 (2008) 481–488. doi:10.1007/s10570-008-9197-5.

[90] S. Patai, The chemistry of acyl halides, Interscience, London, 1972. doi:10.1002/9780470771273.

[91] N. Lin, J. Huang, A. Dufresne, Preparation, properties and applications of polysaccharide nanocrystals in advanced functional nanomaterials: a review, Nanoscale. 4 (2012) 3274. doi:10.1039/c2nr30260h.

[92] P. Strazzolini, A.G. Giumanini, G. Verardo, The reaction between acyl halides and alcohols: Alkyl halide vs. ester formation, Tetrahedron. 50 (1994) 217–254. doi:10.1016/S0040-4020(01)80747-X.

[93] D. Xu, B. Li, C. Tate, K.J. Edgar, Studies on regioselective acylation of cellulose with bulky acid chlorides, Cellulose. 18 (2011) 405–419. doi:10.1007/s10570-010-9476-9.

[94] J. Emsley, V. Gold, F. Hibbert, W.T.A. Szeto, Kinetic and equilibrium studies by 19F nuclear magnetic resonance of the formation of acetyl fluoride from acetyl chloride and tetraethylammonium fluoride in acetic acid, J. Chem. Soc. Perkin Trans. 2. (1988) 923. doi:10.1039/p29880000923.

[95] S. Belegrinou, V. Malinova, R. Masciadri, W. Meier, Efficient Two-Step Synthesis of 11,11′-Dithiobis[1-(2-bromo-2-methylpropionyloxy)undecane], a Conventional Initiator for Grafting Polymer Brushes from Gold Surfaces via ATRP, Synth. Commun. 40 (2010) 3000–3007. doi:10.1080/00397910903350008.

[96] Y.H. Zhao, K.H. Wee, R. Bai, A novel electrolyte-responsive membrane with tunable permeation selectivity for protein purification, ACS Appl. Mater. Interfaces. 2 (2010) 203–211. doi:10.1021/am900654d.

[97] L. Fan, H. Chen, Z. Hao, Z. Tan, Cellulose-based macroinitiator for crosslinked poly(butyl methacrylate-co-pentaerythritol triacrylate) oil-absorbing materials by SET-LRP, J. Polym. Sci. Part A Polym. Chem. 51 (2013) 457–462. doi:10.1002/pola.26404.

[98] V. Castelvetro, M. Geppi, S. Giaiacopi, G. Mollica, Cotton fibers encapsulated with homo- and block copolymers: Synthesis by the atom transfer radical polymerization grafting-from technique and solid-state NMR dynamic investigations, Biomacromolecules. 8 (2007) 498–508. doi:10.1021/bm060602w.

[99] C.S.R. Freire, A.J.D. Silvestre, C.P. Neto, M.N. Belgacem, A. Gandini, Controlled heterogeneous modification of cellulose fibers with fatty acids: Effect of reaction conditions on the extent of esterification and fiber properties, J. Appl. Polym. Sci. 100 (2006) 1093–1102. doi:10.1002/app.23454.

[100] J.O. Warwicker, J.W. Clayton, Reactivity of Cotton After Treatment in Alkaline and Acid Swelling Agents, J. Appl. Polym. Sci. 13 (1969) 1037–1048. doi:10.1002/app.1969.070130518.

[101] R. Jeffries, J.G. Roberts, R.N. Robinson, Accessibility and Reaction Sites in Cotton, Text. Res. J. 38 (1968) 234–244. doi:10.1177/004051756803800304.

[102] ATR precautions, Shidmazu Corp. (2015). http://www.shimadzu.com/an/ftir/support/ftirtalk/letter2/atr2.html (accessed May 22, 2015).

[103] A. Aied, Y. Zheng, A. Pandit, W. Wang, DNA immobilization and detection on cellulose paper using a surface grown cationic polymer via ATRP, ACS Appl. Mater. Interfaces. 4 (2012) 826–831. doi:10.1021/am201483h.

[104] D. Keskin, J.I. Clodt, J. Hahn, V. Abetz, V. Filiz, Postmodification of PS-b-P4VP diblock copolymer membranes by ARGET ATRP, Langmuir. 30 (2014) 8907–8914. doi:10.1021/la501478s.

[105] B. Zhu, S. Edmondson, Polydopamine-melanin initiators for Surface-initiated ATRP, Polymer (Guildf). 52 (2011) 2141–2149. doi:10.1016/j.polymer.2011.03.027.

[106] X. Qiu, X. Ren, S. Hu, Fabrication of dual-responsive cellulose-based membrane via simplified surface-initiated ATRP, Carbohydr. Polym. 92 (2013) 1887–1895. doi:10.1016/j.carbpol.2012.11.080.

[107] D.J. Wang, H. Chen, H. Xu, J.M. Sun, Y.Y. Xu, Preparation of Wheat Straw Matrix- g -Polyacrylonitrile-Based Adsorbent by SET-LRP and Its Applications for Heavy Metal Ion Removal, ACS Sustain. Chem. Eng. 2 (2014) 1843–1848. doi:10.1021/sc500308x.

[108] N.S. Çetin, P. Tingaut, N. Özmen, N. Henry, D. Harper, M. Dadmun, G. Sèbe, Acetylation of cellulose nanowhiskers with vinyl acetate under moderate conditions, Macromol. Biosci. 9 (2009) 997–1003. doi:10.1002/mabi.200900073.

[109] A. Ashori, M. Babaee, M. Jonoobi, Y. Hamzeh, Solvent-free acetylation of cellulose nanofibers for improving compatibility and dispersion, Carbohydr. Polym. 102 (2014) 369–375. doi:10.1016/j.carbpol.2013.11.067.

[110] Q. Zhou, L. Greffe, M.J. Baumann, E. Malmström, T.T. Teeri, H. Brumer, Use of xyloglucan as a molecular anchor for the elaboration of polymers from cellulose surfaces: A general route for the design of biocomposites, Macromolecules. 38 (2005) 3547–3549. doi:10.1021/ma047712k.

[111] Z. Wang, Y. Zhang, F. Jiang, H. Fang, Z. Wang, Synthesis and characterization of designed cellulose-graft-polyisoprene copolymers, Polym. Chem. 5 (2014) 3379. doi:10.1039/c3py01574b.

[112] K. Matyjaszewski, P.J. Miller, N. Shukla, B. Immaraporn, A. Gelman, B.B. Luokala, T.M. Siclovan, G. Kickelbick, T. Vallant, H. Hoffmann, T. Pakula, Polymers at Interfaces: Using Atom Transfer Radical Polymerization in the Controlled Growth of Homopolymers and Block Copolymers from Silicon Surfaces in the Absence of Untethered Sacrificial Initiator, Macromolecules. 32 (1999) 8716–8724. doi:10.1021/ma991146p.

[113] J. Kuang, P.B. Messersmith, Universal surface-initiated polymerization of antifouling zwitterionic brushes using a mussel-mimetic peptide initiator, Langmuir. 28 (2012) 7258–7266. doi:10.1021/la300738e.

[114] C. Devaux, J.P. Chapel, E. Beyou, P. Chaumont, Controlled structure and density of "living" polystyrene brushes on flat silica surfaces, Eur. Phys. J. E. 7 (2002) 345–352. doi:10.1140/epje/i2001-10098-2.

[115] J. Yuan, X. Huang, P. Li, L. Li, J. Shen, Surface-initiated RAFT polymerization of sulfobetaine from cellulose membranes to improve hemocompatibility and antibiofouling property, Polym. Chem. 4 (2013) 5074. doi:10.1039/c3py00565h.

[116] M. Barsbay, O. Güven, T.P. Davis, C. Barner-Kowollik, L. Barner, RAFT-mediated polymerization and grafting of sodium 4-styrenesulfonate from cellulose initiated via γ-radiation, Polymer (Guildf). 50 (2009) 973–982. doi:10.1016/j.polymer.2008.12.027.

[117] M. Barsbay, O. Güven, M.H. Stenzel, T.P. Davis, C. Barner-Kowollik, L. Barner, Verification of controlled grafting of styrene from cellulose via radiation-induced RAFT polymerization, Macromolecules. 40 (2007) 7140–7147. doi:10.1021/ma070825u.

[118] F. Tang, L. Zhang, Z. Zhang, Z. Cheng, X. Zhu, Cellulose Filter Paper with Antibacterial Activity from Surface-Initiated ATRP, J. Macromol. Sci. Part A. 46 (2009) 989–996. doi:10.1080/10601320903158651.

[119] P.S. Liu, Q. Chen, X. Liu, B. Yuan, S.S. Wu, J. Shen, S.C. Lin, Grafting of zwitterion from cellulose membranes via ATRP for improving blood compatibility, Biomacromolecules. 10 (2009) 2809–2816. doi:10.1021/bm9006503.

[120] F. Jiang, Z. Wang, Y. Qiao, Z. Wang, C. Tang, A novel architecture toward third-generation thermoplastic elastomers by a grafting strategy, Macromolecules. 46 (2013) 4772–4780. doi:10.1021/ma4007472.

[121] W. Wu, F. Huang, S. Pan, W. Mu, X. Meng, H. Yang, Thermo-responsive and fluorescent cellulose nanocrystals grafted with polymer brushes, J. Mater. Chem. A Mater. Energy Sustain. 3 (2015) 1995–2005. doi:10.1039/C4TA04761C.

[122] W. Muller, New ion exchangers for the chromatography of biopolymers, J. Chromatogr. 510 (1990) 133–140. doi:10.1016/S0021-9673(01)93746-X.

[123] L. Valentine, Moisture Regain and Accessibility of Cellulose Derivatives, Text. Res. J. 24 (1954) 670–672. doi:10.1177/004051755402400713.

[124] R.M. Silverstein, F.X. Webster, Spectrometric identification of organic compounds, 6th ed., Wiley, Chichester, 1998.

[125] E. Kontturi, P.C. Thüne, J.W. Niemantsverdriet, Cellulose Model Surfaces Simplified Preparation by Spin Coating and Characterization by X-ray Photoelectron Spectroscopy, Infrared Spectroscopy, and Atomic Force Microscopy, Langmuir. 19 (2003) 5735–5741. doi:10.1021/la0340394.

[126] S.H. Zeronian, E. Cabradilla, Action of Alkali Metal Hydroxides on Cotton, J. Appl. Polym. Sci. 16 (1972) 129–137.

[127] D. Bontempo, G. Masci, P. De Leonardis, L. Mannina, D. Capitani, V. Crescenzi, Versatile grafting of polysaccharides in homogeneous mild conditions by using atom transfer radical polymerization, Biomacromolecules. 7 (2006) 2154–2161. doi:10.1021/bm0601373.

[128] P. van Beijeren, P. Kreis, T. Zeiner, Ion exchange membrane adsorption of bovine serum albumin-Impact of operating and buffer conditions on breakthrough curves, J. Memb. Sci. 415-416 (2012) 568–576. doi:10.1016/j.memsci.2012.05.051.

[129] Repligen, Recombinant Protein A Affinity Resins, (2015). http://www.repligen.com/protein-a-affinity-resin (accessed August 17, 2015).

[130] J. Wang, R. Faber, M. Ulbricht, Influence of pore structure and architecture of photo-grafted functional layers on separation performance of cellulose-based macroporous membrane adsorbers, J. Chromatogr. A. 1216 (2009) 6490–6501. doi:10.1016/j.chroma.2009.07.042.

[131] A. De Sousa Delgado, M. Leonard, E. Dellacherie, Surface modification of polystyrene nanoparticles using dextrans and dextran-POE copolymers: polymer adsorption and colloidal characterization., J. Biomater. Sci. Polym. Ed. 11 (2000) 1395–1410. doi:10.1163/156856200744309.

Appendix

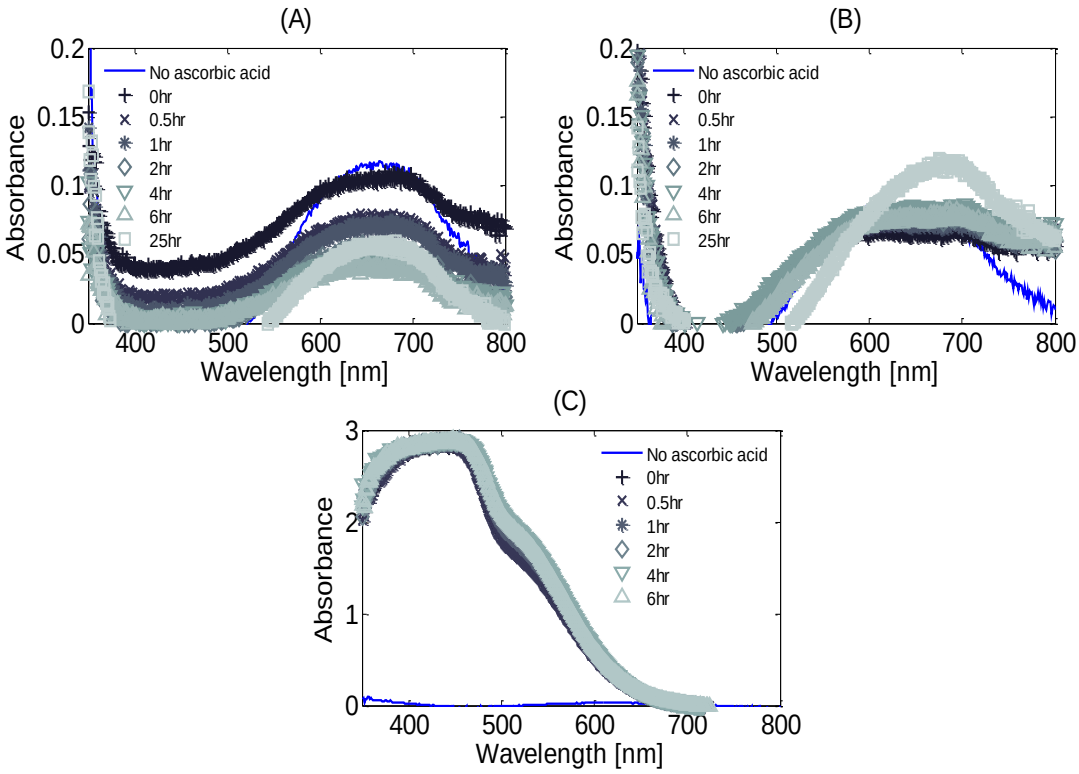

Figure A1: UV-vis spectra over time for the following reagent molar ratios: (A) 1/1/2 $CuBr_2$/PMDETA/ascorbic acid; (B) 1/10/2 $CuBr_2$/PMDETA/ascorbic acid and (C) 1/2/2 $CuBr_2$/bpy/ascorbic acid. All solutions were pH adjusted to 12 before ascorbic acid addition.

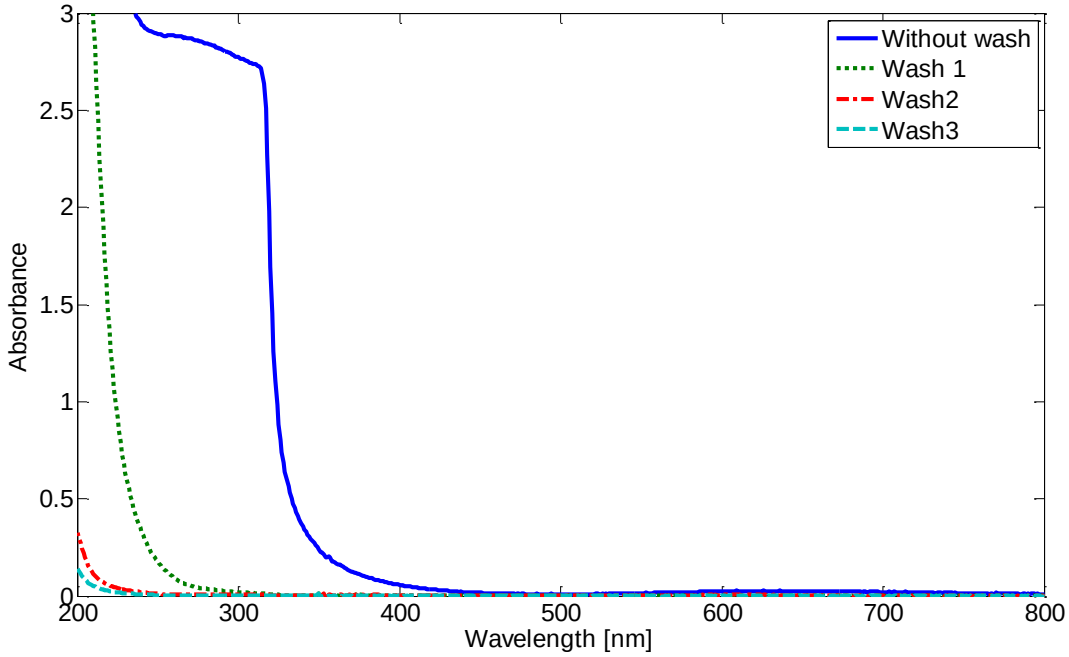

Figure B1: Baseline-corrected UV-vis spectrum of rinsing water after each washing step of PAA-*g*-RC (2 hr) where wash 1 = three quick rinsing stages plus 30-minute soak, all with Milli-Q water, wash 2 = three quick rinsing stages plus 40-minute soak all with Milli-Q water, wash 3 = three quick rinsing stages plus 30-minute soak, where pure Milli-Q water was used as baseline.

Table B1: Carbon, oxygen, bromine, sodium, nitrogen and chlorine weight percentages from EDX

		Weight ± Fitting error %					
RC membrane treatment	BiBB quantity used per membrane disc [mmol]	Carbon	Oxygen	Bromine	Sodium	Nitrogen	Chlorine
0nD	0	52.14 ± 4.85	47.86 ± 8.33	---	---	---	---
	0.74	50.97 ± 5.15	48.37 ± 8.32	0.66 ± 33.82	---	---	---
	2.67	51.51 ± 4.92	48.27 ± 8.25	0.22 ± 58.23	---	---	---
0D	0*	75.35 ± 4.11	24.65 ± 11.73	---	---	---	---
	0.74*	68.92 ± 5.38	26.81 ± 10.12	4.27 ± 9.47	---	---	---
	2.67*	53.74 ± 9.01	18.38 ± 10.53	23.38 ± 4.07	---	4.5 ± 23.54	---
0.5D	0*	72.28 ± 5.30	23.19 ± 11.39	---	3.12 ± 13.72	---	1.41 ± 30.72
	0.74	46 ± 7.70	38.96 ± 9.08	11.65 ± 4.56	---	3.39 ± 28.66	---
	2.67	44.4 ± 8.65	35.07 ± 9.35	17.36 ± 4.51	---	3.17 ± 30.24	---

*Spot measurement rather than full sample area measurement; Percent Error is the fitting error to the EDX spectrum

Table B2: ATR-FTIR peak area ratios at 1680-1800 cm^{-1}/2700-3000 cm^{-1} for the 9 immobilization reaction conditions (n=3, each sample measured 48 times)

	ATR-FTIR peak area ratios at 1680-1800 cm^{-1}/2700-3000 cm^{-1}		
	BiBB quantity used per membrane disc [mmol]		
RC membrane treatment	0	0.74	2.67
0nD	0.064 ± 0.013	0.068 ± 0.014	0.079 ± 0.015
0D	0.063 ± 0.012	0.16 ± 0.035	0.27 ± 0.026
0.5D	0.058 ± 0.014	0.14 ± 0.043	0.24 ± 0.028

Table B3: Estimated degree of substitution for the 9 immobilization reaction conditions (n=3)

	Degree of substitution (DS)	
	BiBB quantity used per membrane disc [mmol]	
RC membrane treatment	0.74	2.67
0nD	0.029 ± 0.0044	0.030 ± 0.0049
0D	0.14 ± 0.050	0.31 ± 0.081
0.5D	0.093 ± 0.086	0.46 ± 0.0070

Sample calculation of BiBB density (molecules g of RC^{-1}), grafting ratio, and $M_{n,theo}$

A. BiBB density

$$\text{BiBB density}\,[\text{molecules g RC}^{-1}] = \frac{(53.9 - 39.8)\ \text{mg}/1000/(2\,29.9 - 79.9)\ \text{g mol}^{-1} \times 6.02 \times 10^{23}\ \text{molecules mol}^{-1}}{39.8\ \text{mg}/1000}$$

$$\text{BiBB density}\,[\text{molecules g RC}^{-1}] = 1.42 \times 10^{21}\ \text{molecules g RC}^{-1}$$

B. Grafting ratio

$$\text{Grafting ratio}\,[\%] = \frac{W_p - W_i}{W_i} \times 100\% = \frac{121.5mg - 53.9mg}{53.9mg} \times 100\% = 125\%$$

C. Theoretical number-average molecular weight ($M_{n,theo}$)

$$M_{n,theo} = \frac{n_{m0}}{n_{BiBB}} \times MW_{monomer} \times conversion$$

$$M_{n,theo} = \frac{3.29\ \text{g}/94\ \text{g mol}^{-1}}{(53.9 - 39.8)\ \text{mg}/1000/(2\,29.9 - 79.9)\ \text{g mol}^{-1}} \times 94\ \text{g mol}^{-1} \times \frac{(121.5 - 53.9)\ \text{mg}/1000}{3.29\ \text{g}}$$

$$M_{n,theo} = 719\ \text{g mol}^{-1}$$

DBC MATLAB code with outlier removal

```
%Matlab code for AKTA weak c membrane chromatography evaluation with one type of protein, no
%contaminations
%Use method #24 for c0 determination
%Use method #27 for chromatography; export UV-, conductivity- and pressure
%curves and logbook; no fraction collection
%Use method #37 for chromatography with fraction collection of
%binding/washing/elution


%Code written by Kamjar Ghofrani 2013
%Edited by Nils Wagner 2014
%Edited by Katharina Hassel 2014
%Edited by Jan Tobias Weggen 2015
%Edited by Priscilla Lai 2015


close all
clear
clc

% input the number of experimental conditions
abcd=input('please input how many files you want to run');
%input the legend titles for the normalized absorbance vs normalized time plot
texta=input('please input legend titles with { quotation} format');
m=[]; %storage matrix
% input whether you want to manually input the wash files and chromatography files or %run a set
of specified files to plot
```

```
blah = input('please input either custom or thesis or thesis2');

for j=1:abcd
    switch blah
        case 'custom'
            cfile=input('input wash file name'); %Define excel sheet with c0 determination
            chromfile=input('input run file name'); %Define excel sheet with AKTA Data
           %thickness of membrane
            thick=input('input average thickness of all membranes in \miu\m in vector format');
            diam=input('input diameter of membrane in mm');   %diameter of membrane holder

        case 'thesis'

washes={'0D_2015Jul30Wash','0D_2015Jun25Wash1','0D_2015Jun30Wash1','0D267_2015Jul7Wash2','0D267_2
015Jun24Wash3','0D267_2015Jun30Wash2','polym_2015Jul24Wash','polym_2015Aug11Wash','polym_2015Aug1
2Wash'}; %Defined set of wash files

runes={'0D_2015Jul30Run','0D_2015Jun25Run1','0D_2015Jun30Run1','0D267_2015Jul7Run2','0D267_2015Ju
n24Run3','0D267_2015Jun30Run2','polym_2015Jul24Run','polym_2015Aug11Run','polym_2015Aug12Run'};
%Defined set of run files

            cfile=washes{j}; %Define excel sheet with c0 determination
            chromfile=runes{j}; %Define excel sheet with AKTA data
            diam=47; %diameter of membrane holder

            thick=[74 74 74 78 78 78 93 93 93]; %thicknesses of the sample

        case 'thesis2'

washes={'2015Jul16Wash2_polym25mmagain','2015Jul16Wash1_polym25mm','polym_2015Jul24Wash','polym_2
015Aug11Wash','polym_2015Aug12Wash'}; %Defined set of wash files

runes={'2015Jul16Run2_polym25mmagain','2015Jul16Run1_polym25mm','polym_2015Jul24Run','polym_2015A
ug11Run','polym_2015Aug12Run'}; %Defined set of run files

            cfile=washes{j}; %Define excel sheet with c0 determination
            chromfile=runes{j}; %Define excel sheet with AKTA data

            diam=47;
            thick=[93 93 93 93 93]; %thicknesses of the sample

    end
    % linestyle for plot; adjust before running code
    colouer={'-',':','-.','-',':','-.','-',':','-.'};

    elurate=2;          %Flow rate (ml/min) during elution
    bindrate=1;         %Flow rate (ml/min) during bind/equ/wash steps
    deadvolume=3.38;    %Deadvolume of the AKTA system in ml (determined by Kayleigh Kuindersma)
    proc= 0.5;          % 0.5mg/mL protein
    bindvolume=50;      %set retention volume for binding from AKTA system

    maxabsor=xlsread(cfile,'B4:B10000');        %Importing c0 absorbance data
    nitr=min(maxabsor(390:end));                %minimum absorbance value in wash data
    nitr2=max(maxabsor(390:end));               %maximum absorbance value in wash data

    %-------------------------Finding c0 calibration from wash data-----------------------------%
    if nitr<0 %if the lowest number is negative, then baseline=0
        nitr=0;
    end

%if the highest number doesnt make sense i.e. >>100 absorbance units, then find the max of the
%binding plateau
    if nitr2>170
        nitr2=max(maxabsor(390:600));
    end

%if the highest number still has absorbance units >>300, then find the mode of the binding
%plateau
    if nitr2>300
        nitr2=mode(maxabsor(400:600));
    end
```

```
    nitr2,nitr                  %Display maximum and minimum absorbance value in wash data
    c0=nitr2-nitr               %Determines c0 (Use AKTA method #24 to collect data!)
    %-------------------------------------------------------------------------------------%

    %--------------Deleting outliers from AKTA Run data ---------------------------------%
    t=xlsread(chromfile,'A4:A10000');      %Importing time data from AKTA run with membrane
    absor=xlsread(chromfile,'B4:B10000');  %Importing absorbance data from AKTA run with membrane
    press=xlsread(chromfile,'F4:F10000');  %Importing pressure data from AKTA run with membrane

   % controls where you want to find outliers change the time to go to particular segment
    absor2=absor(find(t>=0 & t<(xlsread(chromfile,('G17:G17'))+deadvolume/bindrate)));

% if data point is +30 of previous data point, +30 of two previous points higher, -8 of previous
%data point or greater than 170, label the point as NaN
    for i=3:length(absor2) %finding high value outliers at binding plateau
     if absor(i)>absor(i-1)+30 || absor(i)>absor(i-2)+30 || absor(i)<absor(i-1)-8 ||absor(i)>170
            absor(i)= NaN; %identifying the outliers
            press(i)=NaN; %identifying the outliers
        end
    end
    size(absor)
    size(press)
    t(find(isnan(absor)))=[];%deleting the outlier element
    absor(isnan(absor))=[]; %deleting the outlier element
    press(isnan(press))=[];%deleting the outlier element
    %-------------------------------------------------------------------------------------%

    %Imports req.starting time of binding from field G12 and considers the system's dead volume
    %in order to determine real starting time of binding.
    u=abs(t-(xlsread(chromfile,('G12:G12'))+deadvolume/bindrate));
    bindstart=find (u==(min(u)))

    clear u

    %Imports req. ending time of binding and adjusts it
    u=abs(t-(xlsread(chromfile,('G14:G14'))+deadvolume/bindrate));
    bindend=find (u==(min(u)));

    clear u

    %Imports req. starting time of elution and finds real starting time.
    u=abs(t-(xlsread(chromfile,('G17:G17'))+deadvolume/elurate));
    elustart=find (u==(min(u)))
    clear u
    u=abs(t-xlsread(chromfile,('G17:G17')));
    elureq=find (u==(min(u)));


    %----------DBC calculation Method 1-----------------------------------------------%

    %absorbance of binding step
    bindabsor=absor(t>=0 & t<(xlsread(chromfile,('G14:G14'))+deadvolume/bindrate));

    %finding 10% breakthrough time by minimizing abs [30:end] excludes wrong determination of
    %absorption caused by bubbles.
    c10=abs(bindabsor(30:end)-(c0/10));
    k=find(c10==min(c10))+29;                   %add 29 to k again to be consistent with time

    %finding 50% breakthrough time by minimizing abs [30:end] excludes wrong determination of
    %absorption caused by bubbles.
    c50=abs(bindabsor(30:end)-(c0/2));

    %finding 100% breakthrough time by minimizing abs [30:end] excludes wrong determination of
    %absorption caused by bubbles.
    c100=abs(bindabsor(30:end)-(c0));
    k2=find(c100==min(c100))+29;
    k3=find(c50==min(c50))+29;

    vpermeate= bindrate*(t(k)-t(bindstart));    %permeate volume at 10% breakthrough
    vpermeate2=bindrate*(t(k2)-t(bindstart));   %permeate volume at 50% breakthrough
    vpermeate3=bindrate*(t(k3)-t(bindstart));   %permeate volume at 100% breakthrough
```

```
    Area=pi*((diam/10)/2).^2;                   %surface area of membrane [cm^2]
    thickness=(thick(j)/1000000)*100;           %thickness of membrane [cm]
    vmembrane=thickness*Area;                   %volume of membrane [cm^3=mL]

    Qdbc = proc*vpermeate/vmembrane             %Formula to calculate DBC 10%, 50%, 100%
    Qdbc2=proc*vpermeate2/vmembrane
    Qdbc3=proc*vpermeate3/vmembrane


    %-------------------------------------------------------------------------------------------%


    %---------------------------Qdbc,10% Method 2 Integration method-------------------------%
    absnorm=absor/c0;                           %normalize absorbance values
    absnorm (absnorm < 0)=0;
    tbind=t(bindstart:bindend);                 %create vector for binding time
    tbind0=t(bindstart:bindend)-t(bindstart); %create vector for binding time starting with 0.
    tbindnorm=tbind0/max(tbind0);               %normalizing
    absbindnorm=absnorm(bindstart:bindend);   %create vector for binding absorption
    absbind=absor(bindstart:bindend);
    bindpress=press(bindstart:bindend);
    %cbind=absbind/178.91;      %178.91 slope of calibration curve of IgG in 50mM acetate buffer
    slope=c0/0.5;               %two point slope of single point calibration curve from wash step
    cbind=absbind/slope;

    %total volume at every time
    vol=[t(1:elureq);((elurate*(t(elureq+1:end)))-((elurate-1)*(t(elureq))))];

    %vector for volume starting with 0 when binding starts
    volbind = vol(bindstart:bindend)-vol(bindstart);
    volbindnorm = volbind/max(volbind);                     %normalized binding volume

    h=k-bindstart;
    %integration of binding curve
    mass_protein_bound_10percent=volbind(h)*proc-(trapz(volbind(1:h),cbind(1:h)));
    mass_protein_bound=bindvolume*proc-(trapz(volbind(1:end),cbind(1:end)));
    protein_feed_10=proc*bindrate*t(k)
    DBC10=mass_protein_bound_10percent/vmembrane            %DBC 10%,100% calculation
    DBC100=mass_protein_bound/vmembrane

    %-----------------------------------Plot binding curve-----------------------------------%
    k2={'b','b','b','g','g','g','m','m','m'};        %colour values for plot

    %----plot pressure and normalized absorbance binding curves for thesis 2 case---------------%
    wordi='thesis2';
    if strcmp(blah,wordi)==1
        a=j;
        if j==5
            a=5.5;
        end

        subplot(3,2,a)
        [AX,H1,H2] = plotyy(tbindnorm, absbindnorm,tbindnorm,bindpress);
        set(get(AX(1),'Ylabel'),'String','Normalized Absorbance','fontsize',12)
        set(get(AX(2),'Ylabel'),'String','Pressure [MPa]','fontsize',12)
        set(AX,'fontsize',12)
        set(AX(2),'XTickLabel',[])
        set(AX(2),'ylim',[0 0.2])
        set(AX(2),'YTick',[0:0.5:0.2],'yaxislocation','right','ytickmode','auto')
        set(AX(1),'Box','off')
        names={'(A) 25 mm_{low DBC} ','(A) 25 mm_{high DBC}','(B) 47 mm rep 1','(C) 47 mm rep
2','(D) 47 mm rep 3'};
        title(names(j))

    else

        %---------------plot normalized absorbance binding curve for thesis case----------------%
        plot(tbindnorm, absbindnorm,colouer{j},'linewidth',4,'color',k2{j});
        hold on
        %plot(t,absor)
        f=18; %fontsize
```

```
        xlabel('Normailized Time','fontsize',f)
        ylabel('Normalized Absorbance','fontsize',f)
        set(gca,'fontsize',f)

        t(bindstart)
        legend(texta)
    end

%matrix displaying DBC10% values from method 1 and method2
    m=[m;Qdbc,DBC10,mass_protein_bound_10percent]
end
```